STRUCTURE AND FUNCTION STUDIES OF THE

CYTOCHROME bc_1 COMPLEX

By

BUDDHA GURUNG

Bachelor of Science in Biochemistry
Oklahoma State University
Stillwater, Oklahoma
2000

Submitted to the Faculty of the
Graduate College of the
Oklahoma State University
in partial fulfillment of
the requirements for
the Degree of
DOCTOR OF PHILOSOPHY
December, 2007

STRUCTURE AND FUNCTION STUDIES OF THE

CYTOCHROME bc_1 COMPLEX

Dissertation Approved:

Dr. Chang-an Yu (Dissertation Adviser)

Dr. Linda Yu

Dr. Jose L. Soulages

Dr. Robert Burnap

Dr. A. Gordon Emslie (Dean of the Graduate College)

ACKNOWLEDGEMENTS

I wish to express the utmost gratitude to my advisor Dr. Chang-an Yu without whose guidance, support, inspiration, caring and love, I would not be where I am today. I am also equally grateful to Dr. Linda Yu for her supervision, advise, support and friendship during my stay here. Many thanks are also due in part to Dr. Jose L. Soulages and Dr. Robert Burnap for taking time off their hectic schedules to serve on my committee. Their support, guidance and friendship are greatly appreciated.

I would like to thank Dr. Di Xia at the NIH for his support and great collaboration. I am grateful to Dr. Shih-Chia Tso for his help during the early years of my tenure here. My sincere gratitude also extends to students and postdoctorates, both former and current, in Dr. Yu's lab for their assistance, hospitality and stimulating discussions.

Most important of all, I would like to thank my family for their love and constant support in my endeavors, and the sacrifices endured in helping me achieve my dreams. Finally, I would like to thank Ms. Brittany Glenn, my friend and partner in life, for her friendship, understanding, patience and unconditional love.

TABLE OF CONTENTS

LIST OF TABLES

LIST OF FIGURES

NOMENCLATURE

ADP	Adenosine diphosphate
ATP	Adenosine triphosphate
NADH	Nicotinamide adenine dinucleotide (reduced form)
NAD+	Nicotinamide adenine dinucleotide
TCA	Tricarboxylic acid
Pi	Inorganic phosphate
cyt	cytochrome
ISP	Rieske iron-sulfur protein
EPR	Electron Paramagnetic Resonance
[2Fe-2S]	Rieske iron-sulfur cluster
RC	Reaction center
ICM	Intra-cytoplasmic membrane
PL	Phospholipid
CCCP	carbonyl cyanide *m* – chlorophenylhydrazone
DM	n-Dodecyl-β-D-Maltoside
OG	n-Dodecyl-β-D-Glucoside
C*c*O	Cytochrome *c* Oxidase
CD	Circular Dichroism

Ni-NTA	Nickel-NitriloTriAcetic Acid
ISF	Rieske Iron-Sulfur Fragment
SOD	Superoxide dismutase
DTT	Dithiothreitol
DEAE	Diethylaminoethyl
XO	Xanthine Oxidase
MCLA	6-(4- methoxyphenyl)-2-methyl-3,7-dihydroimidazo[1,2-a] pyrazin-3 (7H) – one hydrochloride

CHAPTER I

INTRODUCTION

I: Bioenergetics and oxidative phosphorylation

Mitochondria, described as "the power plants" of cells are the site of eukaryotic oxidative phosphorylation. This process is responsible for more than 95 % of the energy required, and is carried out in the inner mitochondrial membrane by electron transfer complexes and the ATP synthase complex (Fig 1). The mitochondrial electron transport chain is composed of four multi-subunit electron transfer complexes: NADH-ubiquinone oxidoreductase, also called Complex I, succinate-ubiquinone reductase or Complex II, ubiquinol-cytochrome *c* reductase or Complex III, and cytochrome *c* oxidase also known as Complex IV.

NADH and succinate, derived from the TCA cycle and the β-oxidation of fatty acids and amino acids, are oxidized by NADH-ubiquinone oxidoreductase and succinate-ubiquinone oxidoreductase respectively to form NAD^+ and fumerate. The electrons are then transferred to ubiquinol-cytochrome *c* reductase, cytochrome *c* oxidase and eventually to molecular oxygen. Electron transfer through the complexes is coupled to proton translocation across the inner membrane in all complexes except succinate-ubiquinone reductase. This results in the generation of a membrane potential that is utilized by the ATP synthase to synthesize ATP. ATP synthase is comprised of two

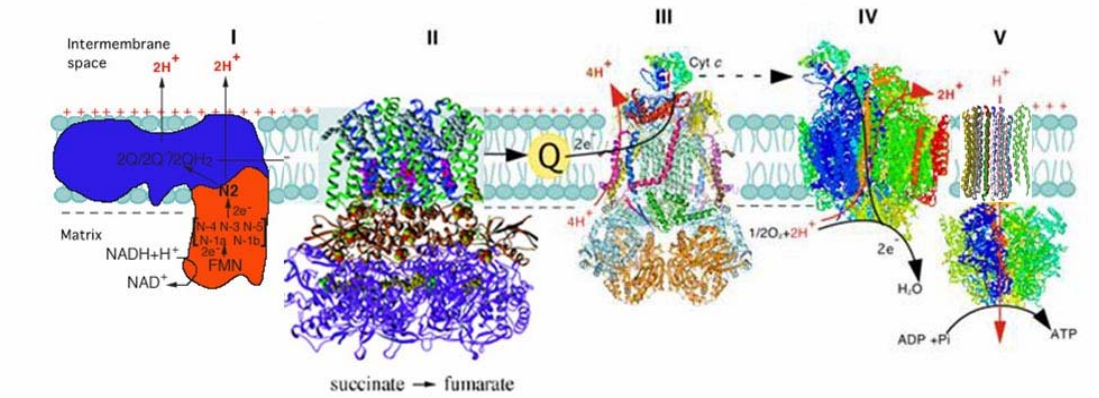

Figure 1. Mitochondrial electron transport chain. Electron transfer complexes are labeled as: Complex I, NADH-Q Oxidoreductase; Complex II, Succinate-Q Oxidoreductase; Complex III, Ubiquinol Cytochrome *c* Oxidoreductase; Complex IV, Cytochrome *c* Oxidase; Complex V, ATP synthase. Electron flow is represented by black arrows while proton transfers are shown in red. The reactions catalyzed by the individual complexes are indicated as well.

functional subunits; F_0 and F_1. F_1 is the water-soluble catalytic subunit that binds ADP and Pi to generate ATP. It consists of a hexagonal array of alternating α and β subunits with a centrally located γ subunit that has been shown to rotate during catalysis (1-3). The detergent soluble F_0 subunit is a hydrophobic trans-membrane protein that contains a proton translocation channel. The ATP synthase operates through a mechanism in which three interacting catalytic protomers undergo a change in binding affinity for the reactants, ATP, ADP and inorganic phosphate (Pi). The change in affinity for the reactants results in a change in the γ-subunit position relative to the $\alpha_3\beta_3$ assembly, which involves a rotation of one relative to the other (2, 4). The rotation of the $\alpha_3\beta_3$ assembly of F_1 is driven in the direction of ATP synthesis by an influx of H^+ down the proton gradient to the matrix from the inter-membrane space. The generation of a proton motive force across the energy-transducing membrane coupled to electron transfer is the central dogma of the chemiosmotic theory, proposed by Nobel laureate Peter Mitchell in 1961 (5).

II. The cytochrome bc_1 complex

1. Cytochrome bc_1 complex and the electron transport chain.

The cytochrome bc_1 complex, or ubiquinol-cytochrome *c* oxidoreductase, is an essential component of the energy-conserving, electron transfer chain of mitochondria and many respiratory and photosynthetic bacteria (6). The complex catalyzes electron transfer from ubiquinol to cytochrome *c* with the concomitant translocation of protons the membrane to generate a proton gradient and membrane potential for ATP synthesis.

The cytochrome bc_1 complex from all species contains three core subunits that house four redox prosthetic groups: cytochrome *b* with heme b_L (b_{566}), and b_H (b_{562}), cytochrome c_1, which houses a *c*-type heme, and a high potential iron sulfur cluster in the Rieske iron-sulfur protein (ISP). In addition to the three core subunits, varying numbers of non-redox group containing subunits called supernumerary subunits are present in the cytochrome bc_1 complexes from different sources. For example, cytochrome bc_1 complexes from *Rhodobacter capsulatus* have no supernumerary subunits, *Rhodobacter sphaeroides* bc_1 complex has one, while complexes from bovine mitochondria have eight. The exact role of supernumerary subunits is uncertain, but it has been reported that complexes without any supernumerary subunits are less stable and have lower activity (7, 8).

2. The Q-cycle mechanism

The simplest arrangement for electron transfer via the cytochrome bc_1 complex is a linear pathway, where the direction of electron transfer is determined by the redox potential of the various prosthetic groups as shown in the scheme below;

$$QH_2 \longrightarrow b_L \longrightarrow b_H \longrightarrow ISP \longrightarrow \text{cyt. } c_1 \longrightarrow \text{cyt. } c$$

However, this scheme fails to explain the 2 H^+/e^- stoichiometry observed in cytochrome bc_1 complex catalysis (9), as it can only account for a 1 H^+/e^- stoichiometry. This linear scheme of electron transfer also fails to explain the phenomenon described as 'oxidant-induced reduction of cytochrome *b*' observed by Chance et. al. (10). Addition of a pulse of oxygen to slowly respiring mitochondria, in the presence of antimycin A, resulted in a

transient increase in cytochrome *b* reduction with a rate comparable to the oxidation of cytochrome c_1.

Peter Mitchell was the first to propose the 'Q-cycle mechanism' (Fig. 2) to explain the electron and proton transfer mechanism within the cytochrome bc_1 complex (11). The 'modified Q-cycle' is now widely accepted as it adequately accounts for most of the experimental results mentioned above, including the 'oxidant-induced reduction of cytochrome *b*' (12-14). There are two key features of the Q-cycle mechanism: (a) the presence of two separate binding sites for ubiquinol and ubiquinone, namely Q_P and Q_N sites, and (b) the bifurcated electron transfer at the Q_P site. Ubiquinol is oxidized at the Q_P site with a relatively high activation barrier (13). The first electron from ubiquinol oxidation is transferred to a high-potential chain consisting of the Rieske iron-sulfur protein, cytochrome c_1 and cytochrome *c*. Two protons are released into the inter-membrane space. The second electron is passed to a lower-potential chain containing the b_L and b_H hemes. The electron then reduces a ubiquinone at the Q_N site to form a stable ubisemiquinone ($Q^{\cdot-}$). At this juncture, only half of the Q-cycle is complete. During the second turnover, a second ubiquinol is oxidized at the Q_P site, and the electron from heme b_H now reduces the ubisemiquinone formed at the Q_N site during the first cycle. Subsequently, two protons are taken up from the N-side to form QH_2 thereby completing one Q-cycle. The end result of one complete Q-cycle is the oxidation of two ubiquinol molecules at the Q_P site, the generation of one ubiquinol molecule at the Q_N site, the production of two molecules of reduced cytochrome *c*, and the deposition of four protons on the P-side of the membrane. The overall Q-cycle reaction is represented by the equation below;

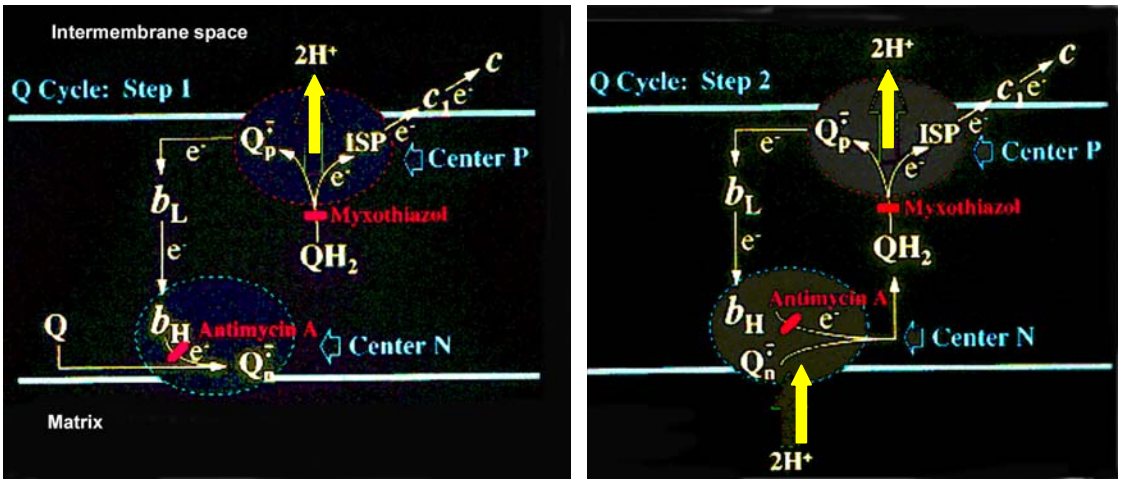

Figure 2. The protonmotive Q-cycle mechanism of electron transfer and proton translocation in the cytochrome *bc*$_1$ complex. The Q_P and Q_N sites are represented by dashed circles and labeled as Center P and Center N respectively. The sites of action of myxothiazol, a Class Ia inhibitor and antimycin A are shown in red. Electron transfer pathways are shown by white arrows while protons are shown in yellow block arrows.

$$QH_2 + 2 \text{ cyt } c^{3+} + 2H^+_{(N)} \longrightarrow Q + 2 \text{ cyt } c^{2+} + 4H^+_{(P)}$$

The bifurcation of the two electrons from ubiquinol between the high and low-potential chains is crucial to the process through which the free-energy drop is utilized to generate a proton gradient. The second electron of ubiquinol is transferred to the low-potential heme b_L almost exclusively, although a thermodynamically favorable pathway to the high-potential pathway is available. Several models on the bifurcated electron transfer at the Q_P site have been proposed. The sequential (15-17) and the concerted mechanism (18-20) are the widely accepted views on ubiquinol oxidation at the Q_P site. In the concerted mechanism, an electron from ubiquinol is transferred to heme b_L at or about the same time an electron is transferred to ISP. This mechanism excludes the generation of a ubisemiquinone radical at the Q_P site. In the sequential mechanism, a ubisemiquinone radical formed after reduction of the high-potential chain reduces heme b_L and the low-potential pathway. However, the existence of such a radical has not been detected yet (13). Suggestions have been made that a relatively stable complex of ISP_{red} with ubisemiquinone might be formed, but both their EPR signals might be lost through interaction between their neighboring spins (18).

3. The Three-Dimensional Crystal Structure of the Cytochrome bc_1 Complex

A. Overall structure of the Cytochrome bc_1 complex.

Three-dimensional structures of mitochondrial bc_1 complexes from bovine (22, 23) and chicken (24) were determined by X-ray diffraction of crystals at 3 Å. The first cytochrome bc_1 complex crystal structure, determined at 2.9 Å was reported by our group

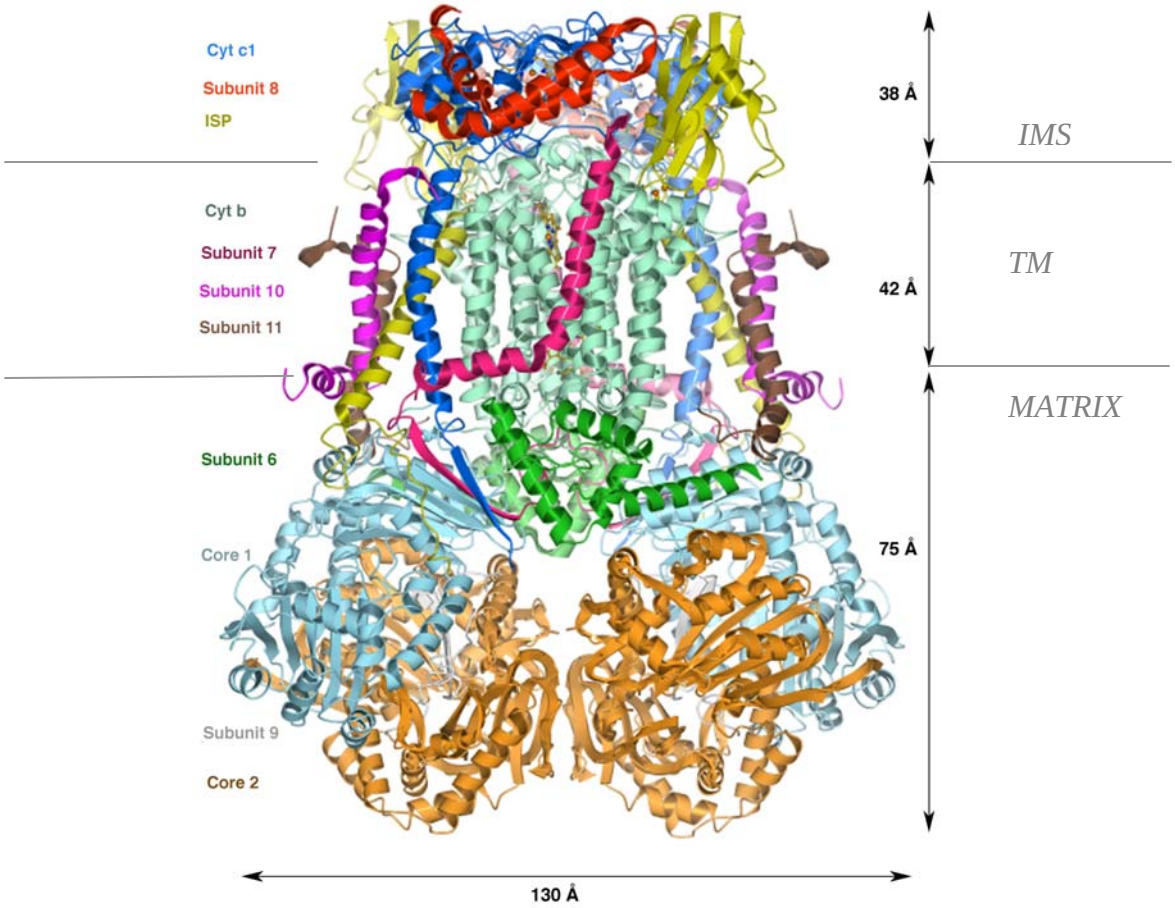

Figure 3. The 3-D structure of the dimeric mitochondrial cytochrome bc_1 complex. The color code for each subunit is given on the side bar. Prosthetic groups are shown in ball-and-stick model. The two parallel lines indicate the membrane-spanning regions. The mitochondrial inter-membrane space (IMS), the membrane spanning region (TM), and the matrix are as labeled.

in 1997 in collaboration with Dr. Deisenhofer's lab at Southwest Medical Center in Dallas, Texas (22). The resolutions were later improved to 2.31 Å using cytochrome bc_1 complex purified from yeast crystallized in the presence of a monoclonal antibody Fv fragment (25). The structure of the cytochrome b_6f complex, a complex that is analogous to the cytochrome bc_1 complex, that provides an electronic connection between photosystems I and II, has also been established for the thermophillic cyanobacterium (blue-green algae) *Mastigocladus laminosus* (26) and in the algae *Chlamydomonas reinhardtii* (27). In our bovine $I4_122$ crystal structure, the cytochrome bc_1 complex is a pear-shaped intertwined dimer with a diameter of 130 Å at its widest point in the matrix, and is 155 Å in height. It can be divided into three regions: matrix, transmembrane, and the inter-membrane space regions (Fig. 3). The majority of the complex is located in the matrix region, extending 75 Å deep. This region consists of subunits I, II, VI, IX, the N-terminal part of subunit VII and the C-terminal of ISP. The transmembrane region is approximately 42 Å, and consists of thirteen transmembrane helices in each monomer, eight from cytochrome *b*, one each from cytochrome c_1, ISP, subunits VII, X, and XI. The transmembrane region of cytochrome *b* houses hemes b_L and b_H, and the two ubiquinol binding sites, Q_P and Q_N. The inter-membrane space region, 38 Å tall, houses heme c_1 and the Rieske iron-sulfur cluster.

In native crystals, a bound ubiquinone molecule that occupies the same region as antimycin A has been described (25, 35). However, no ubiquinol / ubiquinone molecule(s) have been identified at the Q_P inhibitor binding site. Therefore, any discussions on the mechanisms of electron transfer are based primarily on the positions

occupied by inhibitors at the Q_P site, and assumptions are made to reflect a similar site for binding of the natural substrate, ubiquinol.

B. The structure of the Rieske iron-sulfur protein (ISP)

The presence of an iron-sulfur cluster in the bc_1 complex was first recognized by its contribution to the EPR spectrum (28). The structure of the Rieske iron-sulfur protein (Fig 4) is divided into three domains: the membrane-spanning N-terminal domain (tail) including residues 1-62, the soluble C-terminal domain (head) covering residues 73-96, and the flexible domain that links the head and tail domains containing residues 63-72 (29). The soluble, extra-membrane head domain of ISP from bovine heart containing the intact iron-sulfur cluster was crystallized and its structure determined at 1.5 Å (29). It is a rigid, compact, and flat-spherical shaped structure containing three layers of anti-parallel β-sheets composed of ten β-strands. Unlike classical ferrodoxin-type [2Fe-2S] centers where the ligands are all cysteines, the [2Fe-2S] cluster of the Rieske ISP is coordinated by two cysteine and two histidine residues. Loops β4-β5 and β6-β7, each contributes one cysteine and one histidine residue. An additional cysteine residue is present in each loop, forming a disulfide bond connecting the two loops contributing to the stability of the protein. A complex salt bridge and hydrogen-bond network exists, which further stabilizes the protein. Multiple factors contribute to the high redox potential of the cluster: the overall charge of the cluster, 0 and -1 for the oxidized and reduced state, respectively, compared with -2 and -3 for [2Fe-2S] clusters with four cysteine coordination in ferrodoxins; the electronegativity of the histidine ligands and the solvent exposure of the Fe(II). The transmembrane helix of ISP is in one monomer while its extrinsic domain crosses over and associates with cytochrome *b* and c_1 of the other

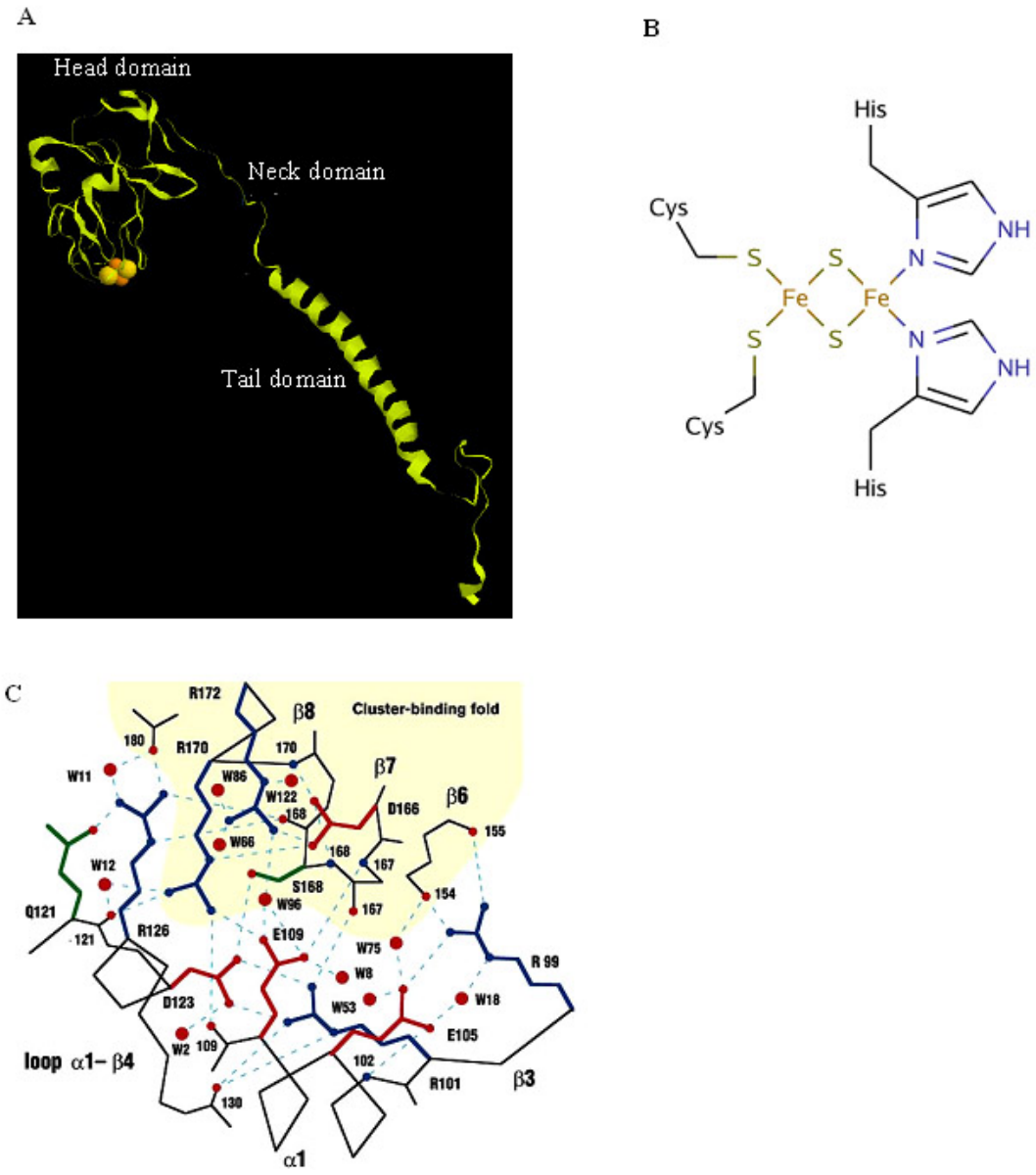

Figure 4. Structure of the Rieske iron-sulfur protein (ISP). The overall structure of ISP (A), the ligands of the Rieske iron-sulfur cluster (B), and the salt bridge / hydrogen bond network around the iron-sulfur cluster (C). The head, neck and tail domains of the Rieske ISP are shown.

monomer. Therefore, the bc_1 complex is a functional dimer, since dimerization is necessary to complete the high-potential chain consisting of the Rieske ISP and cytochrome c_1. A functional unit of bc1 complex consists of cytochromes *b* and c_1 from one monomer, and a Rieske ISP from the other monomer.

C. Structure of cytochrome *b*

Cytochrome *b* is the only mitochondrially encoded protein in the cytochrome bc_1 complex. It has eight trans-membrane helices designated with capital letters A-H, and the linker regions are labeled with lower case letters (Fig 5). The trans-membrane regions can be divided into two groups; helices A-E in one group and F-H in the other. The crystal structures indicate that both the N- and C- terminals are located in the matrix region. The high-potential heme (b_H) is close to the matrix side of the cytochrome *b* subunit, while the low potential-heme (b_L) lies close to the exterior surface of the subunit, but is shielded from the aqueous phase by cytochrome c_1. The iron-iron distance between the high-potential and low-potential hemes is 20.7 Å, and is in good agreement with the predicted distance of 22 Å derived from biochemical and biophysical studies (30). The low potential hemes in the two monomers are quite close; the distance between the two irons is 21.2 Å, and electron transfer between the two monomers via the two heme b_L's has been reported (31). Histidines serve as the axial ligands for both the low and high-potential hemes. His- 83 and His-182 co-ordinate heme b_L while that role is fulfilled by His-97 and His-196 in heme b_H. The putative ubiquinol / ubiquinone binding sites, Q_P and Q_N, are located at the P-side and the N-side, and in close vicinity of hemes b_L and b_H respectively.

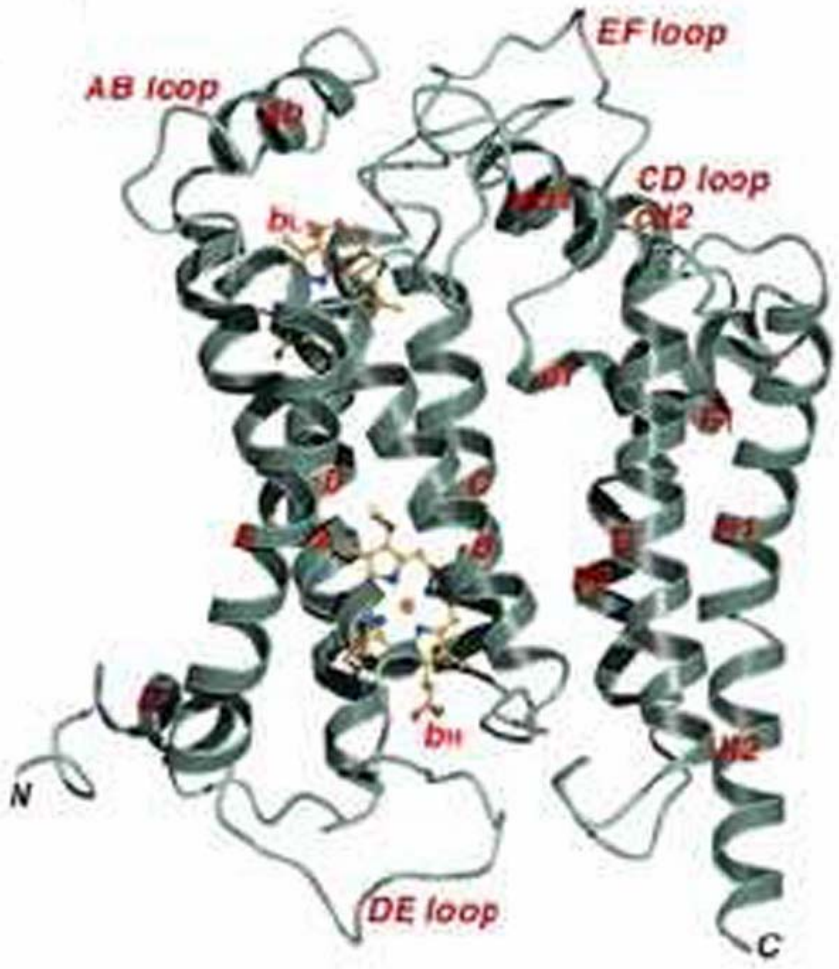

Figure 5. Structure of the mitochondrial cytochrome *b* subunit. Ribbon representation of cyt *b* showing its eight trans-membrane helices. Hemes b_L and b_H are shown as stick models with carbon atoms in yellow, nitrogen blue and oxygen red. The helices are individually labeled, and the loops connecting the helices are also shown.

D. *Crystal Structure of the cytochrome bc_1 complex loaded with inhibitors*

Historically, cytochrome bc_1 complex inhibitors were divided into two classes depending upon their site of action. Class I inhibitors bind at the Q_P site while Class II inhibitors bind at the Q_N site (32-34). The Class I inhibitors were further divided into sub-groups based upon the chemical characteristics of the inhibitors, and on biophysical and spectroscopic effects of the b_L heme and the iron-sulfur cluster upon binding of inhibitors. Class Ia inhibitors include myxothiazol and β-methoxyacrylate stilbene (MOAS); they presumably block electron transfer from quinol to the ISP accompanying a red-shift in the α and β-bands of the reduced cytochrome *b*. Class Ib inhibitors possess a chromone ring system, and inhibit electron transfer from ISP to cytochrome c_1. A pronounced increase in the redox potential of the ISP is observed upon binding of Class Ib inhibitors. Like the Class Ia inhibitors, Class Ib inhibitors cause a red-shift in the absorption spectrum of reduced cytochrome *b*. Stigmatellin is an example of a Class Ib inhibitor.

It was recognized in the first bc_1 complex structures that the extrinsic head domain of ISP was highly mobile (22). It was further demonstrated that, when the soluble head domain of ISP is not restricted in motion by crystallographic contacts, it assumes one of two states in response to binding of different Class I inhibitors: a fixed or mobile state (35-37). In the crystals of native cytochrome bc_1 complex (i.e. Q_P site empty), the soluble head domains are partitioned between a fixed and loose state. The binding of Class Ib inhibitors, or 'P_F' inhibitors like stigmatellin and UHDBT, results in the ISP head in the fixed state, while Class Ia or 'P_M' inhibitors exhibit a dramatic increase in the mobility. The binding of Q_P site inhibitors has a considerable effect on the

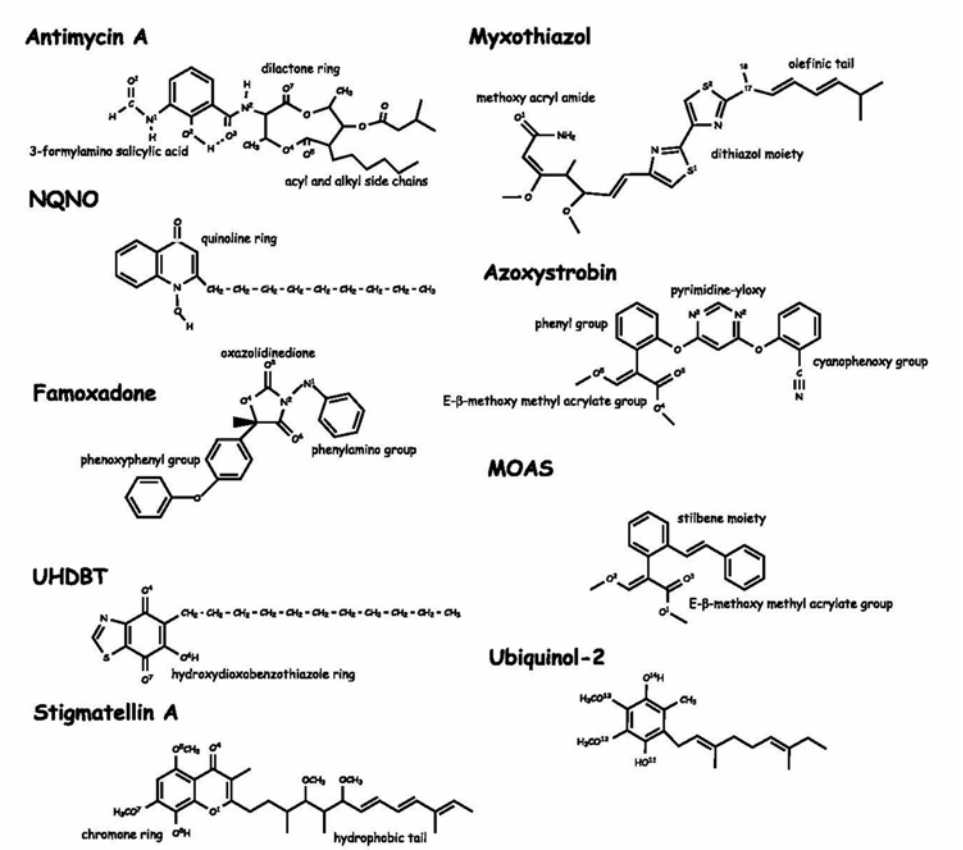

Figure 6. Chemical structures of some cytochrome bc_1 complex inhibitors.

Table 1

Effects of Q_P site inhibitors on the relative anomalous peak heights of the [2Fe-2S] cluster of the ISP normalized to the heme b_H peak

Crystal preparation	Normalized peak heights [a]
Native bc_1 (Q_P binding pocket empty)	0.52
+ MOAS	0.23
+ Myxothiazol	0.46
+ Azoxystrobin	0.36
+ Stigmatellin	1.20
+UHDBT	0.96
+ Fomaxodone	1.02

[a] Peaks are normalized against anomalous signals of their respective b_H heme irons.

electron density of the anomalous scattering of the FeS peak heights (38). All iron anomalous peaks were normalized by the peak height of the b_H heme iron, and the values in the presence of different inhibitors are presented in Table 1. The use of the b_H heme peak as an internal standard is justified because of the structural stability of the heme environment due to its proximity to the core proteins of the bc_1 complex where most of the crystal contacts are made. Binding of Class Ib inhibitors like stigmatellin or UHDBT enhances the electron density of the anomalous scattering peak of the [2Fe-2S] cluster, while Class Ia inhibitors like myxothiazol and MOAS abolish the electron density.

Conformational variations in cytochrome *b* upon binding of P_F inhibitors are limited to a few regions: the inhibitor binding sites, the ISP neck contact area, and parts of the *ef* loop (35). Alignment of inhibitor-bound structures with the native bc_1 structure reveals complexity both in terms of magnitude and the direction of displacement of certain amino acid residues. Antimycin A binding to the bc_1 complex does not induce significant conformational change in cytochrome *b* residues, except for small displacements of 0.5 – 1 Å to facilitate the binding of the inhibitor (36). However, the binding of stigmatellin led to significant conformational changes, particularly in the cd-1 and cd-2 helices and the *ef* loop. The hydroxyl group of stigmatellin forms a hydrogen bond with Glu-271 whose side-chain has rotated 160^o from the inhibitor-free state. Displacement vectors, measured between C^α atoms of inhibitor bound and native structures for residues that are in direct contact with the P_F and P_M inhibitors are given in Tables 2A, and 3 respectively (38).

Table 2

Displacement vector (V_d) length for residues of cyt. b upon inhibitor binding.

A

Cyt. *b* residue	Fomaxodone	Stigmatellin	UHDBT	NQNO
M124	0.37	0.43	0.35	0.26
F128	0.37	0.41	0.60	0.36
Y131	0.28	0.18	0.42	0.28
V132	0.11	0.20	0.29	0.25
M138	0.27	0.57	1.06	0.66
G142	0.23	1.31	1.20	0.75
A143	0.17	1.16	1.05	0.60
V145	0.68	1.41	1.40	1.06
I146	0.69	1.33	1.37	0.98
I268	0.75	1.16	0.84	0.25
P270	1.56	1.19	0.46	0.61
E271	1.21	0.77	0.32	0.54
Y273	0.61	0.52	0.20	0.25
F274	0.47	0.51	0.48	0.17
Y278	0.25	0.13	0.63	0.36
L294	0.22	0.28	0.24	0.24
I298	0.24	0.20	0.27	0.26

B

Cyt. *b* residue	Myxothiazol	MOAS	Azoxystrobin
M124	0.49	0.26	0.25
F128	0.29	0.19	0.15
Y131	0.40	0.34	0.51
V132	0.27	0.13	0.38
M138	0.20	0.26	0.33
G142	0.49	0.42	0.48
A143	0.42	0.20	0.43
V145	0.39	0.32	0.49
I146	0.45	0.51	0.65
I268	0.94	0.55	0.72
P270	1.29	1.23	1.51
E271	1.15	1.23	1.52
Y273	0.39	0.24	0.53
F274	0.43	0.18	0.57
Y278	0.47	0.43	0.66
L294	0.69	0.53	0.71
I298	0.23	0.49	0.89

4. Study System

The photosynthetic bacterium, *Rhodobacter sphaeroides* is used as the model system for our studies. *R. sphaeroides* is an anoxygenic purple facultative bacterium. In plants and algae, photosynthesis occurs in an aerobic environment resulting in the release of oxygen as a result of the water splitting process. However, in *R. sphaeroides*, photosynthesis occurs in an anaerobic environment, and does not result in the production of oxygen. The synthesis of some photosynthetic pigments in *R. sphaeroides* is actually repressed by oxygen (40). The preferred growth mode of *R. sphaeroides* is photoheterotrophic, under anaerobic conditions in light with various organic substrates. The ecological niches of *R. sphaeroides* are anoxic parts of waters and sediments, which receive light of sufficient quantity and quality to allow phototrophic development (40).

In *R. sphaeroides*, ATP is synthesized either via the cyclic or non-cyclic electron transfer pathway (Fig 7). The cyclic electron transfer pathway involves two membrane-bound components; the reaction center (RC) where the initial light-dependant electron transfer occurs, and the cytochrome bc_1 complex. Upon excitation by light energy, P_{870}, a bacteriochlorophyll inside the photosynthetic reaction center, becomes a strong reducing agent. It transfers its electron to a second bacteriochlorophyll, a bacteriopheophytin, a bound quinone at site Q_A, and eventually to a bound quinone at Q_B. Upon reduction by two electrons, the quinone at the site Q_B becomes fully reduced as Q^{2-}, and two protons are taken up from the cytoplasm to form QH_2 (41). The QH_2 leaves the RC and diffuses through the membrane towards the cytochrome bc_1 complex, which in turn transfers the electrons to cytochrome c_2. As in the mitochondrion, four protons are translocated across the membrane for every two electrons that pass through the bc_1 complex. The reduced

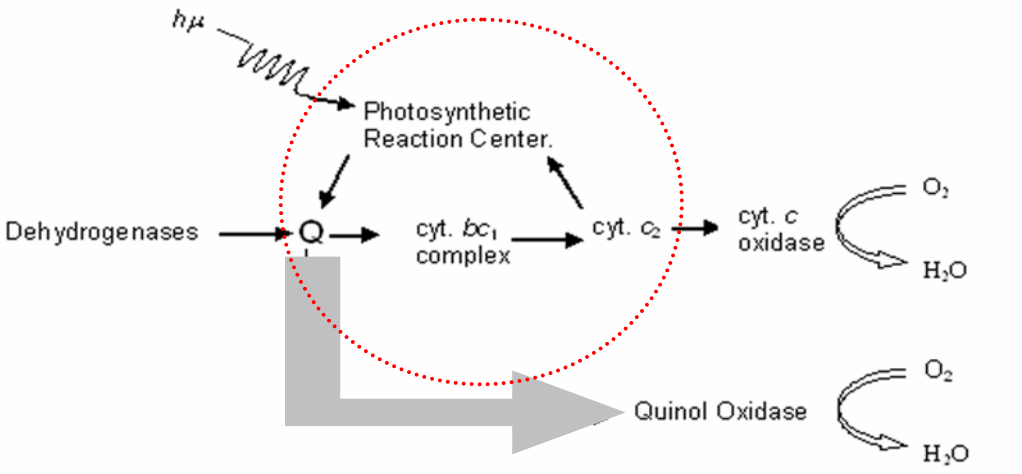

Figure 7. Electron transfer pathways in *Rhodobacter sphaeroides*. Cyclic electron transfer in *R. sphaeroides* is shown enclosed within the red circle, while non-cyclic electron transfer is depicted by the gray block arrow.

cytochrome c_2 then transfers its electron back to the reaction center where it reduces P_{870}. As a result of this cyclic electron transfer, there is no need for an exogenous electron donor or a terminal electron acceptor, and continuous synthesis of ATP is made possible.

R. sphaeroides is not a strict anaerobe. When the oxygen tension is high, *R. sphaeroides* can also undergo respiratory growth. Under these conditions, the photosynthetic apparatus is repressed, and there is an increase in the content of quinol oxidases. A very important feature and advantage of using *R. sphaeroides* is that the bc_1 complex is not essential for aerobic growth by the non-cyclic pathway. Under these conditions, the electrons can be transferred to oxygen by the aforementioned quinol oxidases. Under aerobic growth, the synthesis of bacteriochlorophyll is repressed, resulting in a brownish / pink cell-culture rather than the brownish-green color observed in photosynthetically-grown cells.

The use of *R. sphaeroides* as model system for our studies of the cytochrome bc_1 complex has several advantages.

1. Simplicity – The cytochrome bc_1 complex from *R. sphaeroides* contains only four subunits; the three core subunits and one supernumerary subunit. The three core subunits, i.e. cytochrome *b*, cytochrome c_1 and ISP are homologous to their mitochondrial counterparts.
2. Readily applied molecular engineering protocols – In eukaryotes, cytochrome *b* is encoded in the mitochondrion and is hence inconvenient for site-directed mutagenesis. In *R. sphaeroides*, the three catalytic core subunits are encoded by genes organized in an *fbc*FBC operon. This operon has been deleted from the chromosome in order to facilitate the mutagenic studies.

3. Mutant cytochrome bc_1 complexes incapable of supporting photosynthetic growth can still be purified and characterized. *R. sphaeroides* strains over-expressing the defective cytochrome bc_1 complexes can be grown in semi-aerobic conditions in the dark to induce extensive intra-cytoplasmic membrane (ICM) generation (42 - 44).

REFERENCES

1. Duncan, T.M., Bulygin, V. S., Zhou, Y., Hutcheon, M. L., and Cross, R. L. (1995) *Proc. Natl. Acad. Sci. U.S.A.*, **92**, 10964-10968
2. Noji, H., Yasuda, R., Yoshida, M., and Kinosita, K. Jr. (1997) *Nature* **386**, 299-302
3. Itoh, H., Takahashi, A., Adachi, K., Noji, H., Yasuda, R., Yoshida, M., and Kinosita, K. Jr. *Nature*, **427** (2004) 465-468
4. Pedersen, P. L., Ko, Y. H., and Hong. S. (2000) *J. Bioenerg. Biomembr*. **32**, 325-332
5. Peter Mitchell (1961) *Nature* **191**: 144–148
6. Trumpower, B. L., and Gennis, R. B. (1994) *Annu. Rev. Biochem.* **63**, 675-716
7. Ljungdahl, P. O., Pennoyer, J. D., Robertson, D. E., and Trumpower, B. L. (1987) *Biochim. Biophys. Acta.* **891**, 227-241
8. Yu, L., Tso, S. C., Shenoy, S. K., Quinn, B. N., and Xia, D. (1999) *J. Bioenerg. Biomembr.* **31**, 251-257
9. Trumpower, B. L. (1990) *J. Biol. Chem.* **265**, 11409-11412
10. Erecinska, M., Chance, B., Wilson, D. F., and Dutton, P. L. (1972) *Proc. Natl. Acad. Sci. U.S.A.* **69**, 50-54
11. Mitchell, P. (1976) *J. Theor. Biol.* **62**, 327-367
12. Brandt, U., and Trumpower, B. L. (1994) *Crit. Rev. Biochem. Mol. Biol.* **29**, 165-197
13. Crofts, A., and Wang, Z. (1989) *Photosynth. Res.* **22**, 69-87
14. Robertson, D. and Dutton, P. (1988) *Biochim. Biophys. Acta.* **726**, 149-186

15. de Vries, S., Albracht, S. P., Berden, J. A., and Slater, E. C. (1981) *J. Biol. Chem.* **256**, 11996-11998

16. Orii, Y., and Miki, T. (1997) *J. Biol. Chem.* **272**, 17594-17604

17. Brandt, U. (1998) *Biochim. Biophys. Acta* **1365**, 261-268

18. Link, T. A. (1997) *FEBS Lett.* **412**, 257-264

19. Junemann, S., Heathcote, P., and Rich, P. R. (1998) *J. Biol. Chem.* **273**, 21603-21607

20. Snyder, C. H., Gutierrez-Cirlos, E. B., and Trumpower, B. L., (2000) *J. Biol. Chem.* **275**, 13535-13541

21. Zhu, J., Egawa, T., Yeh, S. R., Yu, L., and Yu, C. A. (2007) *Proc. Natl. Acad. Sci. U.S.A.* **104**, 4864-4869

22. Xia, D., Yu, C. A., Kim, H., Xia, J. Z., Zhang, L., and Deisenhofer, J. (1997) *Science* **277,** 60-66

23. Iwata, S., Lee, J. W., Okada, K., Lee, J. K., Iwata, M., Rasmussen, B., Link, T. A., Ramaswamy, S., and Jap, B. K. (1998) *Science* **281**, 64-71

24. Zhang, Z., Huang, L., Shulmeister, V. M., Chi, Y. I., Kim, K. K., Hung, L. W., Crofts, A. R., Berry, E., A., and Kim, S. H. (1998) *Nature* **392**, 677-684

25. Hunte, C., Koepke, J., Lange, C., Rossmanith, T., and Michel, H. (2000) *Struct. Fold. Des.* **8,** 669-684

26. Kurisu, G., Zhang, H., Smith, J. L., and Cramer, W. A., (2003) *Science* **302**, 1009-1014

27. Stroebel, D., Choquet, Y., Popot, J. L., and Picot, D. (2003) *Nature* **426**, 413-418

28. Rieske, J. S., Zaugg, W. S., and Hansen, R. E. (1964) *J. Biol. Chem.* **239**, 3023-3030

29. Link, T. A., and Iwata, S. (1996) *Biochim. Biophys. Acta.* **1275,** 54-60

30. Ohnishi, T. H., Schagger, H., Meinhardt, S. W., Lobrutto, R., Link, T. A., and von Jagow, G. (1989) *J. Biol. Chem.* **264**, 735-744

31. Gong, X., Yu, L., Xia, D. and Yu C. A. (2005) *J. Biol. Chem*. **280**, 9251-9257

32. Geier, B. M., Haase, U. and von Jagow, G. (1993) *Biol. Soc. Trans*. **22**, 203-209

33. Link, T. A., Haase, U., Brandt, U. and von Jagow, G. (1993) *J. Bioenerg. Biomembr*. **25**, 221-232

34. von Jagow, G., and Link, T. A. (1986) *Methods Enzymol.* **126**, 253-271

35. Gao, X., Wen, X., Yu, C. -A., Esser, L., Tsao, S., Quinn, B., Zhang, L., Yu, L., and Xia, D. (2002) *Biochemistry*, **41**, 11692-11702

36. Gao, X., Wen, X., Esser, L., Yu, L., Yu, C. –A., and Xia, D. (2003) *Biochemistry*, **42**, 9067-9080

37. Kim. H., Xia, D., Yu, C. A., Xia, J. Z., Kachurin, A. M., Zhang, L., Yu, L., and Deisenhofer, J. (1998) *Proc. Natl. Acad. Sci. USA*, **95**, 8026-8033

38. Esser, L., Quinn, B., Li, Y. F., Zhang, M., Elberry, M., Yu, L., Yu, C. A., and Xia, D. (2004) *J. Mol. Biol.* **341**, 281-302

39. Crofts, A. R., Barquera, B., Gennis, R. B., Kuras, R., Guergova-Kuras, M., and Berry, E. A. (1999) *Biochemistry*, **38**, 15807-15826

40. Imhoff, J. F. (1992) in *Photosynthetic Prokaryotes* (Carr, N. H. M. a N. G., ed), pp 53-92, Plenum Press, New York

41. Clayton, R. K., and Sistrom, W. R. (1979) "The Photosynthetic Bacteria". Plenum, New York

42. Knaff, D. B., (1990) T*rends Biochem. Sci*. **15**, 289-291

43. Gennis, R. B., Barquera, B., Hacker, B., van Doren, S. R., Arnaud, S., Crofts, A. R., Davidson, E., Gray, K. A., and Daldal, F. (1993) *J. Bioenerg. Biomembr.* **25**, 195-209

44. Thöny-Meyer, L. (1997) *Microbiol. Mol. Biol. Rev.* **61**, 337-376

Chapter II

The Iron Sulfur Cluster of the Rieske Iron Sulfur Protein Functions as a Proton-exiting Gate in the Cytochrome bc_1 Complex

Buddha Gurung, Linda Yu, Xia Di, and Chang-an Yu

The Journal of Biological Chemistry (2005) **280**, 24897-24902

ABSTRACT

Destruction of the Rieske iron-sulfur cluster ([2Fe-2S]) in the bc_1 complex by hematoporphyrin-promoted photo-inactivation results in the complex becoming proton-permeable (Miki, T., Yu, L., and Yu, C, -A. (1991) *Biochemistry* **30**, 230-238). To further study the role of this [2Fe-2S] cluster in proton translocation of the bc_1 complex, *Rhodobacter sphaeroides* mutants expressing His-tagged cytochrome bc_1 complexes with mutations at the histidine ligands of the [2Fe-2S] cluster were generated and characterized. These mutants lack the [2Fe-2S] cluster and possess no bc_1 activity. When the mutant complex is co-inlaid in phospholipid vesicles with intact bovine mitochondrial bc_1 complex or cytochrome *c* oxidase, the proton ejection, normally observed in intact reductase or oxidase vesicles during the oxidation of their corresponding substrates, disappears. This indicates the creation of a proton-leaking channel in the mutant complex, whose [2Fe-2S] cluster is lacking. Insertion of bc_1 complex lacking the head domain of ISP, removed by thermolysin digestion, into PL vesicles together with mitochondrial bc_1 complex also renders the vesicles proton-permeable. Addition of excess purified head domain of ISP partially restores proton-pumping activity. These results indicate that elimination of the [2Fe-2S] cluster in mutant bc_1 complexes opens up an otherwise closed proton-channel within the bc_1 complex. It is speculated that in the normal catalytic cycle of the bc_1 complex, the [2Fe-2S] cluster may function as a proton-exiting gate.

INTRODUCTION

The cytochrome bc_1 complex, also known as ubiquinol-cytochrome *c* reductase or Complex III is the central segment of the energy conserving, electron transfer chain of mitochondria and many respiratory and photosynthetic bacteria (1). This enzyme complex catalyzes electron transfer from ubiquinol to cytochrome *c* (c_2 in bacteria) with concomitant translocation of protons across the membrane to generate a proton electrochemical gradient required for ATP synthesis by ATP synthase. The cytochrome bc_1 complexes from all species contain three core subunits, cytochrome *b*, cytochrome c_1 and Rieske Iron-Sulfur protein (ISP), that house two *b* type cytochromes (b_{566} and b_{562}), one *c*-type cytochrome (c_1) and a high potential Rieske [2Fe-2S] cluster respectively. However, the number of non-redox group containing subunits, also called supernumerary subunits, in the complex varies from species to species.

Recently the 3-D crystal structures of mitochondrial bc_1 complexes from bovine (2, 3), chicken (4) and yeast (5), which contain seven to eight supernumerary subunits in addition to the three core subunits, have been obtained. The structures of the cytochrome b_6f complex, a complex analogous to the cytochrome bc_1 complex that provides an electronic connection between photosystems I and II, have also been established for the thermophilic cyanobacterium *Mastigocladus laminosus* (6), and in the algae, *Chlamydomonas reinhardtii* (7), respectively. The 3-D structural information for the mitochondrial bc_1 complex establishes the location of the redox centers, the number of transmembrane helices, quinone binding at the Q_N site, and inhibitor binding at both the Q_P and Q_N sites (2-4, 8, 9). Moreover, it suggests mobility of the extrinsic head domain

of ISP during bc_1 catalysis. Strong evidence in support of this movement has been reported (10-19).

The proton-motive Q-cycle model (20, 21) has been favored for describing electron and proton translocation in the cytochrome bc_1 complex. The key feature of this model is the presence of two separate ubiquinol/ubiquinone binding sites; a ubiquinol oxidation site (Q_P) near the P (inter-membranes space) side of the mitochondrial inner membrane, and a ubiquinone reduction site (Q_N) near the N (matrix) side. Due to a lack of information on the binding of ubiquinol at the putative Q_P site from the 3-D structures, the detailed bifurcation of ubiquinol oxidation, the key step in the Q-cycle mechanism is difficult to establish. Several models of the bifurcated oxidation of ubiquinol at the Q_P site have been proposed (22-28).

It has been established that for every electron transferred through the bc_1 complex two protons are translocated across the membrane. This 2 H^+/e^- stoichiometry has been verified in a wide variety of species, *in vitro,* by studying bc_1 complexes in phospholipid (PL) vesicles. Proton-pumping by bc_1 complex inlaid PL vesicles requires an intact membrane which prevents non-specific proton leakage. Any compromise of membrane integrity results in loss of the proton electrochemical gradient, as is observed when an uncoupler like carbonyl cyanide *m* - chlorophenylhydrazone (CCCP) is added to either intact mitochondria or PL vesicles harboring electron transfer complexes. The integrity of the membrane is maintained by its protein and lipid components.

Although the proton translocation pathway in the cytochrome bc_1 complex is not fully understood, the involvement of the [2Fe-2S] cluster of ISP has been suggested. When bovine mitochondrial bc_1 complex is illuminated with a projector light in the

presence of hematoporphyrin under aerobic conditions, the complex becomes inactivated as the [2Fe-2S] cluster in the treated complex is destroyed (29). When photo-inactivated bc_1 complex is co-inlaid in PL vesicles with intact bovine bc_1 complex, no proton ejection is detected during ubiquinol oxidation. These findings suggest that a proton-permeable channel is created in the photo-inactivated complex. However, since the hematoporphyrin promoted photo-inactivation site in the bc_1 complex is not specific, the formation of a proton-leaking channel in the photo-inactivated complex may result from the oxidation of key amino acid residues in the bc_1 complex, rather than from destruction of the [2Fe-2S] cluster alone. Therefore, in order to unambiguously establish the involvement of the [2Fe-2S] cluster in the proton transfer pathway, a bc_1 complex either lacking the cluster, or possessing a damaged one, is necessary. We think that such a bc_1 complex can be obtained by site-directed mutagenesis of histidine residues H131 and H152 of the ISP, that serve as ligands to the [2Fe-2S] cluster.

Herein, we report the generation and characterization of *R. sphaeroides* strains expressing cytochrome bc_1 complexes with substitutions at one or both the histidine ligands of the [2Fe-2S] cluster. The proton-pumping activities of the protein-PL vesicles containing intact bovine mitochondrial bc_1 complex, or cytochrome *c* oxidase, and the mutant complex were determined, and compared to those of protein-PL vesicles containing intact mitochondrial bc_1 complex or cytochrome *c* oxidase and wild-type bacterial bc_1 complex. Restoration of proton-pumping activity was explored by adding excess amounts of ISP head domain containing the [2Fe-2S] cluster to proton-leaking PL vesicles embedding mitochondrial bc_1 complex and thermolysin digested bacterial bc_1 complex.

EXPERIMENTAL PROCEDURES

Materials - Cytochrome *c* (horse heart, Type-III), carbonyl cyanide *m*-chlorophenylhydrazone, and thermolysin were from Sigma. Azolectin was obtained from Associate Concentrate and purified according to the method of Racker and Kagawa (30). n-Dodecyl-β-D-Maltoside and n-Dodecyl-β-D-Glucoside were from Anatrace. Ni-NTA gel and Qiaprep Spin Miniprep kit were from Qiagen. 2, 3-Dimethoxy-5-methyl-6-bromodecyl-1, 4-benzoquinol ($Q_0C_{10}BrH_2$) was prepared in our laboratory as previously reported (11). All other chemicals were of the highest purity commercially available.

Generation of R. sphaeroides Strains Expressing the His_6-tagged bc_1 Complexes with Mutation at the Histidine Ligand of the [2Fe-2S] cluster of ISP - Mutations were constructed with the Quik Change™ site-directed-mutagenesis kit from Sratagene using a supercoiled double-stranded pGEM7Zf(+)-*fbc*FB as template, and a forward and reverse primer for PCR amplification. The pGEM7Zf(+)-*fbc*FB plasmid (31) was constructed by ligating the *Eco*RI - *Xba*I fragment from pSELNB3503 into the *Eco*RI and *Xba*I sites of the pGEM7Zf(+) plasmid. The primers used were;

H131C (F): GCGTCTGCACCTGCCTCGGCTGCGTGC

H131C(R): GCACGCAGCCGAGGCAGGTGCAGACGC

H152C (F): GTTCTGCCCCTGCTGCGGATCGCACTACG

H152C (R): CGTAGTGCGATCCGCAGCAGGGGCAGAAC

F and R in parenthesis denote forward and reverse primers respectively. The *Eco*RI - *Xba*I fragment from the pGEM7Zf(+)-*fbc*F_mB plasmid was ligated into the pRKD418-*fbc*$FB_{Km}C_HQ$ plasmid to generate the pRKD418-*fbc*F_mBC_HQ plasmid. A plate-mating

procedure was used to mobilize the pRKD418-*fbc*F_mBC_HQ plasmid from *Escherichia coli* S17-1 cells into *R. sphaeroides* BC-17 cells, as previously described (32). The presence of the engineered mutations was confirmed by DNA sequencing, before and after semi-aerobic growth of the cells. The expression plasmid, pRKD*fbc*F_mBC_HQ, was purified from an aliquot of semi-aerobically grown culture using the Qiagen Plasmid Mini Prep kit. Since *R. sphaeroides* cells contain four types of endogenous plasmids, the isolated plasmids lack the purity and concentration needed for direct sequencing. Therefore, a 2-kilobase pair DNA segment containing the mutation sequence was amplified from the isolated plasmids by polymerase chain reaction (PCR), and sequenced. DNA sequencing and oligonucleotide syntheses were carried out at the Recombinant DNA / Protein Core Facility at Oklahoma State University.

Growth of bacteria - *Escherichia coli* cells were grown at 37^oC in LB medium. For semi-aerobic growth of the plasmid-bearing *R. sphaeroides* BC-17 cells, an enriched Sistrom's medium (33) supplemented with twenty amino acids, and extra-rich vitamins were used. Cells harboring the mutated *fbc* genes on the pRKD*fbc*F_mBC_HQ plasmid were grown semi-aerobically for only one or two serial passages, in order to minimize any pressure for reversion. The semi-aerobic cultures were grown in 800 ml of enriched Sistrom's medium in 2 L Bellco flasks with vigorous shaking (150 rpm) for about 26 hours at 30 ^oC in the dark. The inoculation volumes used for semi-aerobic growth were at least 5 % of the total volume. Antibiotics were added to the following concentrations: ampicillin (125 μg/ml), kanamycin sulfate (30 μg/ml for *E. coli* and 20 μg/ml for *R. sphaeroides*), tetracycline (10 μg/ml for *E. coli* and 1 μg/ml for *R. sphaeroides*), and trimethoprim (100 μg/ml for *E. coli* and 30 μg/ml for *R. sphaeroides*).

Enzyme Preparations and Activity Assay - Chromatophores and intra-cytoplasmic membranes (ICM's) were prepared as described previously (10), and stored at –80 ^{o}C in the presence of 20 % glycerol. The His_6-tagged cytochrome *b*c$_1$ complexes were purified from frozen ICM's or chromatophores by the method of Tian *et al.* (10). Purified cytochrome *bc*$_1$ complexes were stored at –80 ˚C in the presence of 10% glycerol. To assay ubiquinol-cytochrome *c* reductase activity, membrane preparations or purified cytochrome *bc*$_1$ complexes were diluted with 50 mM Tris-Cl, pH 8.0 containing 200 mM NaCl and 0.01% n-dodecyl-β-D-maltopyranoside (DM) to a final cytochrome *b* concentration of 1 μM. 5 μl of the diluted samples were added to 1 ml of assay mixture containing 100 mM of sodium phosphate buffer (pH 7.4), 0.3 mM EDTA, 50 μM ferricytochrome *c*, and 25 μM $Q_0C_{10}BrH_2$. Activities were determined by measuring the reduction of cytochrome *c*, by following the increase in the absorbance at 550 nm, in a Shimadzu UV-2101 PC spectrophotometer at 23 ˚C using a millimolar extinction coefficient of 18.5 $mM^{-1}cm^{-1}$ for calculations. The non-enzymatic oxidation of $Q_0C_{10}BrH_2$, determined under similar conditions in the absence of the enzyme, was subtracted during calculations for the specific activity. Potassium cyanide was added to a final concentration of 30 μM in the assay mixture, to inhibit cytochrome *c* oxidase (C*c*O) when determining the *bc*$_1$ activity in ICM's or chromatophores.

Preparation of Electron-Transfer Complex Inlaid PL Vesicles - Protein-PL vesicles were prepared by the cholate dialysis method of Racker and Kagawa (30). Bovine heart ubiquinol-cytochrome *c* reductase or C*c*O, either singly, or in combination with *R. sphaeroides* wild-type or mutant *b*c$_1$ complex, was mixed with 1 ml of asolectin micellar solution to give an asolectin (mg) / protein (mg) ratio of 40. The asolectin

micellar solution was prepared by sonicating 200 mg of acetone-washed asolectin in 4 ml of 50 mM sodium phosphate buffer, pH 7.4, containing 2 % sodium cholate and 100 mM KCl (for use in preparation of bc_1 complex-PL vesicles), and in 4 ml of 100 mM Hepes-KOH, pH 7.3, containing 10 mM KCl and 2 % sodium cholate (for use in preparation of C*c*O-PL vesicles), in an ice-water bath. Sonication was performed in an anaerobic environment by continually passing argon into the vessel.

The bc_1 complex-PL mixtures were incubated at 0˚C for 30 minutes before overnight dialysis at 4 °C against 100 volumes of 50 mM sodium phosphate buffer, pH 7.4 containing 100 mM KCl with three changes of buffer. The mixture was then dialyzed against 100 volumes of 150 mM KCl for 3 to 4 hours. The C*c*O-PL mixture was dialyzed against 100 mM Hepes-KOH, pH 7.3, containing 10 mM KCl for 4 hours followed by 10 mM Hepes-KOH, pH 7.3, containing 50 mM KCl and 50 mM sucrose with one change of buffer for 12 hours each. Subsequently, the vesicles were dialyzed against two changes of 50 µM Hepes-KOH buffer, pH 7.3, containing 55 mM KCl and 55 mM sucrose, for 12 hours and 4 hours (34).

Determination of Proton Translocating Activity of bc_1 complex-PL Vesicles - Proton translocation coupled to electron flow through the bc_1 complex-PL vesicles was measured at room temperature using an Accumet Model 10 pH meter and a Model 13-620-96 combination pH electrode. Twenty-five nmoles of $Q_0C_{10}BrH_2$ was added to 1.6 ml reaction mixture containing 150 mM KCl, 4 µM ferricytochrome *c*, 1 µM valinomycin, and an appropriate amount of bc_1-PL vesicles (30 to 50 µl). Electron flow was initiated by the addition of 5 nmoles of ferricyanide, which oxidizes the cytochrome *c*, and thus provides an electron acceptor for the complex. Electron flow under

conditions where no transmembrane ΔpH formed was measured in an identical manner except that the protonophore, CCCP, was present at a concentration of 2 μM to make the vesicles permeable to protons. Proton-pumping (H^+/e^-) was calculated as the ratio of the decrease in pH upon ferricyanide addition to bc_1-PL vesicles before and after treatment with CCCP.

Determination of Proton Pumping Activity of CcO-PL vesicles - Proton-pumping experiments involving C*c*O-PL vesicles were conducted at 23°C in a stopped-flow spectrophotometer from Applied Photophysics, SX.18MV. Reaction vessel A contains 2 μM C*c*O-PL vesicles, 110 μM phenol red, 2 μM valinomycin in 50 μM Hepes-KOH, pH 7.3, and 55 mM KCl. Reaction vessel B contains 30 μM horse heart ferrocytochrome *c* in the same buffer (34). Electron flow was initiated by mixing equal volumes of the reaction components in vessels A and B. Proton pumping was measured by monitoring the absorbance changes of phenol red at 556.6 nm. At this wavelength, the absorption change due to cytochrome *c* is minimal as it is the isobestic point for cytochrome *c*. Since the pH of the components of vessels A and B were the same, no non-specific absorbance changes should be observed.

Preparation of the head domain of ISP (ISF) from R. sphaeroides bc_1 complex – The method used for the preparation of ISF from mitochondrial bc_1 complex (35) was adapted to prepare the ISF from wild-type *R. sphaeroides* bc_1 complex. Two μM wild-type *R. sphaeroides* bc_1 complex was suspended in 50 mM Tris-Cl, pH 8, containing 5 mM $CaCl_2$ and 100 mM NaCl. 0.2 μM thermolysin was added, and the reaction mixture was incubated at room temperature for three hours. Thermolysin digestion of the bc_1 complex was stopped by the addition of 10 mM EDTA. The EDTA containing reaction

mixture was dialyzed overnight against 10 mM NaCl, 10 mM EDTA, and 10 mM phosphate buffer pH 7.2 with one change of buffer. The dialyzed sample was centrifuged at 150,000 x *g* for 3 hours. The precipitate was discarded and the supernatant was applied to a calcium phosphate: cellulose column (36) equilibrated with 150 mM NaCl, and 10 mM phosphate buffer, pH 7.2. Calcium phosphate was prepared according to Jenner (37) and mixed at a 3:1 ratio with cellulose powder, prior to use in column chromatography, for enhancement of the flow rate. The ISF did not bind to the column under these conditions and was recovered in the column effluent, which was then concentrated to about 0.5 mg/ml using Centriprep YM-3 from Amicon. The concentrated ISF was applied to a Mono-Q column (from Amersham Pharmacia) equilibrated with 20 mM MOPS, pH 6.2, containing 20 mM NaCl. Thermolysin was not absorbed by the column and therefore removed in the effluent. The ISF-absorbed column was subjected to a stepwise NaCl gradient wash; and ISF was eluted at 100 mM NaCl. The complete removal of thermolysin in the ISF containing fractions was assured by the absence of protease activity, assayed using casein as substrate.

Other Biochemical and Biophysical Techniques - Protein concentration was determined by the method of Lowry *et al*. (38). Cytochrome *b* (39) and cytochrome c_1 (40) concentrations were determined according to published methods. SDS-polyacrylamide gel electrophoresis (SDS-PAGE) was performed according to Laemelli (41) using a Bio-Rad Mini-protean dual slab vertical cell. The polypeptides separated in the SDS-PAGE gel were transferred electrophoretically to a 22 micron nitrocellulose membrane for Western blotting. Polyclonal antibodies generated against ISP of the *R. sphaeroides* bc_1 complex were used as the primary antibody to detect their respective

antigens (10). Protein A conjugated to horseradish peroxidase, from Biorad, was used as the second antibody. The [2Fe-2S] cluster of ISP was determined by EPR, using a Bruker EMX spectrometer equipped with an Air Products flow cryostat, and by circular dichroism (42, 43), using a Jasco J-715 spectropolarimeter. Instrument settings are detailed in the legends of the relevant figures.

RESULTS AND DISCUSSION

Characterizations of Mutants Carrying Mutations at the Histidine Ligands of [2Fe-2S] cluster in ISP - Four *R. sphaeroides* mutants expressing His_6-tagged bc_1 complexes with mutations at the histidine ligands of [2Fe-2S] cluster were generated for this study. They are: three single mutants, H131N, H152N, and H131C and a double mutant, H131C-H151C. For mutants to be useful for this study, the resulting mutant complexes must lack the [2Fe-2S] cluster but have protein and redox components similar to those in the wild-type complex.

When mid-log phase, aerobically dark grown wild-type and mutant cells were inoculated into enriched Sistrom's medium and subjected to anaerobic photosynthetic growth conditions, all four mutants did not grow. However, these mutants grew aerobically and semi-aerobically at rates comparable with that of wild-type cells. These results indicate that the four mutants have a defective cytochrome bc_1 complex, since this complex is absolutely required for photosynthetic growth of this bacterium (See Fig. 7). When ICM's were prepared from semi-aerobically grown mutant cells and assayed for ubiquinol-cytochrome *c* reductase activity, none was detected in the four mutant membranes. Absorption spectral analysis reveals that the content and absorption spectral

properties of cytochrome *b* and cytochromes (c_1+c_2) in all these mutant membranes are similar to those in the complement chromatophores or ICM (See Table 3), indicating that the mutation does not affect the assembly of cytochrome *b* and c_1 into the membrane. EPR analysis reveals that these four mutant membranes contain no [2Fe-2S] cluster of ISP, indicating that the mutation results in an inability of the [2Fe-2S] cluster to be ligated to apo-ISP, thereby leading to loss of bc_1 activity. Western blot analysis using antibodies against *R. sphaeroides* ISP shows that H131N, H152N, H131C, and H131C-H151C mutant ICM's have 9, 58, 64, and 98 % of the apo-ISP in the wild-type chromatophores respectively as determined by densitometer scan analysis (See Table 3). Apparently, the stability of apo-ISP is affected by the type of amino acid substituting for the histidine ligand, and whether the alteration is at H131 or H152. The finding, that the H152N mutant ICM has more apo-ISP than does the H131N mutant membrane, is similar to observations in yeast mutants of H161R and H181R (44). However, it differs from reports on mutation at histidine ligands of [2Fe-2S] cluster in *R. capsulatus,* in which less than 3 % of the apo-ISP is found in the mutant membranes (45).

When the His_6-tagged bc_1 complexes were purified from the ICM of the four mutants, none of them had bc_1 activity or the [2Fe-2S] cluster of ISP. As shown in Fig. 8, EPR signals at g = 2.03, 1.90 and 1.80, characteristics of the [2Fe-2S] cluster of ISP, are observed only in the purified wild-type complex. Similarly, a negative CD peak around 500 nm, a characteristic of the [2Fe-2S] cluster of ISP, is observed only in the purified wild-type complex. Therefore, EPR and CD analysis of the mutant complexes clearly indicates the loss of the [2Fe-2S] cluster.

Table 3

Characterizations of mutants lacking the Rieske [2Fe-2S] cluster

Strains	Cytochrome bc_1 complex			
	Membrane		Purified complex	
	Cyt b/(cyt c_1+c_2)	ISP content[a]	Cyt b/(cyt c_1)	ISP content[a]
Complement	1.20	1.00	1.31	1.00
H131N	1.16	0.09	0.46	0.00
H152N	1.20	0.58	0.50	0.40
H131C	1.21	0.64	0.80	0.55
H131C/H152C	1.20	0.98	1.10	0.82

[a] ISP content was quantified using a Biorad GS-700 Imaging Densitometer. It is expressed as a fraction of the amount present in the complement wild type. complex.

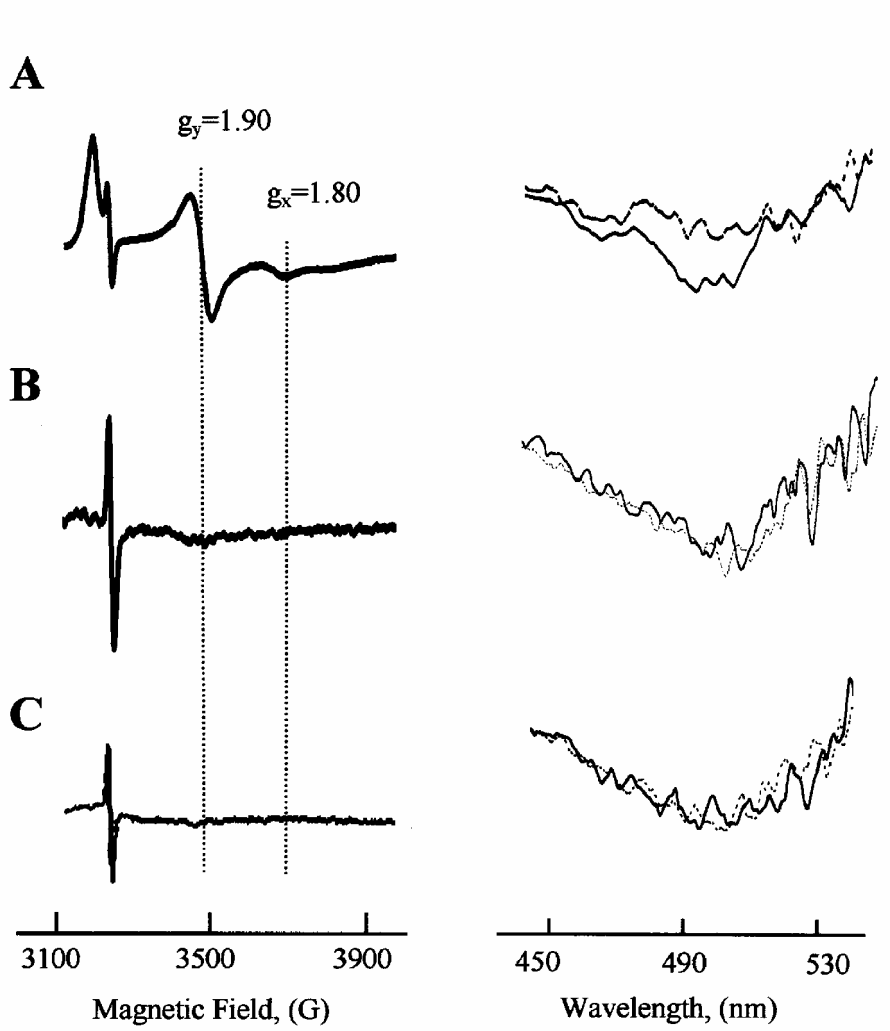

Figure 8. **EPR and CD characterization of the [2Fe-2S] cluster in the cytochrome bc_1 of complement and mutant complexes.** EPR spectra of purified bc_1 complexes of wild-type (A), H131C (B) and H131C-H152C (C) are shown in the left hand panel. The bc_1 complexes were incubated with 1.5 mM ascorbate on ice for 30 minutes and frozen in liquid nitrogen. EPR spectra were recorded at 8 K with the following instrument settings: microwave frequency, 9.3 GHz; modulation frequency, 100 kHz; modulation amplitude, 6.3 G; time constant, 655.4 ms; and sweep time, 167.8 s. CD spectra for purified bc_1 complexes of complement (A), H131C (B) and H131C-H152C (C) are shown in the right hand panel. The bc_1 complexes were diluted to a final concentration of 5.5 μM in 50 mM Tris-HCl, pH 7.5, 100 mM NaCl and 0.01 % DM. The experimental conditions were: band width, 1.0 nm; step resolution, 1.0 nm; cell length, 1 cm; and scan speed, 50 nm/min. Each trace represents an average of four data sets. Reduced (solid lines), and oxidized (dotted lines) bc_1 complexes were prepared by the addition of ascorbate and ferricyanide, respectively.

The b/c_1 ratios in the complement and mutants H131N, H152N, H131C, H131C-H152C, determined by absorption spectra (see Fig. 9 and Table 3), are 1.31, 0.46, 0.50, 0.80 and 1.10 respectively, indicating that the binding affinity between cytochrome *b* and cytochrome c_1 is affected by the nature and position of the substituting amino acids. A decrease in the b/c_1 ratio indicates a decrease in binding affinity between the two cytochromes. Since the expressed *R. sphaeroides* bc_1 complex is His_6 tagged at the C-terminus of cytochrome c_1, all cytochrome c_1 from the dodecylmaltoside solubilized membrane, regardless of whether or not it is associated with cytochrome *b*, will be absorbed to the Ni-NTA column used in the one-step purification of the complex. The cytochrome *b* which is not tightly associated with cytochrome c_1 will appear in the effluent. Consequently the eluted complex would have a lower b/c_1 ratio as compared to the wild-type complex. The possibility that the lower cytochrome b/c_1 ratio observed in the mutant complexes results from a difference in the effectiveness of DM solubilization of the mutant complex from the membrane has been ruled out. DM solubilization of the bc_1 complexes from the mutant membranes was comparable to that of the complement (wild-type) chromatophores. It should be mentioned that EPR signals for both b_L (g =3.76) and b_H (g =3.49) are detected in the H131N mutant complex, indicating that this mutation does not affect the heme environments of cytochrome *b,* despite the loss of more than 65 % of the cytochrome *b* from the DM-solubilized membrane during purification by an Ni-NTA column. The EPR signals for b_L and b_H are observed in all of the [2Fe-2S] cluster lacking mutants (Fig. 10).

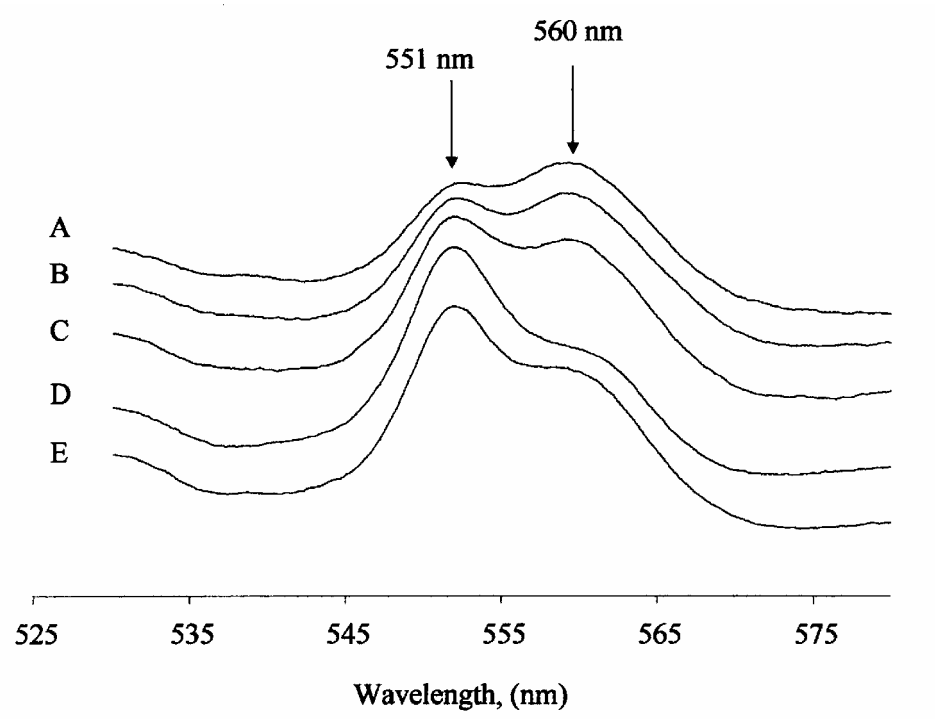

Figure 9. Absorption spectra of purified bc_1 complexes of the complement wild-type, and mutants lacking the [2Fe-2S] cluster. Purified protein complexes from wild type (A), H131C-H152C (B), H131C (C), H131N (D), and H152N (E) were diluted in 50 mM Tris-Cl, pH 8, containing 200 mM NaCl and 0.01 % DM. A few granules of dithionite were added to reduce cytochrome *b*. Each optical spectrum is a calculated difference spectrum of the dithionite-reduced minus ferricyanide-oxidized cytochromes (Abs_{max} = 551 nm for cytochrome c_1, and Abs_{max} = 560 nm for cytochrome *b*).

Table 4

Proton-pumping ratios (H^+/e^-) for PL vesicles harboring mitochondrial bc_1 and bacterial bc_1 complexes.

Vesicle Type	(H^+/e^-)[a]
mitochondrial bc_1 (m-bc_1)	1.9
wild type *R. sphaeroides* bc_1	1.5
m-bc_1 + wild type	1.7
m-bc_1 + H131C-H152C	1.0
m-bc_1 + (thermolysin digested bacterial bc_1)	1.0
m-bc_1 + (thermolysin digested bacterial bc_1 + ISF)[b]	1.3

[a] H^+/e^- is defined under 'Experimental Procedures.' For the experimental conditions, see legend to Fig. 14.

[b] ISF, Rieske Iron-Sulfur Fragment

Fig. 11 shows Western blot analysis of ISP in the complement and mutant complexes. Although the purified H131N mutant complex contains no detectable apo-ISP or subunit IV, purified mutant complexes of H152N, H131C, and H131C-H152C have 40, 55, and 82 % respectively, of the amount of apo-ISP or subunit IV found in the complement complex. When the latter three mutant complexes are subjected to SDS-PAGE analysis, four major protein bands corresponding to cytochrome *b*, cytochrome c_1, ISP and Subunit IV are observed, as in the complement wild-type complex (see Fig. 11). Thus a significant amount of ISP, 40 - 82 %, is still present in the [2Fe-2S] cluster lacking mutant complexes but not in H131N. It has been reported that a yeast mutant strain whose [2Fe-2S] cluster is lacking has about 83 % of the ISP, relative to cytochrome c_1, in the purified complex, when compared to its wild-type counterpart (46).

Clearly, the assembly of the bc_1 complex depends critically on the structural integrity of the head domain of ISP, particularly at the tip of ISP where interaction between ISP and cyt. *b* takes place. A unique feature of the ISP head domain structure is the tip area where the [2Fe-2S] cluster is located; the surface topology of the tip is strikingly smooth with only main chain atoms facing the solvent environment. Substitutions of H131C and H152C by molecular modeling using the bovine ISP structure as a template demonstrated (Fig. 12) the formation of two possible disulfide bonds, between C141 and C161 for one pair, and between C139 and C158 for the other, in the absence of the [2Fe-2S] cluster. Together with the disulfide pair in the native structure between C144 and C160, the three pairs of disulfide-bridge in the mutant would stabilize the structure of ISP at the tip region and perhaps more importantly maintain the smooth surface topology of the wild-type ISP, whereas any of the other single amino acid

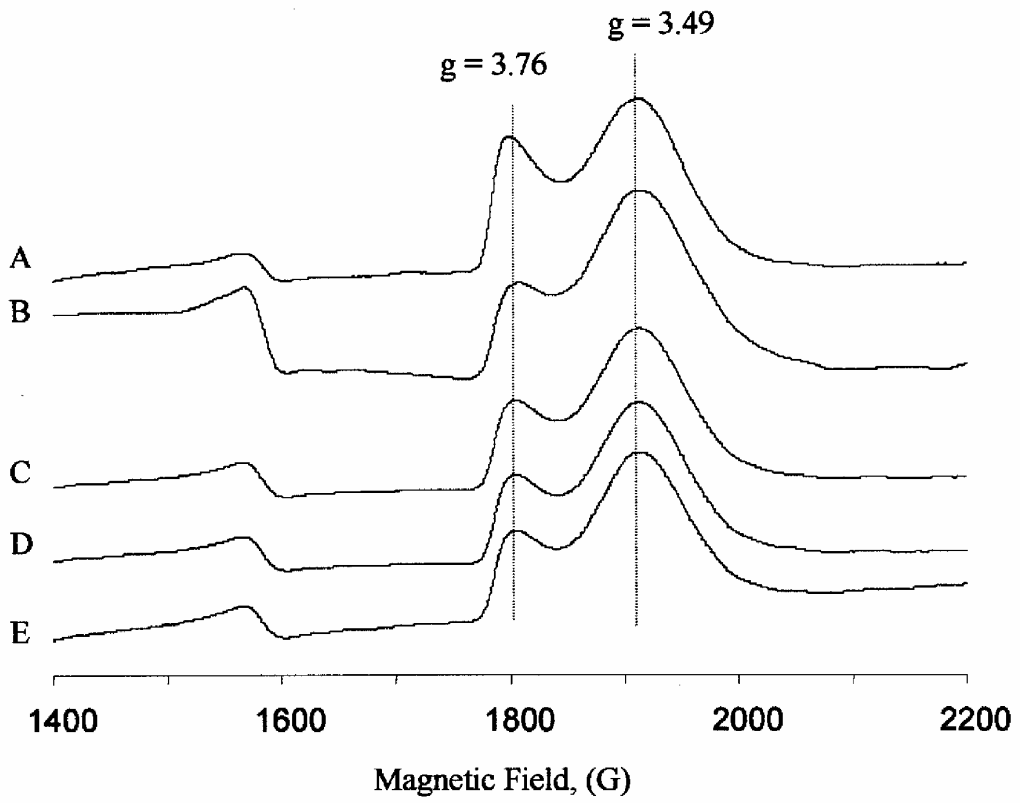

Figure 10. EPR spectra of cytochromes *b* in the cytochrome bc_1 complexes of complement wild type and the [2Fe-2S] cluster lacking mutants. Purified cytochrome bc_1 complexes from wild type (A), H131N (B), H152N (C), H131C (D), and H131C-H152C (E) was diluted in 50 mM Tris-Cl, pH 8, containing 200 mM NaCl and 0.01 % DM. Instrument settings were the same as in Fig. 8, except that the microwave power used was 108.1 mW, and the modulation amplitude was 20 G.

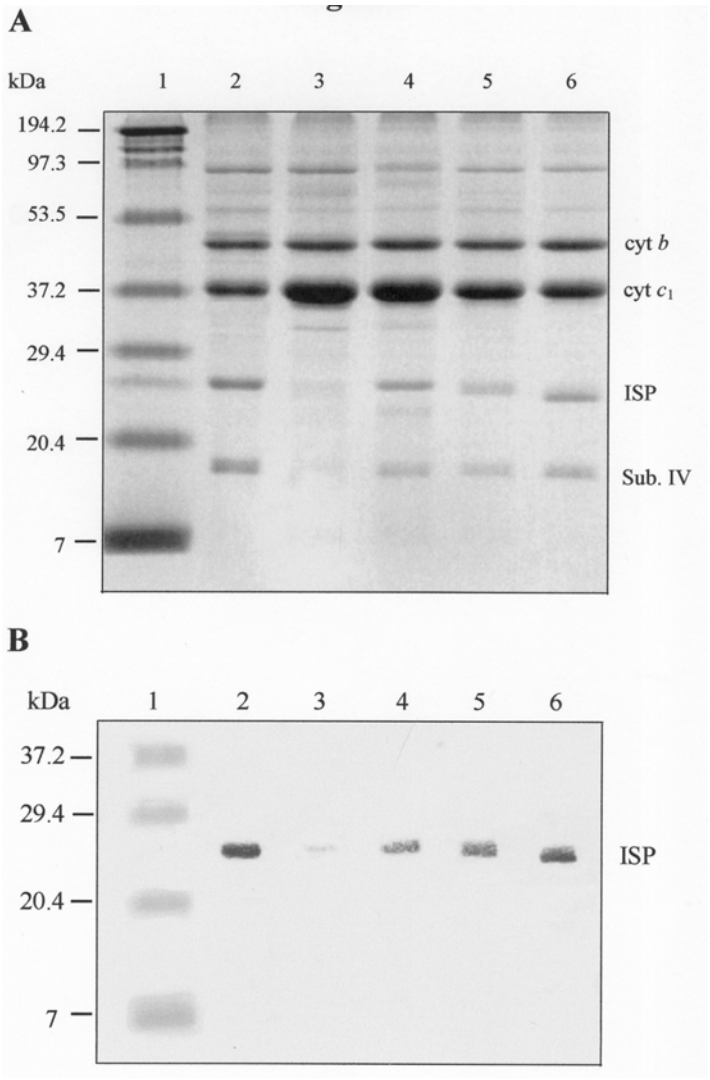

Figure 11. SDS-PAGE and Western Blot analysis of purified cytochrome bc_1 complexes of complement wild-type and [2Fe-2S] cluster lacking mutants. Aliquots of wild-type, and the mutant purified complexes were incubated with 1 % SDS and 0.4 % β-mercaptoethanol at room temperature for 30 minutes. Digested samples containing 100 pmoles of cytochrome *b* were subjected to electrophoresis (panel A). *Lane 1*, pre-stained molecular weight standard; *Lane 2*, wild-type; *Lane 3*, H131N; *Lane 4,* H152N; *Lane 5*, H131C; *Lane 6*, H131C-H152C. The proteins in the gel were transferred electrophoretically to a 22 micron nitrocellulose membrane, and reacted with antibodies against *R. sphaeroides* ISP. The horseradish peroxidase system was used to develop the membrane (panel B). Lane designations are the same as above.

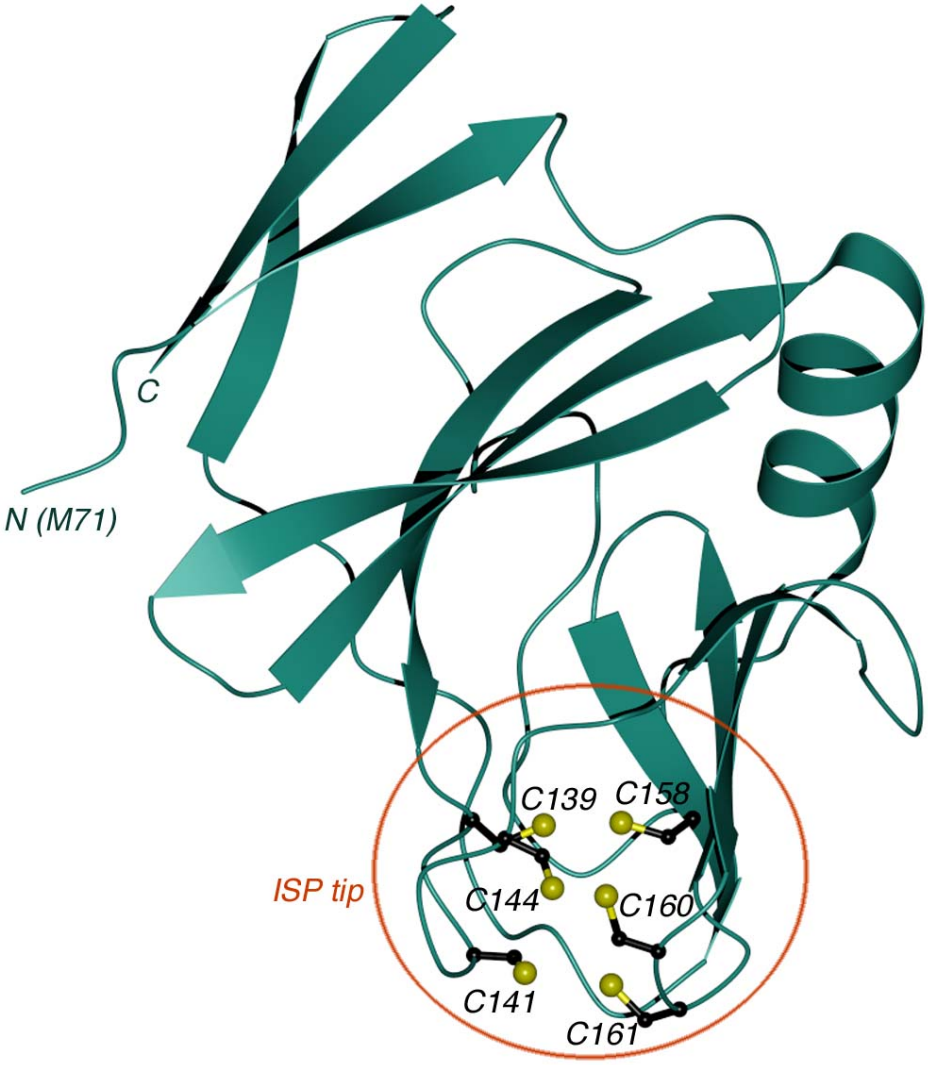

Figure 12. Ribbon representation for the structural model of the mutant lacking the Rieske [2Fe-2S] cluster. The model is represented with the bovine iron sulfur protein (ISP) structure, and the double mutation in ISP of *R. sphaeroides* bc_1 corresponds to H141C / H161C of the bovine sequence. The tip area of the ISP is highlighted with a red circle. The three pairs of disulfide bonds are depicted with the ball-and-stick model with carbon atoms in black and sulfur atom in yellow, and are as labeled.

substitutions would inevitably destroy to a different extent this important feature. The H131N and H152N mutations are particularly unfavorable due to exposed large side chains.

Among the four [2Fe-2S] cluster lacking mutant bc_1 complexes, H131C and H131C-152C are suitable for probing the function of the [2Fe-2S] cluster in proton translocation, because they differ from the wild-type complex only in the lack of the [2Fe-2S] cluster. The content of subunits and spectral properties of cytochromes *b* & c_1 in these two mutant complexes are similar to those in the complement complex. Moreover, the amount of ISP in the purified complexes is over 50 % compared to the complement (wild type) complex. Therefore, any changes in proton translocation activity detected in these two mutant complexes can be unambiguously attributed to the lack of [2Fe-2S] cluster.

Proton Translocation Activity of Intact Mitochondrial bc_1 Complex Co-inlaid in PL Vesicles with Wild-Type and H131C / H152C Mutant of R. sphaeroides complexes - An important property of the cytochrome bc_1 complex is the ability to pump protons across the membrane during electron flow from ubiquinol to cytochrome *c*. This property has been well demonstrated in PL vesicles embedding purified mitochondrial bc_1 complex (47-50). A simplified, cartoon representation of proton translocation coupled to electron transfer by a cytochrome bc_1 complex embedded in a PL vesicle is shown in Fig. 13. Fig. 14-A shows a typical proton translocation activity assay for PL vesicles embedding bovine bc_1 complex. After pH equilibrium is reached for a mixture containing $Q_0C_{10}BrH_2$, valinomycin, ferricytochrome *c*, and bovine bc_1 complex-PL vesicles, an aliquot of ferricyanide solution (addition 1) is added to initiate electron

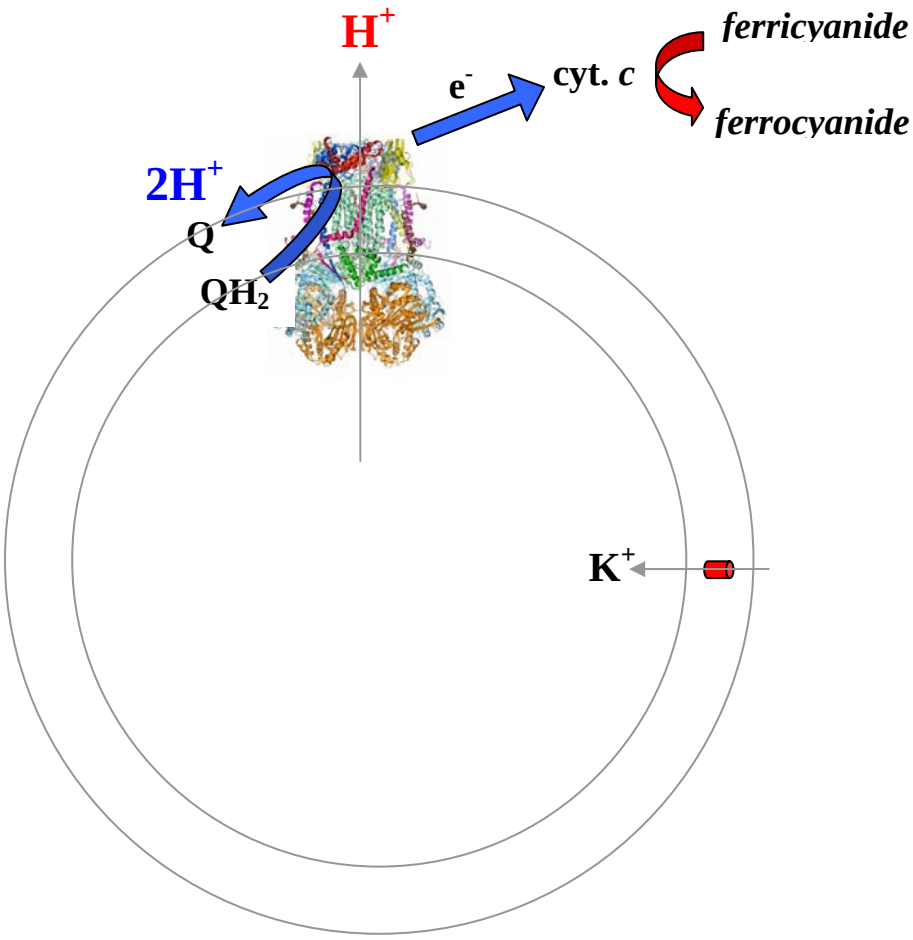

Figure 13. Cartoon depiction and scheme of proton translocation in phospholipids (PL) vesicles embedded with active bc_1 complexes. Protein embedded PL vesicles were generated as described in "Experimental Procedures". The reaction was started by adding ferricyanide, which oxidizes cytochrome *c* triggering electron flow from QH_2 to cytochrome *c* via the PL-embedded bc_1 complex. Scalar protons released by direct oxidation of QH2 (blue), and vectorially translocated protons (red) are shown. Proton pumping, from inside the vesicle to the outside, was measured as a function of the decrease in pH of the reaction mixture, i.e. outside the PL vesicles using an Accumet pH electrode. Valinomycin (red cylinder), a potassium specific ionophore, facilitating the movement of potassium ions through lipid membranes down an electrochemical gradient, was used to negate the contribution of electric potential to the proton motive force. The buffer trapped inside the vesicle was 50 mM Na^+/ K^+ phosphate, pH 7.4, containing 100 mM KCl. Only one bc_1 dimer is shown embedded in the PL vesicle for simplicity, as the total number of bc_1 complexes embedded in the vesicles was not determined.

flow from $Q_0C_{10}BrH_2$ to cytochrome *c*. Ferricyanide oxidizes the cytochrome *c* in the reaction mixture triggering electron flow from ubiquinol to the bc_1 complex that is coupled to proton translocation and acidification of the reaction mixture (Fig 13). Two types of protons, scalar and vectorial, contribute towards the generated electrochemical potential. 'Scalar protons' arise as a result of the direct oxidation of ubiquinol by the bc_1 complex while 'vectorial protons' are translocated from the inside of the PL vesicle to the outside (Fig. 13). In the presence of valinomycin, the electrochemical potential gradient generated consists of only the chemical potential. Valinomycin, a potassium specific ionophore, facilitates the movement of potassium ions through lipid membranes down an electrochemical gradient preventing the build-up of electric potential across the PL vesicle. Failure to dississipate the electric potential across the PL vesicle prevents further electron transfer and proton translocation resulting in inhibition of the reaction. After pH equilibrium is attained, a protonophore, CCCP, is added (Fig. 14, addition 2) to render the liposome membrane freely permeable to protons, and then a second aliquot of ferricyanide is added (addition 3). In the presence of CCCP, the integrity of the PL vesicle is compromised as proton flow is readily permissible. Compartmentalization no longer exists, resulting in abolishment of proton pumping. The ratio of the pH changes produced by the addition of equal amounts of ferricyanide, before (x) and after (y) the addition of CCCP, is taken as a measure of the H^+/ e^- ratio for proton translocation activity of the bc_1 complex. The protons released after CCCP addition are the 'scalar' protons only, as no contribution from the accumulation of 'vectorially' translocated protons is possible. Ratios (i.e. x/y) between 1.6 and 2.0 are routinely obtained with liposomes containing the bovine mitochondrial bc_1 complex (48).

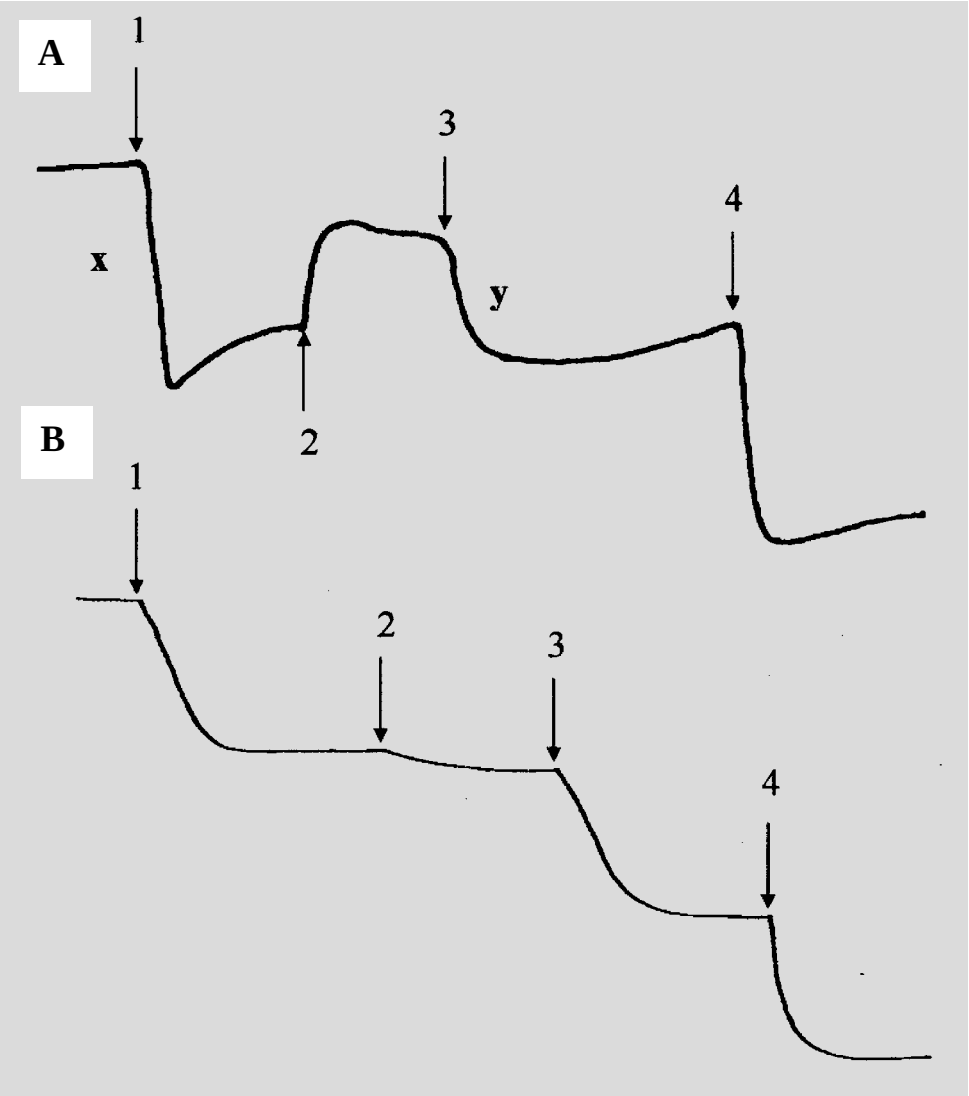

Figure 14. The proton-pumping of cytochrome bc_1 complexes embedded PL vesicles. Measurement of the proton-pumping activity of PL vesicles embedded with mitochondria bc_1 complex only (A), and mitochondrial bc_1 complex co-embedded with the [2Fe-2S] cluster lacking mutant complex, H131C-H152C (B) using ubiquinol as the substrate. Arrows indicate the points of addition of 6 nmoles of ferricyanide (1), 3 uM CCCP (2), 6 nmoles of ferricyanide (3), and 5 nmoles HCl (4). Note: proton-pumping ratio (H^+/e^-) = x / y.

When wild-type *R. sphaeroides* bc_1-PL vesicles, prepared in the same manner as that of mitochondrial-PL vesicles, are subjected to proton pumping activity measurement, a H^+/e^- ratio of 1.5 - 1.6 is obtained (see Table 4). The proton pumping ratio for vesicles embedding bacterial bc_1 complex is lower than that obtained for PL vesicles embedding mitochondrial bc_1 complex probably because the vesicles are not as tightly sealed. As expected, no proton translocation activity is found in PL vesicles embedding the H131C-H152C mutant complex, since it lacks ubiquinol-cytochrome *c* reductase activity. When the wild-type bacterial bc_1 complex is co-embedded in PL vesicles with the intact mitochondrial bc_1 complex, a H^+/e- ratio of 1.7 is obtained. However, when the H131C-H152C mutant complex is co-inlaid in PL vesicles with the mitochondrial bc_1 complex, no proton-pumping is observed; i.e., H^+/ e^- ratio equals 1.0 (see Fig. 14B and Table 4). This indicates that a proton-leaking channel is present in the H131C-H152C mutant complex whose [2Fe-2S] cluster is lacking. Incorporation of the mutant complex into actively proton-pumping liposomes has a similar effect as the addition of CCCP; i.e. they both allow the free flow of protons across the PL vesicle, preventing the generation of a gradient. It should be noted that the proton translocation activity (H^+/e^-) in protein-PL vesicles containing intact mitochondrial bc_1 and the H131C-H152C mutant complexes decreases as the relative amount of mutant complex in the vesicle increases. A complete loss of proton-pumping activity is observed when the mutant complex concentration is three-fold that of the mitochondrial bc_1 complex. An excess of the [2Fe-2S] cluster lacking mutant complex is necessary to ensure that every PL vesicle harbors at least one mutant complex in addition to a mitochondrial bc_1 complex.

Proton Translocation Activity of Intact Mitochondrial Cytochrome c Oxidase Co-inlaid in PL Vesicles with Wild-type and Mutant Bacterial Complexes – The ability of the H131C-H152C mutant bc_1 complexes to form proton-leaking channels is further demonstrated by co-embedding with bovine mitochondrial C*c*O. Like the cytochrome bc_1 complex, electron transfer through C*c*O is coupled to proton translocation across the membrane in which the complex is housed. When purified bovine C*c*O is embedded in PL vesicles, the accumulation of vectorially translocated protons is detected during the oxidation of reduced cytochrome *c* as indicated by acidification of the external medium (Fig. 15). However, when C*c*O is co-inlaid in PL vesicles with a five-fold or higher molar excess of the H131C-H152C mutant bc_1 complex, the vesicles produce an instant alkalization phase during the oxidation of reduced cytochrome *c*. The pattern of pH increase is similar to that observed in CCCP treated PL vesicles embedding C*c*O, thereby further indicating the presence of a proton leaking channel in the bc_1 complex lacking the [2Fe-2S] cluster. It should be noted that the proton translocation activity of C*c*O remains unchanged when co-inlaid in PL vesicles with a five-fold molar excess of wild-type bc_1 complex.

Restoration of Proton Translocation Activity to Protein-PL Vesicles Containing Intact Mitochondrial bc_1 and the Thermolysin-digested Bacterial Complex with the Head Domain of ISP – Since the cytochrome bc_1 complex lacking the [2Fe-2S] cluster has a proton-leaking channel, the cluster may function as a proton-exiting gate regulating the controlled, vectorial extrusion of protons across the bc_1 complex. If removal of the [2Fe-2S] cluster of ISP makes the bc_1 complex proton permeable, a bc_1 complex with the ISP head domain removed should be similar, since the [2Fe-2S] cluster is located in the head

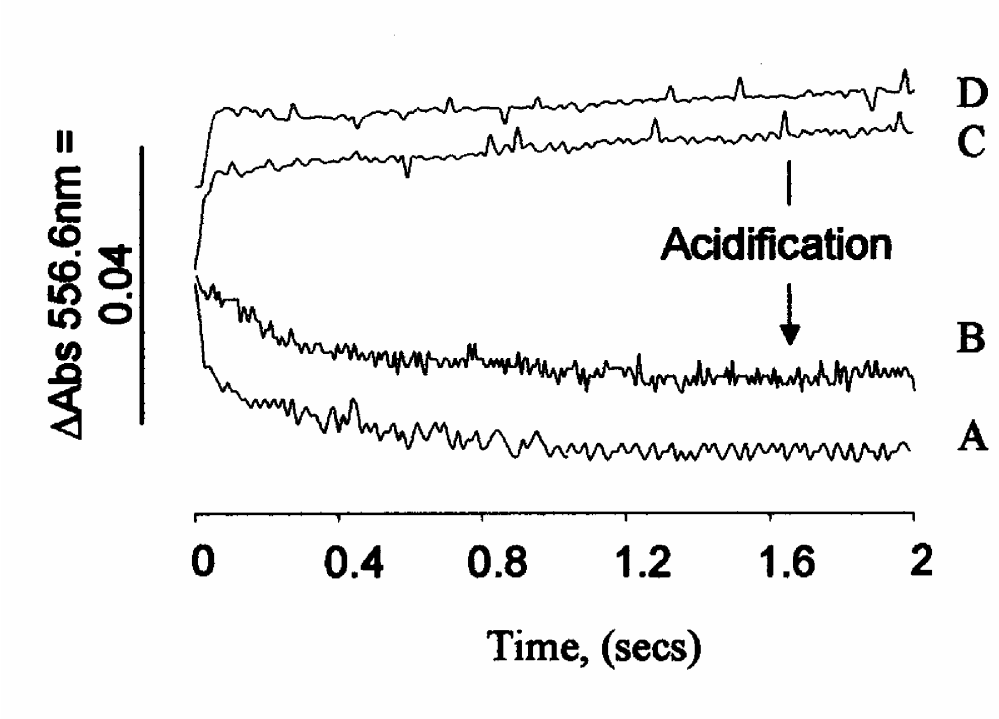

Figure 15. Determination of proton translocation of PL vesicles embedded with cytochrome *c* oxidase (C*c*O) and bacterial bc_1 complex using stopped-flow spectrophotometer. Reaction conditions were as described in Materials and Methods. pH changes were monitored by following the change in absorbance of phenol red at the isobestic point of horse heart cytochrome *c*, 556.6 nm. Reaction of 15 μM reduced cytochrome *c* with vesicles embedded with 0.75 μM bovine mitochondrial C*c*O only (A), C*c*O and complement *R. sphaeroides* bc_1 complex (B), CCCP treated vesicles embedded with C*c*O (C), and vesicles embedded with C*c*O and [2Fe-2S] cluster lacking mutant bc_1 complex, H131C-H152C (D).

domain of ISP. To confirm this prediction, a bacterial bc_1 complex lacking the ISP head domain was prepared by thermolysin digestion and co-inlaid into PL-vesicles with intact mitochondrial bc_1 complex. The proton pumping activity of the resulting protein-PL vesicles was measured. No proton-pumping is observed in protein-PL vesicles containing thermolysin-digested bacterial bc_1 complex and mitochondrial bc_1 complex at an 8:1 molar ratio. The requirement of a large excess of thermolysin digested complex to completely abolish proton transfer activity may be due to incomplete removal of the head domain of ISP by thermolysin. To examine this possibility, the digested complex, which has no ubiquinol-cytochrome *c* reductase activity, was subjected to SDS-PAGE and Western Blot analysis. About 30 % of the ISP in the complex is resistant to thermolysin digestion (see Fig. 16). Similar observations were made with *R. capsulatus*, where incubation of the bc_1 complex with thermolysin for prolonged periods, with fresh additions of protease at 4 hr intervals does not yield complete digestion (51).

Addition of excess purified ISF to proton-leaking PL vesicles co-embedding mitochondrial bc_1 and thermolysin digested bacterial bc_1 complex partially restores the proton-pumping capability with H^+/e^- ratios ranging from 1.35 to 1.40. Probably the purified ISF docks at the vacant position once occupied by the cleaved head domain of ISP of the bacterial complex. Reintroduction of the [2Fe-2S] cluster containing head domain seals the proton channel across the bc_1 complex, preventing the uncontrolled and unimpeded proton flow across the protein-PL vesicles. As expected, the addition of excess ISF to PL vesicles embedding mitochondrial bc_1 complex, and the mutant complex, H131C-H152C, does not restore the proton-pumping activity because the mutant complex lacks only the [2Fe-2S] cluster, not the entire ISF, providing no room

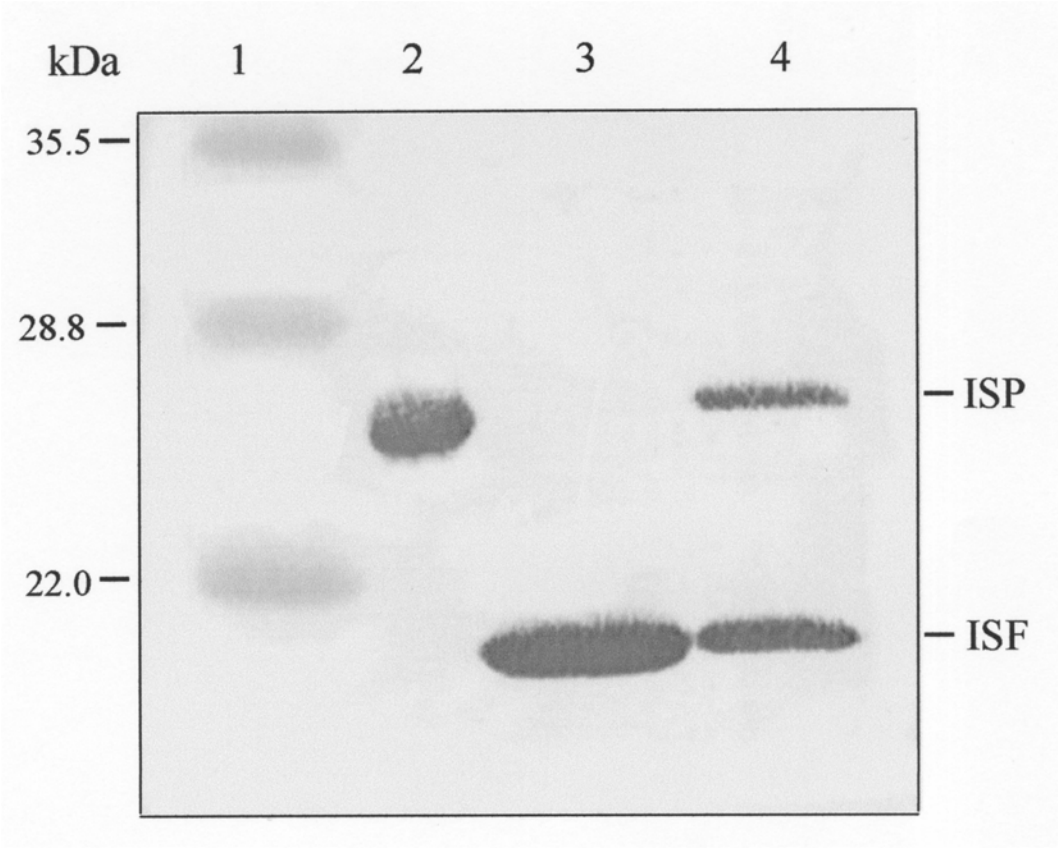

Figure 16. Western blot analysis of thermolysin-mediated proteolysis of purified *R. sphaeroides* bc_1 complex. The *R. sphaeroides* bc_1 complex was treated with thermolysin and incubated at room temperature as detailed in Methods. Samples containing 100 pmoles of cytochrome *b* were loaded into each well and subjected to SDS-PAGE. The proteins in the gel were transferred electrophoretically to a 22 micron nitrocellulose membrane and reacted with antibodies against *R. sphaeroides* ISP. The horseradish peroxidase system was used to develop the membrane. *Lane 1*, pre-stained molecular weight standard; *Lane 2*, undigested wild-type *R. sphaeroides* bc_1 complex; *Lane 3*, purified 18 kDa iron-sulfur fragment (ISF); *Lane 4*, thermolysin digested *R. sphaeroides* bc_1 complex.

for added ISF to dock. Similarly, the addition of excess ISF to PL vesicles embedding mitochondrial bc_1 complex and 2-band bc_1 complex (a mutant bc_1 complex containing only the cytochrome *b* and cytochrome c_1 subunits) does not restore the proton-pumping capability of such vesicles. The tail domain of ISP which is present in the thermolysin digested complex and absent in the 2-subunit bc_1 complex may play a role in maintaining the conformation of the bc_1 complex required for the docking of ISF.

The Existence of Proton Pathway in the Cytochrome bc_1 Complex - The observation of proton leakage in the bc_1 complex with damaged ISP suggests a passage in the complex, channeling proton back-flow from the periplasmic to cytoplasmic side (from the inter-membrane space to matrix in mitochondria). It is unlikely, although it can't be ruled out, that such a channel exists in the trans-membrane (TM) region at the interfaces of different subunits, such as that between cyt. *b* and c_1, because the only damage needed to produce the proton leakage is removal of the [2Fe-2S] cluster. It is conceivable that the culprit lies in the cyt. *b* subunit as it contributes most to the TM region of the complex. Based on the crystallographically refined structures (5, 8, 9), a solvent distribution around the subunit cyt. *b* was generated (Fig. 17), from which three principle solvent accessible regions in cyt. *b* could be defined where water molecules penetrate deep into the subunit: they are the Qi site, the Qo site, and the dimer interface at the matrix side (Fig. 17). There is however a gap of roughly 17 Å in the mid-section of the TM domain where no ordered water molecules were found crystallographically. Proton transfer pathways involving internal water molecules that provide hydrogen bonds and facilitate proton diffusion have been identified in other membrane proteins like bacteriorhodopsin (52), and C*c*O (53). Although the mechanisms for proton

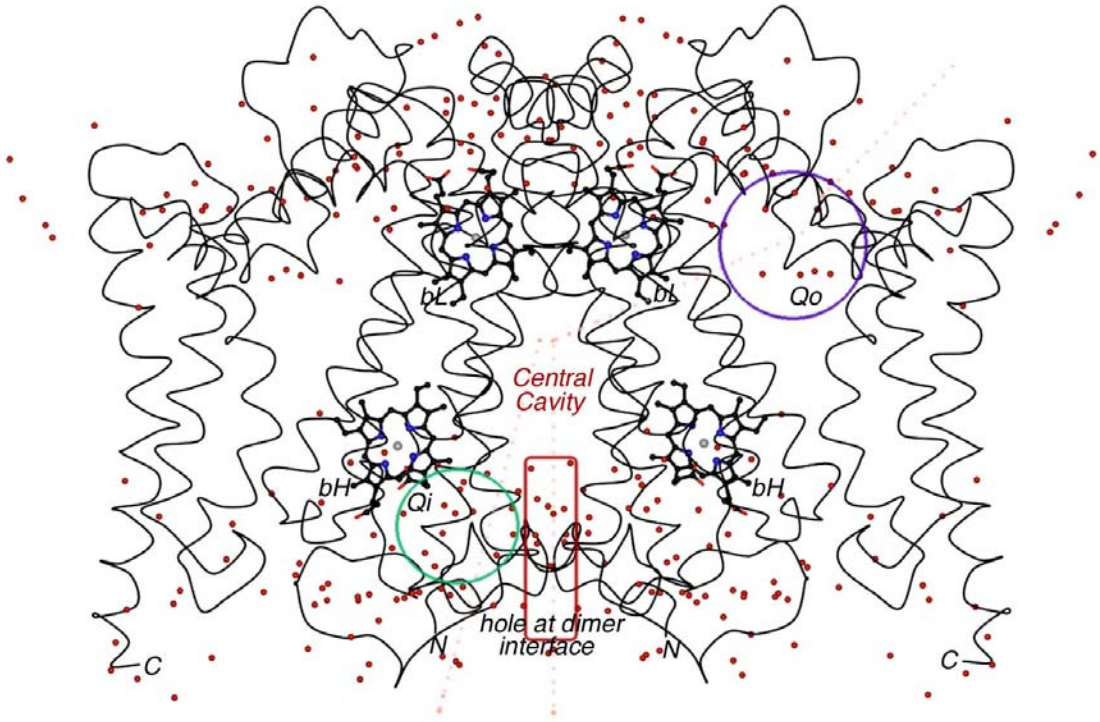

Figure 17. Solvent molecule distribution for the bovine cytochrome *b* dimer. The structure of cytochrome *b* dimer is shown as a Cα tracing, and associated water molecules are shown as red balls. Heme moieties are given as the ball-and-stick models and are as labeled. Highlighted in purple circle is the Qo site, in green circle is the Qi site, and in red rectangle is the hole at the dimer interface near the matrix. The central cavity is also indicated.

translocations are different for different proteins, the underlying principle for bringing water molecules or protons to the active sites is similar. Several pathways for proton leakage are possible. As indicated in Fig. 17, the proton entry for the leakage must be located at the Qo site where protons are ejected under normal circumstance. All other venues near the intermembrane space side are sealed. In the native cytochrome bc_1 complex, the [2Fe-2S] cluster undergoes redox state changes during the catalytic cycle. The ejection of protons must be controlled by the protonation and deprotonation of the histidine ligands of the [2Fe-2S] cluster. The histidine ligands uptake a proton from the substrate, ubiquinol, upon reduction of the [2Fe-2S] cluster, and releases them to the inter-membrane space when oxidized by cytochrome c_1 as was suggested recently (54). It is less clear how the second proton is pumped out, although Glu271 of cytochrome *b* is speculated to be the acceptor of the second proton from ubiquinol (54). The absence of the histidine ligands, and thus the loss of the [2Fe-2S] cluster, explain well the loss of the proton-pumping capability in PL vesicles incorporating the mutant bc_1 complexes. The exact mechanism of how protons leak into the Q_P site in the absence of the [2Fe-2S] cluster remains to be seen.

There are two likely exit pathways for the proton leakage: one is via the Qi site and the other is through a hole at the dimer interface (Fig. 17). We have suggested earlier (9) that two residues in the Qi pocket may be involved in fetching protons from the matrix side; K227 and H201 undergo conformational changes that are coupled to ubiquinone reduction at the Qi site. The same residues could serve as an exit gate in the case of proton leakage except that the gate is decoupled to ubiquinone reduction and is spontaneously open. Alternatively, the proton could exit from the hole at the dimer

interface near the matrix side (Fig. 17). The hole is just outside H201 and filled with ordered water molecules.

The possibility of a direct proton translocation path going through the interior of cyt. *b* is slim since the overall structure is rather rigid as analyzed by the binding of various inhibitors (8). A likely pathway linking the entrance at the Q_o site to the exit gate at the Qi site for spontaneous proton leakage is the large cavity formed between the two symmetry-related cyt. *b* subunits. Although this cavity is fairly hydrophobic, one could argue that the existence of the membrane potential (pH gradient) could overcome the thermodynamic barrier and facilitate proton movement from one side to the other.

REFERENCES

1. Trumpower, B. L., and Gennis, R. B. (1994) *Annu. Rev. Biochem.* **63,** 675-716
2. Xia, D., Yu, C.-A., Kim, H., Xia, J. Z., Kachurin, A.M., Zhang, L., Yu, L. and Deisenhofer, J. (1997) *Science* **277**, 60-66
3. Iwata, S., Lee, J. W., Okada, K., Lee, J. K., Iwata, M., Ramussen, B., Link, T. A., Ramaswamy, S., and Jap, B.K. (1998) *Science* **281**, 64-71
4. Zhang, Z. L., Huang, L. S., Shulmeister, V. M., Chi, Y. I., Kim, K. K., Huang, L. W., Crofts, A. R., Berry, E. A., and Kim, S. H. (1998) *Nature* **392**, 677-684
5. Hunte, C., Koepke, J., Lange, C., Rossmanith, T., and Michel, H. (2000) *Structure Fold. Des.* **8**, 669-684
6. Kurisu, G., Zhang, H., Smith, J. L., Cramer, W. A. (2003) *Science* **302**, 1009-1014
7. Stroebel, D., Choquet, Y., Popot, J. L., and Picot, D. (2003) *Nature* **426**, 413-418
8. Gao, X., Wen, X., Esser, L., Quinn, B., Yu, L., Yu, C.-A, and Xia, D. (2003) *Biochemistry* **42**, 9067-9080
9. Esser, L., Quinn, B., Li, Y. -F, Zhang, M., Elberry, M., Yu, L., Yu, C. –A., and Xia, D. (2004) *J. Mol. Biol.* **341**, 281-302
10. Tian, H., Yu, L., Michael, W., and Yu, C. -A. (1998) *J. Biol. Chem*. **273**, 27953-27959
11. Tian, H., White, S., Yu, L., and Yu, C. -A. (1999) *J. Biol. Chem.* **274**, 7146-7152
12. Xiao, K., Yu, L., and Yu, C. -A. (2000) *J. Biol. Chem.* **275**, 38597-38604
13. Darrouzet, E, Valkova-Valchanova, M., Christopher, C., Moser, P., Dutton, L., and Daldal, F. (2000) *Proc. Natl. Acad. Sci. U.S.A.* **97**, 4567-4572

14. Zhang, Z., Huang, L., Shulmeister, V. M., Chi, Y. -I., Kim, K. K., Huang, L.-W., Crofts, A. R., Berry, E. A., and Kim, S-H. (1998) *Nature* **392**, 677-684

15. Kim, H., Xia, D., Yu, C. -A., Kachurin, A., Zhang, L., Yu, L., and Deisenhofer, J. (1998) *Proc. Natl. Acad. Sci. U.S.A.* **95**, 8026-8033

16. Berry, E. A., Guergova-Kuras, M., Huang, L. S., and Crofts, A. R. (2000) *Annu. Rev. Biochem.*, **69**, 1005-1075

17. Nett, J. H., Hunte, C., and Trumpower, B. L. (2000) *Eur. J. Biochem.* **267**, 5777-5782

18. Obungu, V. H., Wang, Y., Amyot, S. M., Gocke, C. B., and Beattie, D. S. (2000) *Biochim. Biophys. Acta*., **1457**, 36-44

19. Ghosh, M., Wang, Y., Ebert, E. C., Vadlamuri, S., and Beattie, D. S. (2001) *Biochemistry,* **40**, 327-335

20. Mitchell, P. (1976) *J. Theor. Biol.* **62**, 327-367

21. Crofts, A. R., Meinhardt, S. W., Jones, K. R., and Snozzi, M. (1983) *Biochim. Biophys. Acta.* **723**, 202-218

22. Link, T. A., (1997) *FEBS Lett.* **412**, 257-264

23. Brandt, U., Okun, J. G. (1997) *Biochemistry* **36**, 11234-11240

24. Juneman, S., Heathcote, P., and Rich, P. R. (1998) *J. Biol. Chem.* **273**, 2163-21607

25. Osyczka, A., Moser, C. C., Daldal, F., and Dutton, L. P. (2004) *Nature* **427**, 607-612

26. Covian, R., Gutierrez-Cirlos, E. B., and Trumpower, B. L. (2004) *J. Biol. Chem.* **279**, 15040-15049

27. Crofts, A. R. (2004) *Biochim. Biophys. Acta*. **1665**, 77-92

28. Snyder, C. H., Gutierrez-Cirlos, E. B., and Trumpower, B. L. (2000) *J. Biol. Chem.* **275**, 13535-13541

29. Miki, T., Yu, L., Yu, C. -A. (1991) *Biochemistry* **30**, 230-238

30. Kagawa, Y., and Racker, E. (1971) *J. Biol. Chem.* **246**, 5477-5487

31. Xiao, K., Liu, X., Yu, C. –A., and Yu, L. (2004) *Biochemistry* **43**, 1488-1495

32. Mather, M. W., Yu, L., and Yu, C. -A. (1995) *J. Biol. Chem.* **270**, 28668-28675

33. Sistrom, W. R., (1960) *J. Gen. Microbiology*. **22**, 778-785

34. Kannt, A., Soulimane, T., Buse, G., Becker, A., Bamberg, E., and Michel, H. (1998), *FEBS Lett.* **434**, 17-22

35. Link, T. A., Saynovits, M., Assman, C., Iwata, S., Ohnishi, T., and Von Jagow, G., (1996) *Eur. J. Biochem*. **237**, 71-75

36. Lee, G. Y., He, D.-Y., Yu, L., and Yu, C.-A. (1995) *J. Biol. Chem.* **270**, 6193-6198

37. Jenner, E. R., (June 5, 1973) US Patent 3737516

38. Lowry, O. H., Rosebrough, N. J., Farr, A. L., and Randall, R. J., (1951) *J. Biol. Chem.* **193**, 265-275

39. Berden, J. A., and Slater, E.C. (1970) *Biochem. Biophys. Acta*. **216**, 237-249

40. Yu, L., Doug, J. H., and Yu, C. -A., (1986) *Biochem. Biophys. Acta.* **852**, 203-211

41. Laemelli, V. K., (1970) *Nature* **227**, 680-685

42. Link, T. A., Hatzfied, O. Unalkat, P., Shergill, J. K., Cammack, R., and Mason, J. R. (1996) *Biochemistry* **35**, 7546-7552

43. Crofts, A. R., and Ugulava, N. B. (1998) *FEBS Lett.* **440**, 409-413

44. Graham, L. A., and Trumpower, B. L. (1991) *J. Biol. Chem.* **266**, 22485-33492

45. Davidson, E., Ohnishi, T., Tokiti, M., and Daldal, F. (1992), *Biochemistry* **31**, 3351-3358

46. Gutierrez-Cirlos, E. B., Merbitz-Zahradnik, T., and Trumpower, B. L. (2002) *J. Biol. Chem.* **277**, 50703-50709

47. Leung, K. H., and Hinkle, P. C. (1975) *J. Biol. Chem.* **250**, 8467-8471

48. Güner, S., Robertson, D. E., Yu, L., Qui, Z. -H., Yu, C.-A., and Knaff, D. B. (1991) *Biochim. Biophys. Acta.* **1058,** 269-279.

49. Lorusso, M., Gatti, D., Boffoli, D., Bellomo, E., and Papa, S. (1983) *Eur. J. Biochem.* **137**, 413-420

50. Cocco, T., Lorusso, M., Di Paola, M., Minuto, M., and Papa, S. (1992) *Eur. J. Biochem.* **209**, 475-481

51. Valkova-Valchanova, M., Darrouzet, E., Moomaw, C. R., Slaughter, C. A., and Daldal, F. (2000) *Biochemistry* **39**, 15484-15492

52. Gennis, R. B., and Ebrey, T. G. (1999) *Science* **286**, 252-253

53. Wikstrom, M., Verkhovsky, M. I., and Hummer, G. (2003) *Biochim. Biophys. Acta.* **1604**, 61-65

54. Crofts, A. R., Hong, S., Ugulava, N., Barquera, B., Gennis, R., Guergova-Kuras, M., and Berry, E. A. (1999) *Proc. Natl. Acad. Sci. USA* **96**, 10021-10026

Chapter III

Stigmatellin Induces Reduction of the Rieske Iron-Sulfur Protein in the Absence of an Apparent Electron Source

Buddha Gurung, Linda Yu, and Chang-an Yu

ABSTRACT

Stigmatellin, a Q_P site inhibitor, inhibits electron transfer from iron-sulfur protein (ISP) to cytochrome c_1 in the bc_1 complex. Stigmatellin raises the midpoint potential of ISP from +290 mV to +540 mV. The binding of stigmatellin to the fully oxidized complex, oxidized by catalytic amounts of cytochrome *c* oxidase and cytochrome *c*, causes ISP reduction. The extent of ISP reduction is proportional to the amount of inhibitor used and reaches a maximum when the ratio of inhibitor to enzyme complex reaches unity. A g = 2.005 EPR peak, characteristic of an organic free radical, is also observed when stigmatellin is added to the oxidized complex and its signal intensity is dependent on the amount of stigmatellin. Addition of ferricyanide, a strong oxidant, to the oxidized complex also results in the generation of a g = 2.005 EPR peak that is oxidant concentration dependent. Oxygen radicals are generated when stigmatellin is added to the oxidized complex in the absence of the exogenous substrate, ubiquinol. The amount of oxygen radical formed is proportional to the amount of stigmatellin. Oxygen radicals are not generated when stigmatellin is added to a mutant bc_1 complex lacking the Rieske iron-sulfur cluster. Slow reduction of cytochrome *b* is observed in bc_1 complexes treated with either stigmatellin or fericyanide. Based on these results, it is proposed that ISP becomes a strong oxidant upon stigmatellin binding, extracting electrons from an organic compound, likely an amino acid residue. This results in the reduction of ISP and generation of organic radicals.

INTRODUCTION

The cytochrome (cyt) [1] bc_1 complex, also known as ubiquinol-cytochrome *c* reductase or Complex III is the central segment of the energy conserving, electron transfer chain of mitochondria and many respiratory and photosynthetic bacteria (1). This enzyme complex catalyzes electron transfer from ubiquinol to cyt *c* (c_2 in bacteria) with concomitant translocation of protons across the membrane to generate a proton electrochemical gradient required for ATP synthesis by ATP synthase. The cyt bc_1 complexes from all species contain three core subunits, cyt *b*, cyt c_1 and Rieske Iron-Sulfur protein (ISP), that house two *b* type cyt (b_{566} and b_{562}), one *c*-type cyt (c_1) and a high potential Rieske [2Fe-2S] cluster. Depending on the source, the cyt bc_1 complex contains various numbers (0 to 8) of non-redox group containing subunits, also called supernumerary subunits.

Recently, the 3-D crystal structures of mitochondrial bc_1 complexes from bovine (2, 3), chicken (4) and yeast (5), which contain seven or eight supernumerary subunits in addition to the three core subunits, have been obtained. The structure of the cyt b_6f complex, a complex analogous to the cyt bc_1 complex that provides an electronic connection between photosystems I and II, have also been established for the thermophilic cyanobacterium *Mastigocladus laminosus* (6), and for the algae *Chlamydomonas reinhardtii* (7). The 3-D structural information for the mitochondrial bc_1 complex establishes the location of the redox centers, the number of trans-membrane helices, quinone binding at the Q_N site, and inhibitor binding at both the Q_P and Q_N sites (2-4, 8, 9). Moreover, these crystal structures suggest mobility of the extrinsic head

domain of ISP during bc_1 catalysis. Strong evidence in support of this movement has been reported (10-19).

The proton-motive Q-cycle model (20, 21) has been favored for describing electron and proton translocation in the cyt bc_1 complex. The key feature of this model is the presence of two separate ubiquinol/ubiquinone binding sites; a ubiquinol oxidation site (Q_P) near the P (inter-membranes space) side of the mitochondrial inner membrane, and a ubiquinone reduction site (Q_N) near the N (matrix) side. X-ray crystallographic analyses revealed binding of ubiquinone at the Q_N site (5) of the cyt bc_1 complex. Unfortunately, ubiquinone or ubiquinol binding at the Q_P site has not been observed in native crystal structures, thereby preventing establishment of the putative Q_P site. Therefore, discussions on the mechanisms of electron transfer are based primarily on the positions occupied by inhibitors, and assumptions are made to reflect a similar site for binding of the natural substrate, ubiquinol. Detailed bifurcation of ubiquinol oxidation, the key step in the Q-cycle mechanism, is difficult to establish, although several models have been proposed (22-28). Stigmatellin, a P_f inhibitor (29) of the cyt bc_1 complex, binds to cyt *b* at a domain distal from heme b_L. It interacts with the Rieske ISP through the formation of an H-bond with His-161, and with cyt *b* by H-bonding with Glu-272, whose side chain undergoes a rotation of ~160^o from its native position (9). The H-bonded configuration of quinone and stigmatellin in the bc_1 complex were shown to be similar (27). Hence, it is likely that the binding of stigmatellin resembles that of a quinol oxidation intermediate (5, 30).

Herein, we report the affect of stigmatellin on the redox state of oxidized cyt bc_1 complexes. The importance of phospholipids for binding of stigmatellin to the bc_1

complex was established. The generation of free radicals upon addition of stigmatellin was explored by analysis of the g = 2.005 EPR signal. Reduction of cyt *b* after addition of stigmatellin to the oxidized complex was examined. Production of superoxide by the bc_1 complex, in the presence of stigmatellin, was determined in wild-type cyt bc_1 complex and compared to a mutant complex lacking the Rieske iron sulfur cluster (ISC).

EXPERIMENTAL PROCEDURES

Materials - Cyt *c* (horse heart, Type-III), stigmatellin, MCLA, superoxide dismutase and thermolysin were from Sigma. Azolectin was obtained from Associate Concentrate and purified according to the method of Racker and Kagawa (31). Octyl sepharose and DEAE-sepharose CL-6 were obtained from Pharmacia. n-dodecyl-β-D-maltopyranoside (DM) and n-dodecyl-β-D-glucopyranoside (DG) were from Anatrace. Ni-NTA gel and Qiaprep Spin Miniprep kit were from Qiagen. 2, 3-Dimethoxy-5-methyl-6-bromodecyl-1, 4-benzoquinol ($Q_0C_{10}BrH_2$) was prepared in our laboratory as previously reported (11). All other chemicals were of the highest purity commercially available.

Enzyme Preparations and Activity Assay - Chromatophores and intra-cytoplasmic membranes (ICM's) were prepared as described previously (10), and stored at –80 ^{o}C in the presence of 20 % glycerol. The His_6-tagged cyt bc_1 complexes were purified from frozen ICM's or chromatophores by the method of Tian *et al.* (10). Purified cyt bc_1 complexes were stored at –80 ˚C in the presence of 10 % glycerol. To assay ubiquinol-cyt *c* reductase activity, membrane preparations or purified cyt bc_1 complexes were

diluted with 50 mM Tris-Cl, pH 8.0, containing 200 mM NaCl and 0.01 % DM to a final cyt *b* concentration of 1 μM. 5 μl of the diluted samples were added to 1 ml of assay mixture containing 100 mM of Na^+/K^+ phosphate buffer, pH 7.4, 0.3 mM EDTA, 50 μM ferricytochrome *c*, and 25 μM $Q_0C_{10}BrH_2$. Activities were determined by measuring the reduction of cyt *c*, by following the increase in the absorbance at 550 nm, in a Shimadzu UV-2450 PC spectrophotometer at 23 ˚C using a millimolar extinction coefficient of 18.5 $mM^{-1}cm^{-1}$ for calculations. The non-enzymatic oxidation of $Q_0C_{10}BrH_2$, determined under similar conditions in the absence of the enzyme, was subtracted during calculations for specific activity. Potassium cyanide was added to a final concentration of 30 μM in the assay mixture to inhibit cyt *c* oxidase (C*c*O) when determining the cyt bc_1 activity in ICM's or chromatophores.

EPR experiments – The redox state of the Rieske ISP was determined by EPR (32) using a Bruker EMX spectrometer equipped with an Air Products flow cryostat. Cyt bc_1 complexes were diluted in 50 mM Tris-Cl, pH 8, containing 200 mM NaCl and 0.01 % DM. The bc_1 complexes were incubated with 5 mM ascorbate on ice for 30 minutes, and frozen in liquid nitrogen. Cyt bc_1 complexes were oxidized by overnight incubation with 1 μM C*c*O and 1 μM cyt *c*. Variable amounts of stigmatellin were added to oxidized bc_1 complexes, and the mixture was incubated on ice for 30 minutes. EPR spectra were recorded at 100 K with the following instrument settings: microwave frequency, 9.3 GHz; modulation frequency, 100 kHz; modulation amplitude, 6.3 G; time constant, 655.4 ms; and sweep time, 167.8 s. Each spectrum represents an average of three different traces.

Isolation of Rieske ISP from R. sphaeroides bc_1 complex – Wild-type cyt bc_1 complex was diluted to 50 μM cyt *b* in 50 mM Tris-Cl, pH 8, containing 100 mM NaCl and 0.1 % DM. The mixture was gently shaken at 4 ^{o}C for ninety minutes and applied to an octyl-sepharose column previously equilibrated with 50 mM Tris-Cl, pH 8 containing 500 mM NaCl, 0.01 % DM and 1mM DTT. The column was washed with 1 gel volume of 50 mM Tris-Cl, pH 8, 100 mM NaCl, 0.1 % DM and 1mM DTT, followed by a stepwise decrease in NaCl concentration to 75 mM and 50 mM. The column was then washed with 50 mM Tris-Cl, pH 8, 50 mM NaCl, 0.05 % DM and 1mM DTT followed by the same buffer containing only 0.01 % DM. The eluates from all five washes were combined, and subsequently passed through a Ni-NTA column equilibrated with 50 mM Tris-Cl, pH 8, containing 1mM $MgSO_4$ and 1 mM DTT. The column was then washed with 1 gel volume of 50 mM Tris-Cl, pH 8 containing 100 mM NaCl and 1 mM DTT. All eluates were combined and passed through a DEAE-Sepharose CL-6 from Pharmacia Biotech that was previously equilibrated with 50 mM Tris-Cl, pH 7.5, containing 0.01 % DM and 1mM DTT. The column was washed with 50 mM Tris-Cl, pH 8 containing 100 mM NaCl, 0.01 % DM and 1 mM DTT. The Rieske ISP was finally eluted with 50 mM Tris-Cl, containing 0.01 % DM, 500 mM NaCl and 1 mM DTT.

Measurement of superoxide anion generation – Superoxide generation by the cyt bc_1 complex was determined by measuring the chemiluminescence of MCLA-$O_2^{\cdot -}$ adduct in an Applied Photophysics stopped-flow reaction analyzer SX.18MV (Leatherhead, England), by leaving the excitation light off and registering light emission (33). Reactions were carried out at 23 ^{o}C by mixing solutions A and B in a 1:1 ratio. Solution A contains 100 mM Na^+/K^+ phosphate buffer, pH 7.4, 1mM EDTA, 1 mM KCN, 1 mM

NaN_3, 0.1 % bovine serum albumin, 0.01 % DM, and 6 μM cyt bc_1 complex. Solution B was the same as solution A except that the cyt bc_1 complex was replaced with either 50 μM $Q_0C_{10}BrH_2$ or 30 μM stigmatellin and 4 μM MCLA.

Preparation of phospholipid-deficient mitochondrial bc_1 complex – Phospholipid and Q-depleted preparation of mitochondrial bc_1 complex was prepared by means of repeated ammonium sulfate fractionation in the presence of 0.5 % sodium cholate in 50 mM Na^+/K^+ phosphate buffer, pH 7.4. Cyt bc_1 complex was diluted to a protein concentration of 10 mg/ml in 50 mM Na^+/K^+ phosphate buffer, pH 7.4 containing 0.5 % sodium cholate. Neutralized saturated ammonium sulfate solution was added to 48 % saturation. After stirring for 5 minutes, the solution was centrifuged at 44000x g for 10 minutes. The precipitate was dissolved in 50 mM Na^+/K^+ phosphate buffer, containing 0.5 % cholate. Neutralized ammonium sulfate solution was added to 45 % saturation, stirred for 5 minutes followed by centrifugation at 44000x g for 10 minutes. This process was repeated three more times with 40 % ammonium sulfate saturation. The precipitate was finally dissolved in 50 mM Na^+/K^+ phosphate buffer, pH 7.4, containing 10 % glycerol.

Extraction of ubiquinone / ubiquinol from cyt bc_1 complex – A semi-micro assay was employed for extraction of ubiquinol / ubiquinone from mitochondrial and bacterial bc_1 complexes (34). 1 ml of protein containing 2-5 mg of protein was placed in a 45 ml glass centrifuge tube. Rapid addition of 4 ml cold methanol using a hypodermic needle was immediately followed by 5 ml hexane. The mixture was vortexed for 1 minute, and centrifuged for 2 minutes to separate the layers. The upper layer of hexane was transferred to another glass centrifuge tube while 3 ml of hexane was added to the lower

layer for further extraction. After vortexing and centrifugation, the upper hexane layer was collected and combined with the first extraction. The combined hexane extract was placed in a vacuum desiccator to evaporate the hexane. Residual lipid was dissolved in spectroscopically pure ethanol, ubiquinone / ubiquinol was quantitated spectroscopically in a Shimadzu UV-2450 PC spectrophotometer.

Determination of Cytochrome b reduction – Reduction of cyt *b* was followed at 23 °C in an SX.18MV stopped flow spectrophotometer from Applied Photophysics. The reaction was started by rapidly mixing 5 μM bc_1 complex in assay buffer containing 50 mM Tris-Cl, pH 8, 200 mM NaCl, and 0.01 % DM against an equal volume of the same buffer containing 50 μM stigmatellin. The reaction kinetics at 578 nm was subtracted from that at 560 nm to obtain the time course and amplitude of cyt *b* reduction induced by stigmatellin.

Other Biochemical and Biophysical Techniques – Protein concentration was determined by the method of Lowry *et al* (35). Cyt *b* (36) and cyt c_1 (37) concentrations were determined according to published methods. SDS-PAGE was performed according to Laemelli (38) using a Bio-Rad mini-protean dual slab vertical cell.

RESULTS AND DISCUSSION

Stigmatellin-induced reduction of the Rieske Iron-Sulfur Cluster – The EPR spectrum of the reduced iron-sulfur cluster (ISC) of the Rieske protein shows rhombic symmetry with three characteristic g values; $g_z = 2.02$, $g_y = 1.89$ and $g_x = 1.80$ (39). In the presence of ascorbate, the EPR spectrum of the cyt bc_1 complex from *Rhodobacter sphaeroides* displays the characteristic g values signaling ISC reduction (Fig. 18, trace A). Interestingly, the addition of stigmatellin to *R. sphaeroides* bc_1 complex, oxidized by incubation overnight with enzymatic amounts of cyt *c* oxidase (C*c*O) and cyt *c*, results in reduction of the ISC in the absence of an apparent electron source (trace B). Reduction of the ISC is also observed in oxidized cyt bc_1 complexes from bovine mitochondria upon the addition of stigmatellin (data not shown). Complete oxidation of the cyt bc_1 complex before the addition of stigmatellin is confirmed by the absence of the characteristic EPR signals of reduced ISC (trace C).

Stigmatellin contains a 5, 7-dimethoxy-8-hydroxychromone system with a hydrophobic alkenyl chain at position 2 (29). Binding of stigmatellin to the cyt bc_1 complex increases its redox midpoint potential from +290 mV to +540 mV (40). Moreover, stigmatellin arrests the head domain of ISP at the 'fixed' or b-position, proximal to cyt *b,* as derived from the anomalous diffraction signals whereby the mobility of the ISC is dramatically reduced (9). Fig. 19A shows the ubiquinol-cyt *c* reductase activity of *R. sphaeroides* bc_1 complex in the presence of varying amounts of stigmatellin. Stigmatellin inhibits the complex with a stoichiometry of 0.5 mole inhibitor per mole (monomer) bc_1 complex. Similar stoichiometric values have been demonstrated

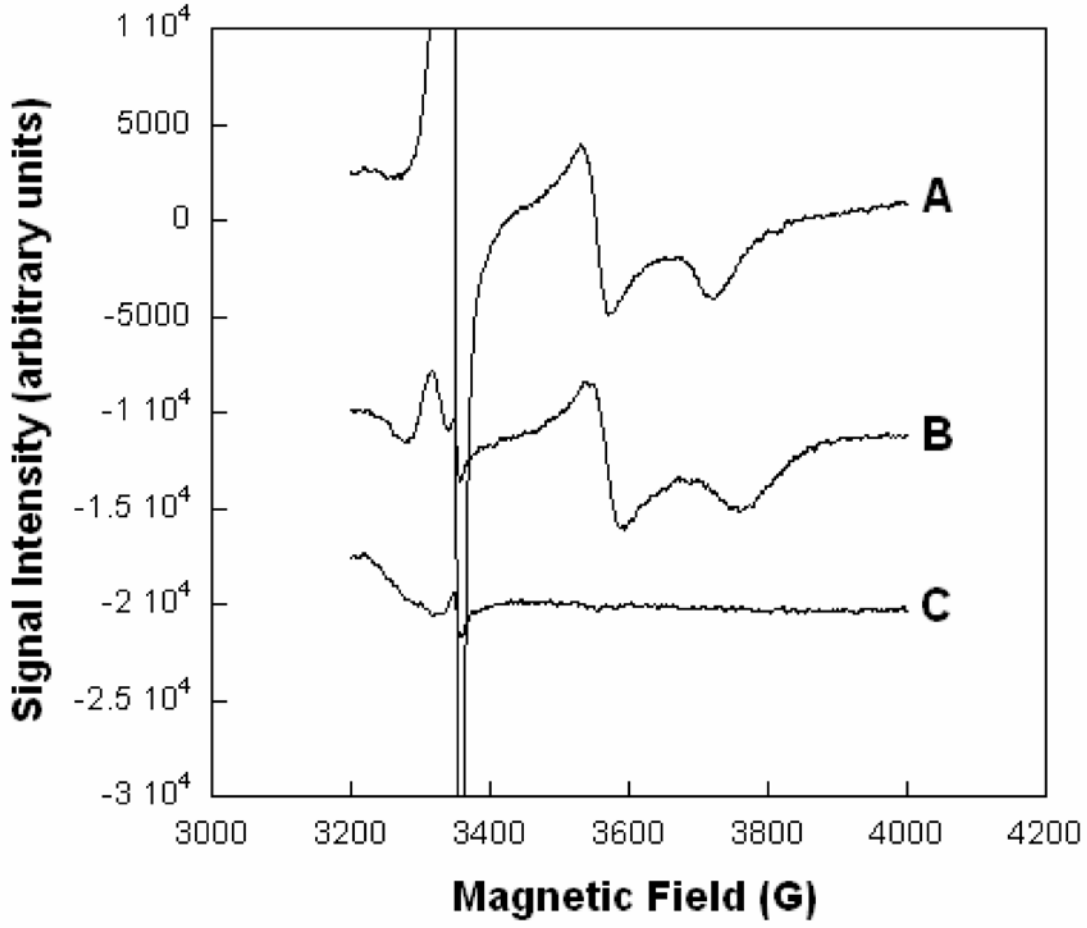

Figure 18. EPR spectra of wild-type *Rhodobacter sphaeroides* bc_1 complex. The bc_1 complexes (100 μM cytochrome *b*) were incubated with 5 mM ascorbate on ice for 30 minutes and subsequently frozen in liquid nitrogen (A). Cytochrome bc_1 complexes were oxidized by overnight incubation with 1 μM cytochrome *c* oxidase and 1 μM cytochrome *c* before 200 μM stigmatellin was added to the bc_1 complex (B). Oxidized bc_1 complex only (C). EPR spectra were recorded at 100 K with the following instrument settings: microwave frequency, 9.3 GHz; modulation frequency, 100 kHz; modulation amplitude, 6.3 G; time constant, 655.4 ms; and sweep time, 167.8 s. Each spectrum represents the average of three separate traces.

in cyt bc_1 complexes from yeast (41) and in submitochondrial particles (40). This indicates that the binding of stigmatellin to only one monomer per dimer is sufficient to abolish bc_1 complex activity. Binding also exhibits negative co-operativity; i.e. stigmatellin binds to a monomer of every inhibitor-free dimer before it binds to the second monomer (41). It must be noted negative co-operativity does not imply that stigmatellin is unable to bind to a monomer where stigmatellin is bound to the other monomer; i.e. negative co-operativity is not absolute. It simply means that the binding or 'ON' rate of the stigmatellin molecule for the monomer in the inhibitor-free dimer is much greater than for a monomer whose interacting monomer already has a bound stigmatellin molecule. ISP reduction induced by stigmatellin binding to oxidized bc_1 complex titrated against varying concentrations of the inhibitor is shown in Fig 19B. Maximal reduction of the ISC by stigmatellin is obtained at a stoichiometry of 1 inhibitor per bc_1 complex monomer indicating that binding to every monomer is necessary for complete ISC reduction. Similarly, one molecule of stigmatellin per bc_1 complex monomer was required to obtain maximal spectral shift of the dithionite-reduced cyt *b* (40). The binding of stigmatellin to the cyt bc_1 complex elevates the mid-point potential of the Rieske ISP, thereby generating a strong electron sink which results in the observed reduction of the ISC in the absence of an apparent electron source.

It is possible that the 8-hydroxy group of the chromone ring system of stigmatellin directly reduces the ISC. This possibility is investigated by adding stigmatellin to pure Rieske ISP isolated from *R. sphaeroides* bc_1 complex (Fig. 20A). Rieske ISP was isolated in the presence of dithiothreitol (DTT) since the ISC is easily lost, when it is not in the reduced state, during the isolation from the bc_1 complex. The

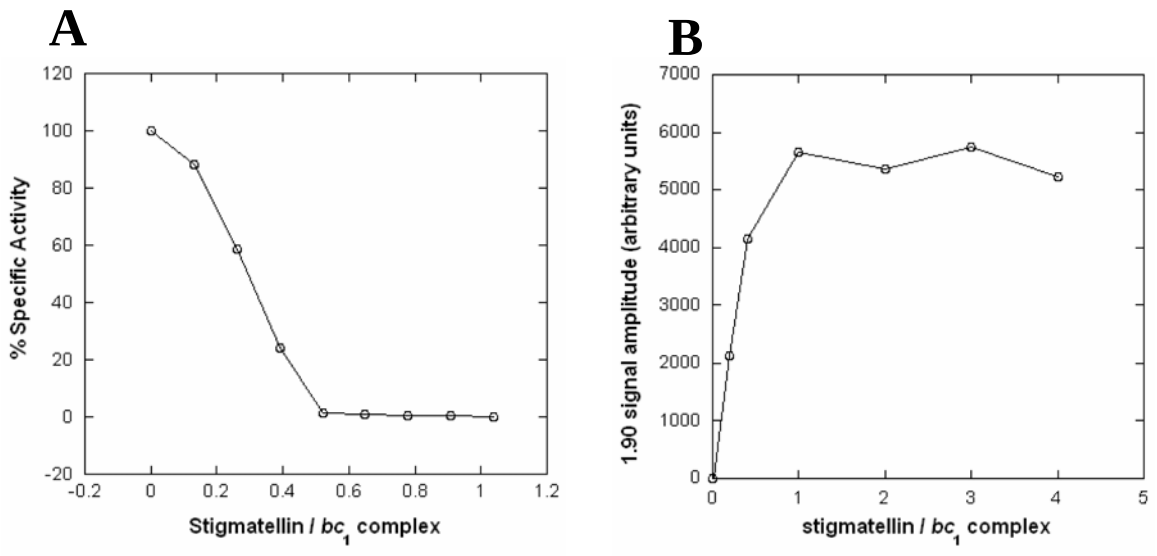

Figure 19. Inhibition of ubiquinol-cytochrome *c* reductase activity (A) and reduction (B) of the Rieske iron-sulfur cluster of oxidized bc_1 complexes by varying amounts of stigmatellin. For specific activity measurements, cyt bc_1 complex was diluted to 1 μM cyt *b* in 50 mM Tris-Cl, pH 8 containing 200 mM NaCl and 0.01 % DM. Stigmatellin was added in varying amounts to the enzyme complex and the mixture was incubated on ice for 20 minutes before collection of data. For determining reduction of the Rieske ISP, the bc_1 complexes were diluted to 100 μM cyt *b* in 50 mM Tris-Cl, pH 8, containing 200 mM NaCl and 0.01 % DM before addition of stigmatellin. The mixture was incubated on ice for 15 minutes and subsequently frozen in liquid nitrogen. The extent of ISP reduction induced by addition of varying amounts of stigmatellin was determined by the intensity of the g_y EPR signal. Sample preparations and instrument settings were the same as in Fig. 18.

EPR spectrum of isolated ISP was recorded in the presence of either stigmatellin or ascorbate (Fig. 20B). In the presence of ascorbate, the characteristic EPR spectrum for the reduced Rieske ISP with its distinct g values is observed indicating that the ISC is not lost during the purification of the ISP from the cyt bc_1 complex. The g_x signal of the isolated Rieske ISP is broad with g = 1.75 - 1.77. Similar broadening of the g_x signal has been reported in bc_1 complexes with either an empty Q_P site, with reduced ubiquinol present or in the presence of an MOA inhibitor (40). Addition of stigmatellin to oxidized ISP does not show any reduction of the ISC as evidenced by lack of the characteristic EPR signals (Fig. 20). Therefore, stigmatellin itself does not reduce the ISC directly, but upon binding to the bc_1 complex induces electron transfer to the ISC. Stigmatellin, like other P_f inhibitors of the cyt bc_1 complex does not bind to isolated Rieske ISP but binds to cyt *b* subunit at the Q_P site proximal to ISP and distal from heme b_L (42).

The necessity of stigmatellin binding to the cyt bc_1 complex for ISC reduction is further evaluated in phospholipid-deficient bovine cyt bc_1 complexes where 90 % of phospholipids and ubiquinone/ubiquinol molecules are removed by repeated cholate-ammonium acetate fractionation (43). Delipidation of mitochondrial bc_1 complexes results in the loss of ubiquinol-cyt *c* reductase activity, but reconstitution with exogenous phospholipids restores a significant amount of the inhibitor-sensitive activity (data not shown). The EPR spectrum of phospholipid-deficient bc_1 complex in the presence of stigmatellin shows no ISC reduction as evidenced by the silent g values while ISC reduction is observed in the presence of ascorbate (data not shown). This indicates that stigmatellin is unable to induce ISC reduction in phospholipid-deficient cyt bc_1 complexes. However, incubation of the phospholipid-deficient cyt bc_1 complex with

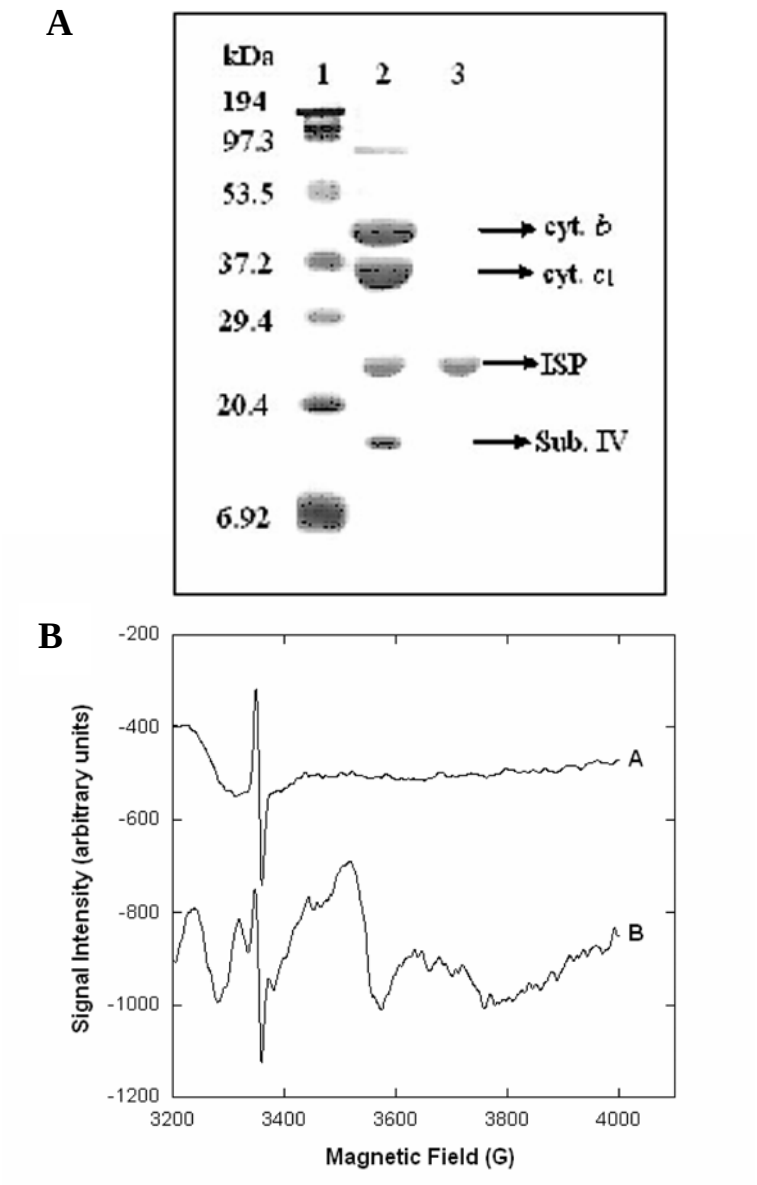

Figure 20. Characterization of purified Rieske ISP isolated from *R. sphaeroides* bc_1 complex. Rieske ISP was isolated from the cytochrome (cyt) bc_1 complex as detailed under "Experimental Procedures", and was subjected to SDS-PAGE (A). The purified Rieske ISP (lane 3) and cyt bc_1 complex (lane 2) was digested with 1 % SDS and 0.4 % β-mercaptoethanol at 23 °C for 15 minutes before loading into the gel. Protein standard contains: myosin (195 kDa), β-galactosidase (115.6 kDa), bovine serum albumin (97.3 kDa), ovalbumin (53.5 kDa), carbonic anhydrase (37.2 kDa), soybean trypsin inhibitor (29.4 kDa), lysozyme (20.4 kDa), and aprotinin (6.92 kDa). EPR spectra of the isolated ISP in the presence of stigmatellin (upper trace) and ascorbate (lower trace) were recorded (B). Instrument settings were as described in Fig. 18.

azolectin, phospholipids from soybean, before adding stigmatellin restores a significant amount of the ISC reduction (data not shown). This demonstrates that phospholipids are essential for the binding of stigmatellin to the cyt bc_1 complex, and correct binding is necessary for the stigmatellin-induced ISC reduction. Furthermore, endogenous ubiquinol can effectively be ruled out as the electron source for ISP reduction induced by stigmatellin, since ISP reduction is observed in phospholipids-supplemented, ubiquinol-deficient mitochondrial bc_1 complex.

It is possible that the Tris (2-amino-2-(hydroxymethyl)-1, 3-propanediol) buffer system used during purification of the bc_1 complex provides the electrons for the Rieske ISC in the presence of stigmatellin. However, stigmatellin reduction of the Rieske ISC is also observed in bc_1 complexes purified using Na^+/K^+ phosphate buffer system, thereby unambiguously eliminating the –OH groups of Tris as possible source of electrons (data not shown).

Characterization of Free Radicals Generated by the Cyt bc_1 Complex in the Presence of Stigmatellin or Ferricyanide – In addition to reduction of the Rieske ISC, an EPR peak with a symmetrical line shape, and g value centered at g = 2.005, typical characteristics of an organic free radical is observed when stigmatellin is added to oxidized cyt bc_1 complex. The intensity of the g = 2.005 EPR signal increases with varying amounts of stigmatellin (Fig. 21). Stigmatellin increases the midpoint potential of the Rieske ISP by approximately 260 mV to 540mV, resulting in the generation of a strong oxidizing agent. Because of its acquired oxidative nature, we speculate that the Rieske ISC extracts an electron from nearby organic residues, leading to its reduction and the subsequent generation of organic free radicals. When stigmatellin is added to the cyt

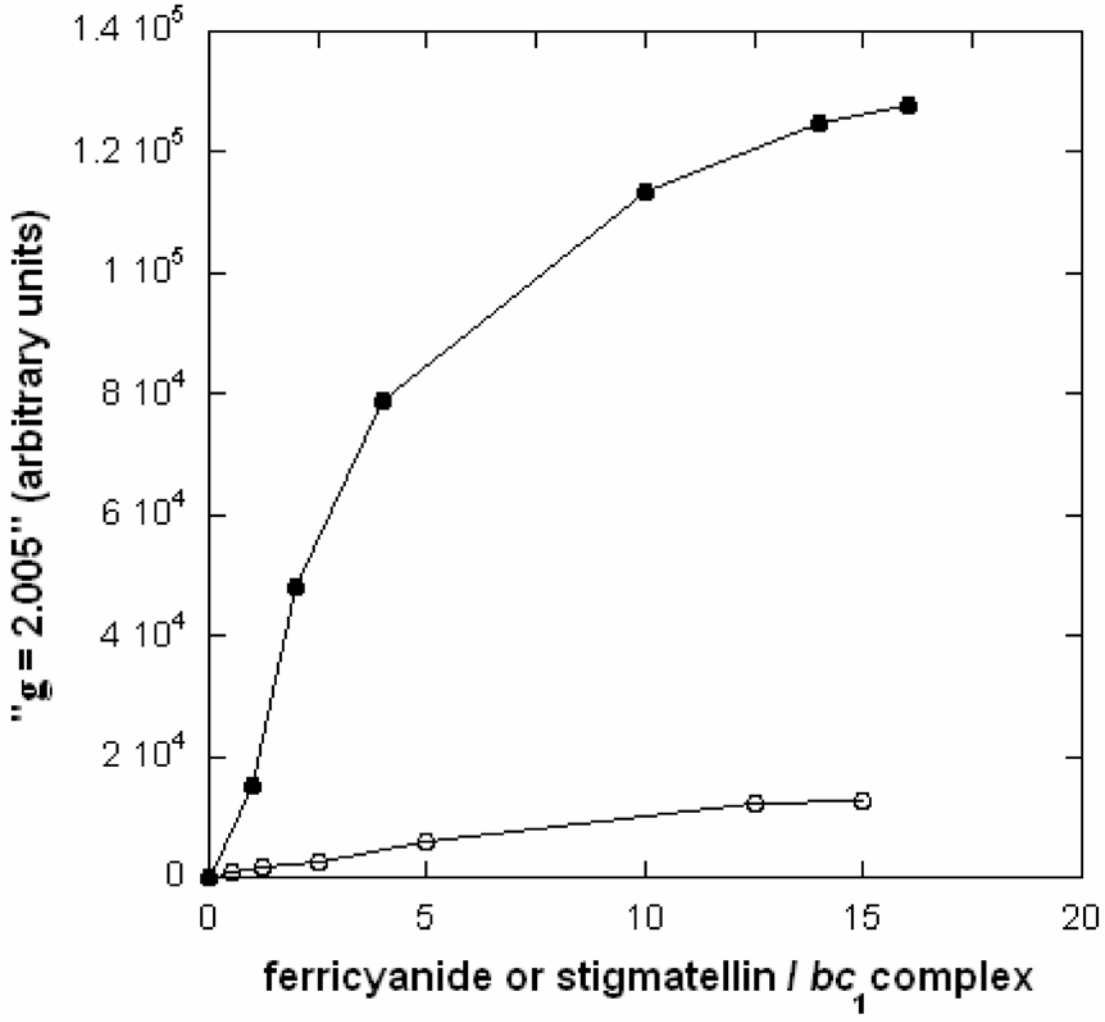

Figure 21. Effect of ferricyanide or stigmatellin concentration on the g = 2.005 EPR signal. Cytochrome bc_1 complex was diluted to 50 μM in 50 mM Tris-Cl, pH 8, containing 200 mM NaCl and 0.01 % DM. Stigmatellin (-○-) and ferricyanide (-●-) were added to the desired concentrations, and the mixtures were incubated on ice for 15 minutes before being frozen in liquid nitrogen. Instrument settings were as described in Fig. 18.

bc_1 complex at molar concentrations of 15 or higher, the mixture turns turbid due to partial precipitation of the bc_1 complex. It is speculated that excessive oxidation of organic residues induced by the high potential Rieske ISC eventually leads to denaturation and unfolding of the native enzyme. Addition of ferricyanide, a strong oxidant ($E_m \sim 420$mV), to oxidized cyt bc_1 complex also results in generation of the g = 2.005 EPR signal (Fig 21). Radical production increases with increasing concentrations of ferricyanide. When ferricyanide is added at a 10 to 15-fold molar excess of bc_1 complex, the g = 2.005 signal shows saturation indicating that possible oxidizable residues in the bc_1 complex become limiting. Moreover, it is speculated that ferricyanide might begin oxidizing some of the generated organic radicals resulting in quasi-equilibrium between oxidation of both organic residues and organic radicals. It must be noted that the amount of radicals produced in the ferricyanide-treated complex is approximately ten-fold greater than that observed in the presence of stigmatellin. Ferricyanide oxidation of organic residues directly proportional to the concentration used whereas stigmatellin induced oxidation is dependant on the amount of ISC available.

Since a symmetrical g = 2.005 EPR signal is often attributed to a ubisemiquinone radical at the Q_N site upon the reduction of ubiquinone by heme b_H (20), it is of interest to determine whether the stigmatellin induced radical is the same as Q_N radical or not. The ubisemiquinone anion generated at the Q_N site is entirely sensitive to the inhibitor, antimycin A, and can thus be distinguished from other organic radicals (44) of the cyt bc_1 complex. Pre-treatment of the bc_1 complex with antimycin A prior to stigmatellin addition reduces the intensity of the g = 2.005 signal by approximately 30 % (Fig 22). This indicates that the vast majority of organic radicals generated upon the

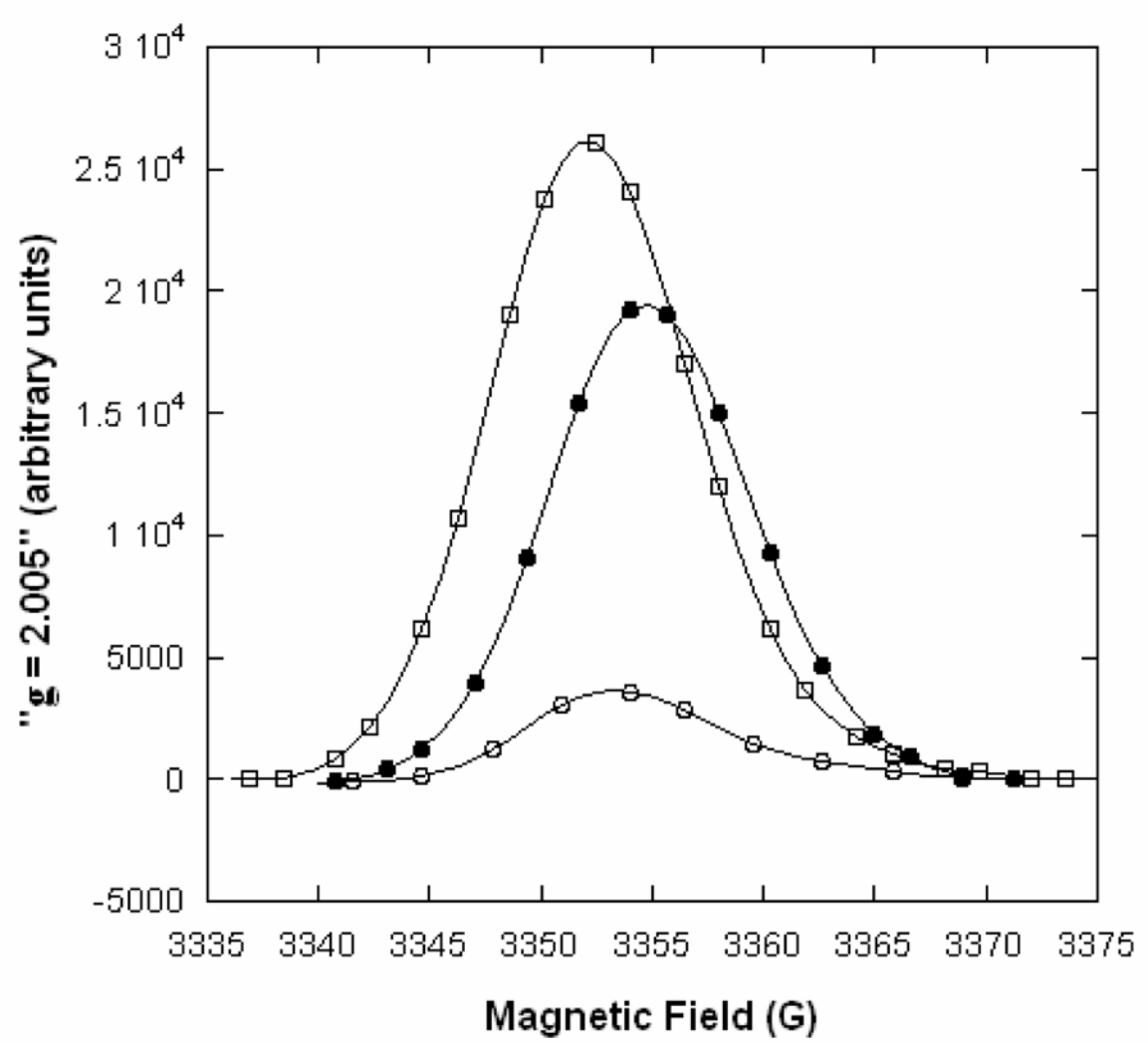

Figure 22. Characterization of the *g* = 2.005 EPR signal in wild type cytochrome bc_1 complexes. Cytochrome (cyt) bc_1 complex was diluted to 50 μM in 50 mM Tris-Cl, pH 8, containing 200 mM NaCl and 0.01 % DM, and oxidized by overnight incubation in the presence of 1 μM cyt *c* oxidase and cytochrome *c*. Curve with open squares (-□-) shows oxidized complex treated with 500 μM stigmatellin, curve with filled circles (-●-) is for 250 μM antimycin A plus 500 μM stigmatellin and curve with open circles (-○-) is for 500 μM stigmatellin plus 5 mM ascorbate. Instrument settings were as described in Fig. 18.

addition of stigmatellin to the cyt bc_1 complex can be attributed to antimycin A-insensitive organic radicals. Moreover, in the presence of ascorbate, an 85 % decrease in the g = 2.005 EPR signal of stigmatellin-treated complex is observed (Fig. 22). Ascorbate likely donates an electron and reduces the organic radicals formed in the stigmatellin-treated complex, resulting in a substantial decrease of the g = 2.005 EPR signal. To further demonstrate the organic radicals generated by the addition of stigmatellin to the complex are different from the ubisemiquinone radical at the Q_N site, power saturation profiles are determined (Fig 23). The g = 2.005 signal produced when bc_1 complex is treated with stigmatellin is monophasic and shows saturation at approximately 0.420 mW. The Q_N radical in the ascorbate-treated wild-type bc_1 complex shows saturation at approximately 0.211 mW. Similar power saturation at 0.251 mW has been previously reported for the Q_N radical generated in mitochondrial bc_1 complex (45). The power saturation profiles of the two free radical species indicate differences in the interactions with paramagnetic cofactors in the aqueous milieu, and also provide information on the relative location of the radical species within the enzyme complex. The significant difference in the power saturation properties confirms that the organic radical generated in the cyt bc_1 complex in the presence of stigmatellin is different from the Q-radical at the Q_N site.

Production of superoxide in cyt bc_1 complexes treated with stigmatellin – Approximately 1-2 % of oxygen consumed during normal respiration is not involved with oxidative phosphorylation, but with the formation of superoxide (46). Complex I and Complex III (bc_1 complex) were identified as two segments responsible for much of the superoxide generated in mitochondria (47-50). Superoxide ($O_2^{\cdot -}$) production, detected as

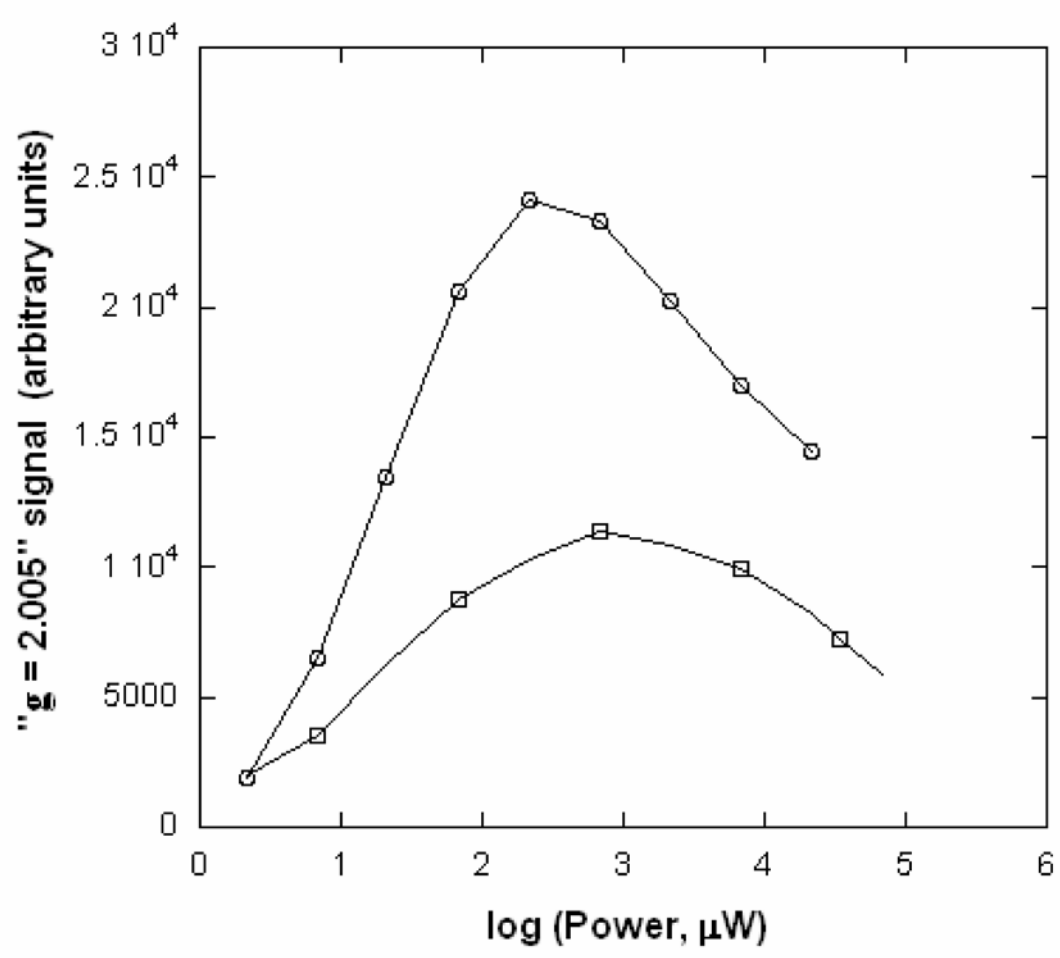

Figure 23. Power saturation properties of the *g* = 2.005 EPR signal. Power saturation of the free radical signal generated in the cytochrome (cyt) bc_1 complex upon treatment with stigmatellin is shown as open squares (-□-) and in the presence of ascorbate as open circles (-○-). Cyt bc_1 complexes were diluted to 50 μM in 50 mM Tris-Cl, pH 8, containing 200 mM NaCl and 0.01 % DM, and incubated with either 500 μM stigmatellin or 5 mM ascorbate on ice for 20 minutes prior to freezing in liquid nitrogen. Instrument settings were the same as in Fig. 18 except various microwave powers were used.

the fluorescence of 6-(4- methoxyphenyl)-2-methyl-3,7-dihydroimidazo[1,2-a] pyrazin-3 (7H) – one hydrochloride (MCLA) - $O_2^{\cdot -}$ adduct, is observed upon adding the substrate, ubiquinol, to the bc_1 complex (Fig 24, trace A). Addition of stigmatellin in the absence of ubiquinol also generates $O_2^{\cdot -}$ (trace B), and its production is dependant on the amount of stigmatellin added. Similarly, when ferricyanide is added to the bc_1 complex, $O_2^{\cdot -}$ is generated (trace C). However, the rate of fluorescence decay is much more rapid as compared to the $O_2^{\cdot -}$ formed in the presence of either ubiquinol or stigmatellin possibly due to alterations in the ionic strength of the radical environment. In the presence of superoxide dismutase (SOD), $O_2^{\cdot -}$ is not observed when either ubiquinol or stigmatellin is added to the wild-type bc_1 complex, confirming the production of $O_2^{\cdot -}$ as a byproduct of the reaction (trace D). It is speculated that the $O_2^{\cdot -}$ is generated as a result of the interaction between molecular oxygen and the organic free radicals generated in the stigmatellin and ferricyanide treated bc_1 complex. To further demonstrate this speculation, $O_2^{\cdot -}$ generation is measured in the double mutant, H131N / H152N, in the Rieske ISP that lacks the ISC (51). In the presence of ubiquinol, $O_2^{\cdot -}$ production is observed in the wild-type, but not in the mutant complex (Fig. 25A). In the normal catalytic cycle of the cyt bc_1 complex, ubisemiquinone radical at the Q_P site (47), and reduced cyt b_{566} (48) are postulated to be the auto-oxidizable factors causing superoxide production. Absence of the Rieske ISC in the mutant complex abolishes the bifurcated electron transfer at the Q_P site preventing the formation of the two individual species responsible for $O_2^{\cdot -}$ production. Similarly, addition of stigmatellin to the mutant bc_1 complex does not generate any $O_2^{\cdot -}$ (Fig 25B), although the mutant bc_1 complex is able to bind stigmatellin as evidenced by the red-shift in the absorption of reduced cyt *b* (data not

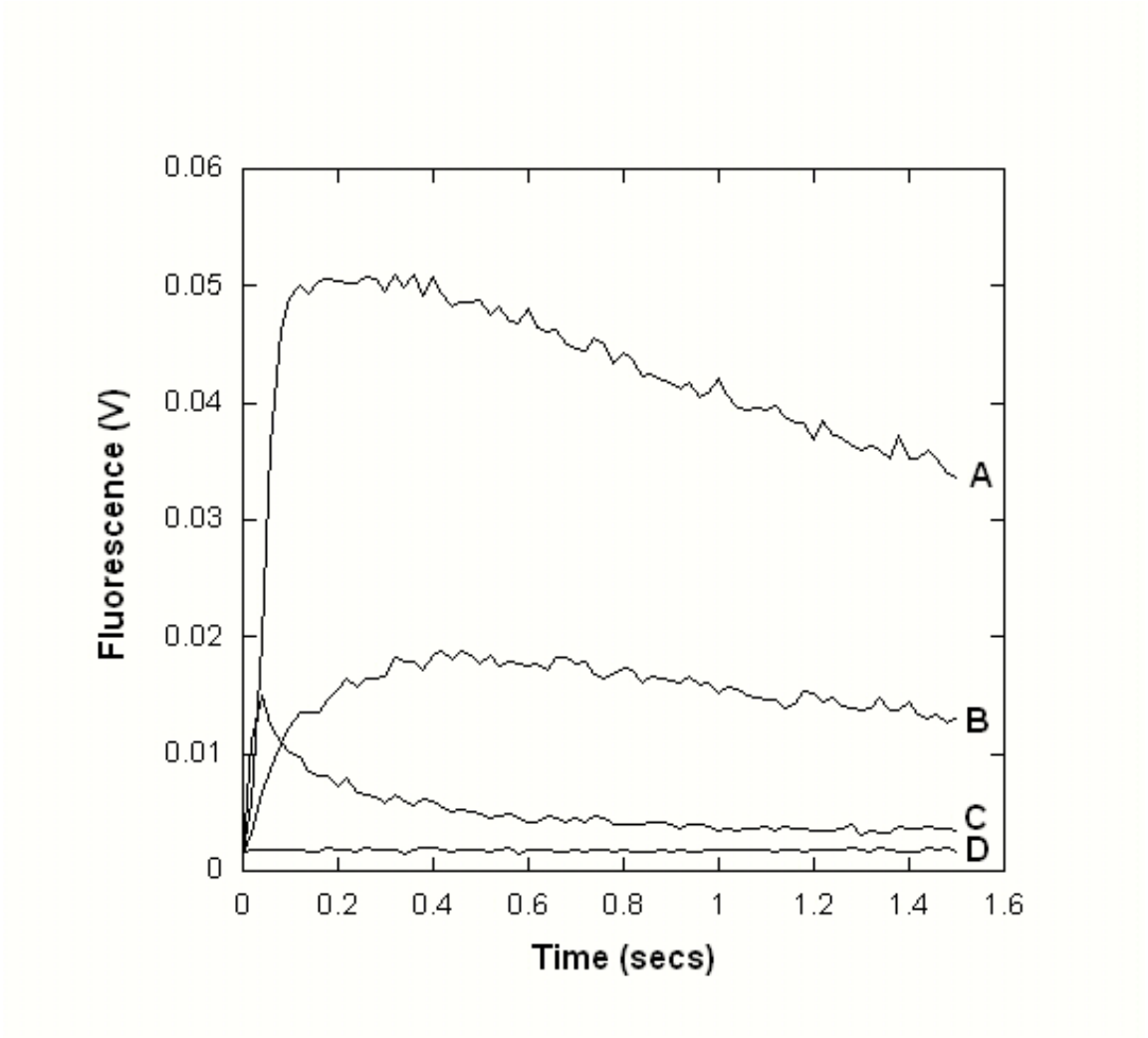

Figure 24. Superoxide generation in wild-type cytochrome (cyt) bc_1 complex. Cytochrome bc1 was diluted to 6 μM cytochrome *b* and superoxide production was determined upon addition of 50 μM ubiquinol (A), 60 μM stigmatellin (B), 60 μM ferricyanide (C), or 60 μM stigmatellin in the presence of superoxide dismutase (D). Superoxide generation was measured at 23 ^{o}C in an Applied Photophysics stopped-flow reaction analyzer SX18MV as described in "Experimental Procedures".

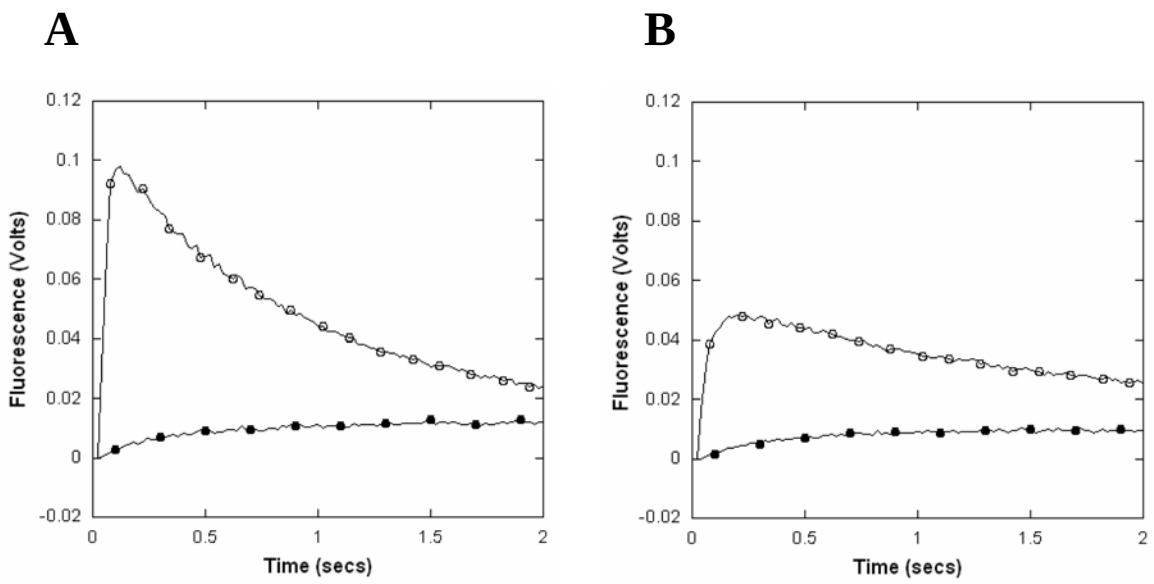

Figure 25. Superoxide generation in mutant lacking the Rieske iron-sulfur cluster. Tracings of superoxide generation in 6 μM wild-type and mutant (Δ 2Fe-2S) cytochrome bc_1 complexes in the presence of 50 μM ubiquinol (A) or 60 μM stigmatellin (B). Curves with open circles (-○-) denote the wild type complex while curves with closed circles (-●-) represent the mutant complex. Sample preparation and instrument settings were as described in Fig. 24.

shown). Binding of stigmatellin to the ISC-deficient mutant complex does not result in the generation of a strong oxidizing agent, i.e. a Rieske ISC with a highly elevated midpoint potential. Consequently, stigmatellin binding to the mutant complex does not induce the extraction of an electron from an organic residue by the Rieske ISC. Therefore, organic radicals are not generated, and no electron source is available for molecular oxygen to form $O_2^{\cdot -}$.

Cyt b reduction in bc_1 complexes treated with stigmatellin or ferricyanide – Addition of stigmatellin to the fully oxidized bc_1 complex results in slow reduction of cyt *b* (Fig 26, trace A). Similarly, when ferricyanide is added to the oxidized complex, cyt *b* reduction is observed with rates and extent comparable to the stigmatellin treated complex (trace B). Organic radicals, generated upon extraction of an electron by the Rieske ISC in stigmatellin-treated complexes or ferricyanide, are responsible for the observed cyt *b* reduction. Moreover, addition of stigmatellin to a mutant complex lacking the Rieske ISC does not show any reduction of cyt *b* (trace D). The absence of the ISC in the mutant complex prevents the formation of a strong oxidizing agent; subsequently no organic radicals capable of reducing cyt *b* are generated. However, in the presence of ferricyanide, cyt *b* reduction is detected in the mutant complex. Unlike with stigmatellin, the generation of organic radicals by ferricyanide is independent of ISC, thereby explaining the observed cyt *b* reduction. It must be noted that the extent of cyt *b* reduction in the mutant is lower than the complement wild-type complex. Altered accessibility of oxidizable residues as a result of possible conformational changes induced by the mutation could account for this decrease. One of the strongest supports for divergent electron flow at the Q_P site specified by the Q-cycle is the phenomenon of

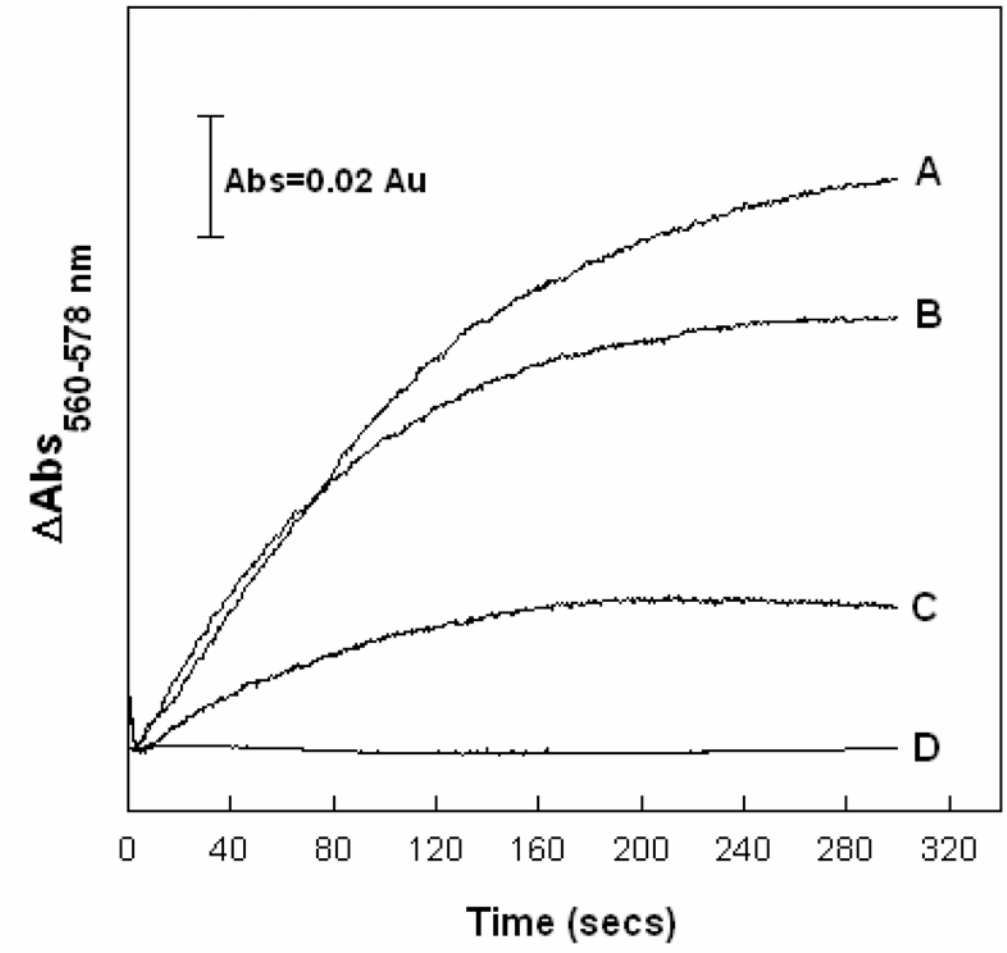

Figure 26. Characterization of cytochrome (cyt) *b* reduction. Fully oxidized wild-type cyt bc_1 complex was diluted to 5 μM in 50 mM Tris-Cl, pH 8, 200 mM NaCl, 0.01 % DM, and cyt *b* reduction was measured upon addition of 50 μM stigmatellin (A) and ferricyanide (B) respectively. Cyt *b* reduction in a mutant complex lacking the Rieske ISC upon addition of ferricyanide (C) or stigmatellin (D) was also determined.

'oxidant-induced reduction of cyt *b*' (52). Oxidation of the high potential chain, including cyt c_1 and ISP, results in a transient increase in cyt *b* reduction that is driven by the ubisemiquinone species generated at the Q_P site. Perhaps part of the cyt *b* reduction, in the presence of an oxidant, comes from oxidized organic radicals, as demonstrated above.

In conclusion - The Rieske ISP is in the fixed '*b*' position when stigmatellin is added to the cyt bc_1 complex. As a result, the redox mid-point potential of the Rieske ISP increases by 250 mV creating a strong oxidant. This elevated redox potential thus serves as the driving force for electron transfer from organic residues to the oxidized Rieske ISC resulting in its reduction, and the subsequent generation of organic radicals. The organic radicals in turn can react with molecular oxygen to yield $O_2^{\cdot -}$ or donate an electron to cyt *b*. The generation of organic radicals by stigmatellin-treated cyt bc_1 complex is severely retarded upon addition of ascorbate whereby the organic radicals are neutralized. Ferricyanide, a strong oxidant, also induces the generation of organic radicals, subsequent formation of $O_2^{\cdot -}$ and reduction of cyt *b*. $O_2^{\cdot -}$ is not observed in cyt bc_1 mutant complexes lacking the Rieske [2Fe-2S] cluster providing further evidence that the elevated mid-point potential of the Rieske ISC drives the reduction of the ISC and radical production. Finally, stigmatellin-induced reduction of the oxidized Rieske ISP might be used to identify cyt bc_1 mutations that confer resistance to the inhibitor, in addition to causing a red-shift in the cyt *b* absorption spectrum.

REFERENCES

1. Trumpower, B. L., and Gennis, R. B. (1994) Energy transduction by cytochrome complexes in mitochondrial and bacterial respiration: The enzymology of coupling electron transfer reactions to transmembrane proton translocation, *Annu. Rev. Biochem. 63*, 675-716.
2. Xia, D., Yu, C. A., Kim, H., Xia, J. Z., Kachurin, A. M., Zhang, L., Yu, L., and Deisenhofer, J. (1997) Crystal structure of the cytochrome bc_1 complex from bovine heart mitochondria, *Science 277*, 60-66.
3. Iwata, S., Lee, J. W., Okada, K., Lee, J. K., Iwata, M., Ramussen, B., Link, T. A., Ramaswamy, S., and Jap, B. K. (1998) Complete structure of the 11-subunit bovine mitochondrial cytochrome bc_1 complex, *Science 281*, 64-71.
4. Zhang, Z., Huang, L., Shulmeister, V. M., Chi, Y. I., Kim, K. K., Huang, L. W., Crofts, A. R., Berry, E. A., and Kim, S. H. (1998) Electron transfer by domain movement in cytochrome bc_1, *Nature 392*, 677-684.
5. Hunte, C., Koepke, J., Lange, C., Rossmanith, T., and Michel, H. (2000) Structure at 2.3 Å resolution of the cytochrome bc(1) complex from the yeast *Saccharomyces cerevisiae* co-crystallized with an antibody Fv fragment, *Structure 8*, 669-684.
6. Kurisu, G., Zhang, H., Smith, J. L., and Cramer, W. A. (2003) Structure of the cytochrome b6f complex of oxygenic photosynthesis: tuning the cavity, *Science 302*, 1009-1014.
7. Stroebel, D., Choquet, Y., Popot, J. L., and Picot, D. (2003) An atypical haem in the cytochrome b(6)f complex, *Nature 426*, 413-418.

8. Gao, X., Wen, X., Esser, L., Quinn, B., Yu, L., Yu, C. A., and Xia, D. (2003) Structural basis for the quinine reduction in the bc1 complex; a comparative analysis of crystal structures of mitochondrial cytochrome bc1 with bound substrate and inhibitors at the Qi site, *Biochemistry 42*, 9067-9080.

9. Esser, L., Quinn, B., Li, Y. F., Zhang, M., Elberry, M., Yu, L., Yu, C. A., and Xia, D. (2004) Crystallographic studies of quinol oxidation site inhibitors: a modified classification of inhibitors for the cytochrome bc(1) complex, *J. Mol. Biol. 341*, 281-302.

10. Tian, H., Yu, L., Michael, W., and Yu, C. A. (1998) Flexibility of the neck region of the Rieske iron-sulfur protein is functionally important in the cytochrome bc_1 complex, *J. Biol. Chem. 273*, 27953-27959.

11. Tian, H., White, S., Yu, L., and Yu, C. A. (1999) Evidence for the head domain movement of the Rieske iron-sulfur protein in electron transfer reaction of the cytochrome bc_1 complex, *J. Biol. Chem. 274*, 7146-7152.

12. Xiao, K., Yu, L., and Yu, C. A. (2000) Confirmation of the involvement of protein domain movement during the catalytic cycle of the cytochrome bc_1 complex by the formation of an intersubunit disulfide bond between cytochrome *b* and the iron-sulfur protein, *J. Biol. Chem. 275*, 38597-38604.

13. Darrouzet, E., Valkova-Valchanova, M., Christopher, C., Moser, P., Dutton, L., and Daldal, F. (2000) Uncovering the [2Fe-2S] domain movement in cytochrome bc1 and its implications for energy conversion, *Proc. Natl. Acad. Sci. U.S.A. 97*, 4567-4572.

14. Zhang, Z., Huang, L., Shulmeister, V. M., Chi, Y. I., Kim, K. K., Huang, L. W., Crofts, A. R., Berry, E. A., and Kim, S. H. (1998) Electron transfer by domain movement in cytochrome bc1, *Nature 392*, 677-684.

15. Kim, H., Xia, D. Yu, C. A., Xia, J., Kachurin, A. M., Zhang, L., Yu, L., and Deisenhofer, J. (1998) Inhibitor binding changes domain mobility in the iron-sulfur protein of the mitochondrial bc1 complex from bovine heart, *Proc. Natl. Acad. Sci. U.S.A. 95*, 8026-8033.

16. Berry, E. A., Guergova-Kuras, M., Huang, L. S., and Crofts, A. R. (2000) Structure and function of cytochrome bc complexes, *Annu. Rev. Biochem., 69*, 1005-1075.

17. Nett, J. H., Hunte, C., and Trumpower, B. L. (2000) Changes to the length of the flexible linker region of the Rieske protein impair the interaction of ubiquinol with the cytochrome bc1 complex, *Eur. J. Biochem. 267*, 5777-5782.

18. Obungu, V. H., Wang, Y., Amyot, S. M., Gocke, C. B., and Beattie, D. S. (2000) Mutations in the tether region of the iron-sulfur protein affect the activity and assembly of the cytochrome bc(1) complex of yeast mitochondria, *Biochim. Biophys. Acta. 1457*, 36-44.

19. Ghosh, M., Wang, Y., Ebert, C. E., Vadlamuri, S., and Beattie, D. S. (2001) Substituting leucine for alanine-86 in the tether region of the iron-sulfur protein of the cytochrome bc1 complex affects the mobility of the [2Fe-2S] domain, *Biochemistry 40*, 327-335.

20. Mitchell, P. (1976) Possible molecular mechanisms of the protonmotive function of cytochrome systems, *J. Theor. Biol. 62*, 327-367.

21. Crofts, A. R., Meinhardt, S. W., Jones, K. R., and Snozzi, M. (1983) The role of the quinine pool in the cyclic electron-transfer chain of *Rhodopseudomonas sphaeroides* - A modified Q-cycle mechanism, *Biohim. Biophys. Acta. 723*, 202-218.

22. Link, T. A. (1997) The role of the 'Rieske' iron sulfur protein in the hydroquinone oxidation (Q(P)) site of the cytochrome bc1 complex, *FEBS Lett. 412*, 257-264.

23. Brandt, U., and Okun, J. G. (1997) Role of deprotonation events in ubihydroquinone: cytochrome c oxidoreductase from bovine heart and yeast mitochondria, *Biochemistry 36*, 11234-11240.

24. Jünemann, S., Heathcote, P., and Rich, P. R. (1998) On the mechanism of quinol oxidation in the bc1 complex, *J. Biol. Chem. 273*, 21603-21607.

25. Osyczka, A., Moser, C. C., Daldal, F., and Dutton, L. P. (2004) Reversible redox energy coupling in electron transfer chains, *Nature 427*, 607-612.

26. Covian, R., Gutierrez-Cirlos, E. B., and Trumpower, B. L. (2004) Anti-cooperative oxidation of ubiquinol by the yeast cytochrome bc1 complex, *J. Biol. Chem. 279*, 15040-15049.

27. Crofts, A. R. (2004) Proton-coupled electron transfer at the Qo site of the bc1 complex controls the rate of ubihydroquinone oxidation, *Biochim. Biophys. Acta. 1655*, 77-92.

28. Snyder, C. H., Gutierrez-Cirlos, E. B., and Trumpower, B. L. (2000) Evidence for a concerted mechanism of ubiquinol oxidation by the cytochrome bc1 complex, *J. Biol. Chem. 275*, 13535-13541.

29. Thierbach, G., Kunze, B., Reichenbach, H., and Höfle, G. (1984) The mode of action of stigmatellin, a new inhibitor of the *b*-c_1 segment of the respiratory chain, *Biochim. Biophys. Acta. 765*, 227-235.

30. Hunte, C. (2001) Insights from the structure of the yeast cytochrome bc1 complex: crystallization of membrane proteins with antibody fragments, *FEBS Lett. 504*, 126-132.

31. Kagawa, Y., and Racker, E. (1971) Partial resolution of the enzymes catalyzing oxidative phosphorylation, *J. Biol. Chem 246*, 5477-5487.

32. McCurley, J. P., Miki, T., Yu, L., and Yu, C. A. (1990) EPR characterization of the cytochrome b-c1 complex from *Rhodobacter sphaeroides*, *Biochim. Biophys. Acta. 1020*, 176-186.

33. Denicola, A., Souza, J. M., Gatti, R. M., Augusto, O. and Radi, R. (1995) Desferrioxamine inhibition of the hydroxyl radical-like reactivity of peroxynitrite: role of the hydroxamic groups, *Free Radic. Biol. Med. 19*, 11-19.

34. Pumphrey, A. M., and Redfearn, E. R. (1960) A method for determining the concentration of ubiquinone in mitochondrial preparations, *Biochem. J. 76*, 61-64.

35. Lowry, O. H., Rosebrough, N. J., Farr, A. L. and Randall, R. J. (1951) Protein measurement with the Folin phenol reagent, *J. Biol. Chem. 193*, 265-275.

36. Berden, J. A., and Slater, E. C. (1970) The reaction of antimycin A with a cytochrome b preparation active in reconstitution of the respiratory chain, *Biochem. Biophys. Acta. 216*, 237-249.

37. Yu, L., Dong, J. H. and Yu, C. A. (1986) Characterization of purified cytochrome c1 from *Rhodobacter sphaeroides* R-26, *Biochem. Biophys. Acta. 852*, 203-211.

38. Laemelli, V. K. (1970) Cleavage of structural proteins during the assembly of the head of bacteriophage T4, *Nature 277*, 680-685.

39. Orme-Johnson, N. R., Hansen, R. E., and Beinert, H. (1974) EPR studies of the cytochrome b-c1 segment of the mitochondrial electron transfer system, *Biochem. Biophys. Res. Commun. 45*, 871-878.

40. von Jagow, G., and Ohnishi, T. (1985) The chromone inhibitor stigmatellin—binding to the ubiquinol oxidation center of the mitochondrial membrane, *FEBS Lett. 185*, 311-315.

41. Gutierrez-Cirlos, E. B., and Trumpower, B. L. (2002) Inhibitory analogs of ubiquinol act anti-cooperatively on the Yeast cytochrome bc1 complex. Evidence for an alternating, half-of-the-sites mechanism of ubiquinol oxidation, *J. Biol. Chem. 277*, 1195-1202.

42. Snyder, C. H., Merbitz-Zahradnik, T., Link, T. A. and Trumpower, B. L. (1999) Role of the Rieske iron-sulfur protein midpoint potential in the protonmotive Q-cycle mechanism of the cytochrome bc1 complex, *J. Bioenerg. Biomembr. 31*, 235-242.

43. Yu, L., Yu, C. A., and King, T. E. (1978) The indispensability of phospholipid and ubiquinone in mitochondrial electron transfer from succinate to cytochrome c, *J. Biol. Chem. 253*, 2657-2663.

44. Yu, C. A., Nagaoka, S., Yu, L., and King, T. E. (1978) Evidence for the existence of a ubiquinone protein and its radical in the cytochrome b and c1 region in the mitochondrial electron transport chain, *Biochem. Biophys. Res. Commun. 82*, 1070-1078.

45. Miki, T., Yu, L., and Yu, C. A. (1992) Characterization of ubisemiquinone radicals in succinate-ubiquinone reductase, *Arch. Biochem. Biophys. 293*, 61-66.

46. Boveris, A., Oshino, N., and Chance, B. (1972) The cellular production of hydrogen peroxide, *Biochem. J. 128*, 617-630.

47. Turrens, J. F., Alexandre, A., and Lehninger, A. L. (1985) Ubisemiquinone is the electron donor for superoxide formation by complex III of heart mitochondria, *Arch. Biochem. Biophys. 237*, 408-414.

48. Nohl, H., and Jordan, W. (1986) The mitochondrial site of superoxide formation, *Biochem. Biophys. Res. Commun. 138,* 533-539.

49. Turrens, J. F., and Boveris, A. (1980) Generation of superoxide anion by the NADH dehydrogenase of bovine heart mitochondria, *Biochem. J. 191*, 421-427.

50. Cadenas, E., Boveris, A., Ragan, C. I., and Stoppani, A. O. (1977) Production of superoxide radicals and hydrogen peroxide by NADH-ubiquinone reductase and ubiquinol-cytochrome c reductase from beef heart mitochondria, *Arch. Biochem. Biophys. 180*, 248-257.

51. Gurung, B., Yu, L. Xia, D., and Yu, C. A. (2005) The iron-sulfur cluster of the Rieske iron-sulfur protein functions as a proton-exiting gate in the cytochrome bc(1) complex, *J. Biol. Chen. 280*, 24895-24902.

52. Wikström, M. K., and Berden, J. A. (1972) Oxidoreduction of cytochrome *b* in the presence of antimycin, *Biochim. Biophys. Acta. 283*, 403-420.

CHAPTER IV

UNPUBLISHED WORKS

EPR spectra of iron sulfur protein (ISP) – ISP reduction by ascorbate in bc_1 complexes, purified using the Tris buffer system and quantitized by the intensity of the g_y EPR signal, is only 50 % of that observed in the presence of stigmatellin (Fig. 27). Similar observations are made when the bc_1 complex is reduced with dithionite. Stigmatellin arrests both Rieske ISP's in the fixed 'b' position, and elevates its E_m from +280 mV to +540 mV. The iron sulfur cluster (ISC) peak heights in anomalous difference maps normalized to the heme b_H peak is 0.47 for native bc_1 complexes, and is increased to 1.18 upon treatment with stigmatellin. In the native, inhibitor-free state, the soluble extra-membrane head domain of ISP is partitioned equally between a fixed and loose state, while it is entirely in the fixed state in the presence of stigmatellin. We speculate that ascorbate reduces only one of the Rieske ISP's, those in the fixed 'b' position, thereby explaining why only 50 % of the ISP's are reduced. This hypothesis is further analyzed in a *R. sphaeroides* bc_1 complex mutant (K70C (ISP)/A185C (cyt. *b*)·N36C (ISP)/G89C (cyt. *b*) whose soluble ISP head domain is covalently fixed onto cytochrome *b* by a pair of genetically engineered disulfide bonds, effectively mimicking the stigmatellin-bound state. Adduct protein bands with apparent molecular masses of 64 and 128 kDa respectively, the size of one cytochrome *b* and one ISP and two

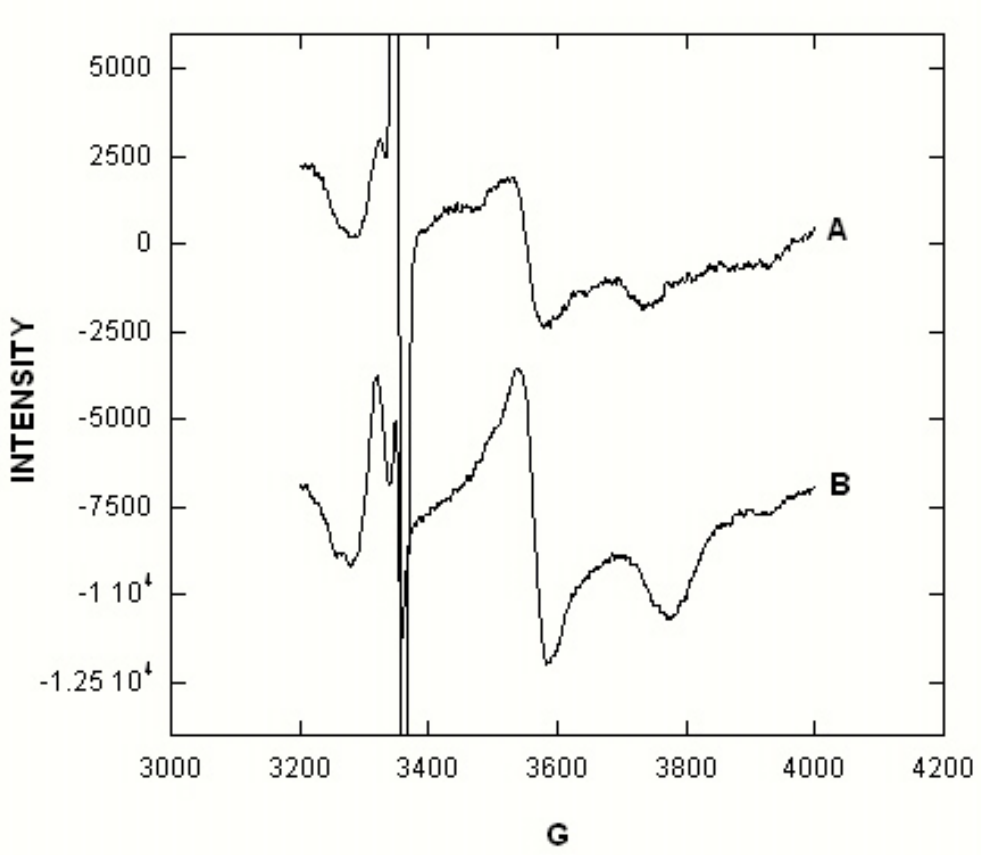

Figure 27. EPR spectra of bc_1 complex in Tris buffer. Cytochrome bc_1 complexes, purified in 50 mM Tris-Cl, pH 8, 200 mM NaCl, 0.5 % DG and 200 mM histidine, were diluted to 70 μM cytochrome *b*. The bc_1 complexes were treated with 5 mM ascorbate (A) or 350 μM stigmatellin (B) and incubated on ice for 20 minutes before freezing in liquid nitrogen. Sample preparations and instrument settings were the same as in Fig. 18.

cytochrome *b*'s and two ISP's respectively, are detected when the mutant bc_1 complex is treated with SDS and subjected to electrophoresis in the absence of β-mercaptoethanol (data not shown). The extent of ISC reduction by ascorbate in the mutant bc_1 complex, as determined by the intensity of the g = 1.89 EPR signal, is approximately two-fold higher than observed in the wild type complex (Fig. 28, left panel). In the presence of stigmatellin, the extent of ISP reduction in the wild type and mutant complexes are similar (Fig 28, right panel) indicating complete ISP reduction.

Cytochrome (cyt) bc_1 complexes were purified from *Rhodobacter sphaeroides* using the following buffer: 50 mM Tris-Cl, pH 8, containing 200 mM NaCl and 200 mM histidine. It has been well established that the pH of Tris buffer is sensitive to temperature, showing a 0.03 unit change in pH per degree change in temperature. Cyt bc_1 complexes are frozen in liquid nitrogen (approx -200 °C) prior to determining the redox state of ISC, and similarly, EPR data is collected at liquid nitrogen temperatures. Such low temperatures undoubtedly lead to large increase in pH of the Tris buffer system containing the bc_1 complex samples, although an exact value is difficult to quantitize. The redox potential of ISP, +280 mV at pH 8, is pH-dependant; it decreases with increasing pH and vice versa. It is possible that the redox potential of ISP in Tris buffer is lowered where it is not readily reducible by ascorbate at liquid nitrogen temperatures. To test this speculation, EPR spectra were recorded for bc_1 complexes solubilized in 50 mM Na^+/ K^+ phosphate buffer, pH 8, containing 200 mM NaCl, 0.5 % DG and 5 mM histidine (Fig. 29). The intensity of the g = 1.89 EPR signal in the presence of ascorbate or stigmatellin is comparable to one another, indicating total reduction of the Rieske ISP in the ascorbate-treated complex. The pH of phosphate buffer is not dependant on

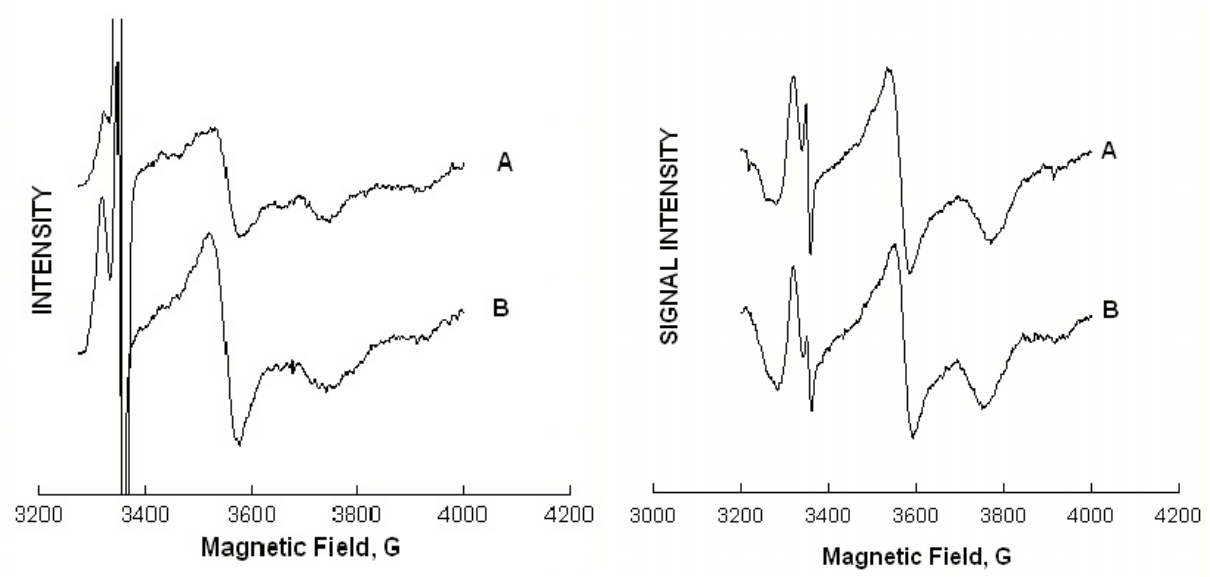

Figure 28. EPR spectra of mutant K70C (ISP) / A185C (cyt. *b*) N36C (ISP)/G89C (cyt. *b*). EPR spectra of WT (traces A) and the mutant complex (traces B)in the presence of ascorbate (left panel) and stigmatellin (right panel) were recorded**.** Ascorbate and stigmatellin were added to 70 μM bc_1 complex to a final concentration of 5 mM and 350 μM respectively. The mixtures were incubated on ice for 20 min prior to freezing in liquid nitrogen. EPR instrument settings are the same as in Fig. 18.

temperature, and consequently the redox potential of Rieske ISP is unaffected when the samples are frozen in liquid nitrogen. The fact that ISP reduction in phosphate buffer is complete demonstrates that ascorbate reduction is not governed by the location of the head domain since ISP's in both the fixed and mobile states were reducible by ascorbate. It was thus necessary to determine why ascorbate reduction of ISP in wild type bc_1 complex in Tris buffer was only half of that observed in phosphate buffer, or ascorbate-treated mutant complex with its ISP head domains tethered to cyt *b*.

We speculate that the redox potential of ISP varies, and is governed by the location of the mobile head domain. When the ISP head domain is in the fixed 'b' state, the redox potential is enhanced, since this is in the natural state for receiving an electron from the substrate, ubiquinol. On the contrary, the redox potential of the ISP in the 'loose' state is lowered possibly to facilitate electron transfer to cytochrome c_1. Therefore, when wild-type bc_1 complex in Tris buffer is frozen in liquid nitrogen, we speculate that the drop in redox potential of ISP as a result of the lowered temperature results in a dramatic lowering of the ISP redox potential. The redox potential of ISP in the 'loose' state, which we ascertain is lower than the fixed state, falls below the threshold where it is no longer reducible by ascorbate. This explains why only 50 % of the ISP in Tris buffer is reduced by ascorbate. The mutant with the ISP head domains tethered to cytochrome *b* has ISP's with elevated redox potential by virtue of their position. The redox potential drop of ISP in mutant complexes in Tris buffer is not sufficient to prevent reduction by ascorbate. A similar argument can be made for stigmatellin treated bc1 complexes in Tris buffer. Moreover, it is well known that stigmatellin raises the redox potential of ISP by a factor of about two. Assumptions can

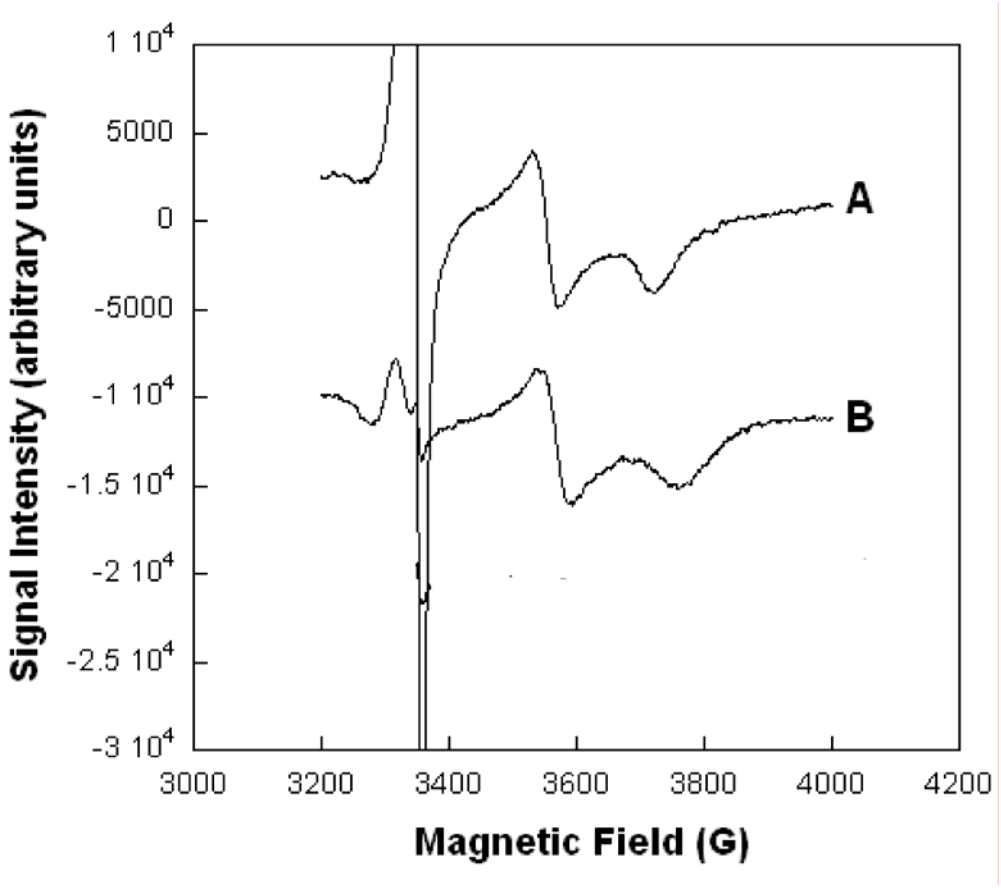

Figure 29. EPR spectra of bc_1 complex purified in Na^+/K^+ phosphate buffer. Cytochrome bc_1 complex purified in 50 mM Tris-Cl, pH 8, 200 mM NaCl, 0.5 % DG and 200 mM histidine was dialyzed in 100x volume of 50 mM Na^+/K^+ phosphate buffer, pH 8, 200 mM NaCl, 0.5 % DG and 5 mM histidine for four hours**,** with two changes of buffer. EPR spectra of bc_1 complex (70μM cyt *b*) in the presence of 5 mM ascorbate (A) and 350 μM stigmatellin (B) were recorded. EPR instrument settings were the same as in Fig. 18.

be made that the redox potential of ISP in the mutant complex increases by a similar manner.

Our experimental data indicate that the redox potential of the Rieske ISP undergoes drastic changes during the catalytic cycle of the bc_1 complex. When it is in the fixed 'b' state, the potential is highly elevated to facilitate electron transfer from ubiquinol. When ISP is in the mobile 'loose' state, its potential is lowered to facilitate electron transfer to cytochrome c_1.

Identifying amino acid residues that donate an electron to oxidized ISP in the presence of stigmatellin – As shown in Chapter III, stigmatellin induces reduction of the Rieske ISP in oxidized bc_1 complexes in the absence of an apparent electron source. It was shown that the elevated redox potential of the ISP upon stigmatellin binding resulted in ISP being a strong oxidant, extracting an electron from an organic residue resulting in its reduction and organic radical formation. Amino acid residues capable of donating an electron include tyrosine, threonine, serine, phenylalanine, histidine, cysteine and methionine. Oxidized cytochrome bc_1 complexes pre-treated with NEM, a cysteine modification agent, prior to addition of stigmatellin resulted in the reduction of ISP. This indicates that cysteine residues within the bc_1 complex are not the electron source for ISP reduction. To identify residues that possibly donate an electron to ISP in the presence of stigmatellin, several amino acid residues were altered by site-directed mutagenesis. The premise of our hypothesis was rather straight-forward: if a particular amino acid residue was responsible for ISP reduction in the presence of stigmatellin, then mutation of this residue would eliminate this observation. Unfortunately, attempts to identify specific

amino acid residues responsible for ISP reduction were unsuccessful. A compilation of mutations generated for this purpose is listed in Table 5.

Table 5

Mutants generated to identify amino acid residues responsible for ISP reduction in oxidized bc_1 complexes treated with stigmatellin

Mutation (*R. sphaeroides* numbering)		
(CYT *b*)	**(CYT c_1)**	**ISP**
Y302A	C145A	Y156F
Y302C		Y156A
Y302F	C169A	
E295K		S154A
E295G		S154C
E295T		
Y147A		
H291A		
T288A		
Y280A		

VITA

Buddha Gurung

Candidate for the Degree of

Doctor of Philosophy

Thesis: STRUCTURE AND FUNCTION STUDIES OF THE CYTOCHROME bc_1 COMPLEX

Major Field: Biochemistry and Molecular Biology

Biographical:

Personal Data:

Born in Manang, Nepal, on June 8, 1976 to Mr. Kami Tsering Gurung and Mrs. Sonam Dolma Gurung.

Education:

Graduated from Oklahoma State University with a Bachelors of Science degree in May 2000.
Completed the requirements for the Doctor of Philosophy in Biochemistry and Molecular Biology at Oklahoma State University, Stillwater, Oklahoma in Dec 2007.

Professional Memberships:

American Association for the Advancement of Science;
American Biophysical Society;
Biochemistry and Molecular Biology Graduate Student Association at Oklahoma State University.

Publications: **Gurung, B.**, Yu, L., Xia, D., and, Yu, C. –A. (2005) *J. Biol. Chem*. **280**, 24895-24902.

Name: Buddha Gurung Date of Degree: December, 2007

Institution: Oklahoma State University Location: Stillwater, Oklahoma

Title of Study: STRUCTURE-FUNCTION STUDY OF THE CYTOCHROME bc_1 COMPLEX

Pages in Study: 108 Candidate for the Degree of Doctor of Philosophy

Major Field: Biochemistry & Molecular Biology

Scope and Method of Study:

The purpose of this study was to gain further insights into the functioning of the bc_1 complex based upon data obtained by X-ray crystallography. Cytochrome bc_1 complexes from bovine heart mitochondrial were used for our study, and the photosynthetic bacterium *Rhodobacter sphaeroides* served as the model of choice for our study because of its simplicity, and the ease with which genetic manipulations could be achieved.

Findings and Conclusions:

Besides its involvement in the catalytic cycle of the cytochrome bc_1 complex, the Rieske iron-sulfur cluster (ISC) of the iron-sulfur protein (ISP) also acts as a proton exit gate. It prevents the non-specific leakage of protons from the inter-membrane space to the matrix, thereby preventing the collapse of the membrane potential which is eventually utilized by ATP synthase to synthesize ATP from ADP and inorganic phosphate. Incorporation of mutants lacking the ISC into vesicles along with actively proton-pumping mitochondrial bc_1 complex results in the loss of the generated membrane potential. Protons ejected by the functional mitochondrial bc_1 complex during electron transfer from ubiquinol to cytochrome *c* flow back via the mutant complex lacking the ISC. Compartmentalization, a key requisite for establishment of a membrane potential, no longer exists when phospholipid vesicles containing functional bc_1 complexes are co-embedded with ISC-lacking bc_1 complexes.

Stigmatellin, a P_f inhibitor of the bc_1 complex elevates the redox midpoint potential of ISP from +280 mV to +540 mV resulting in the generation of a strong oxidant species. Addition of stigmatellin to completely oxidized bc_1 complex leads to reduction of the ISC. Due to the acquired high potential upon stigmatellin binding, the ISC extracts an electron from an organic residue culminating in its reduction and the formation of an organic radical. The radical species can react with molecular oxygen to generate superoxide or donate its electron to cytochrome *b* resulting in its partial reduction. When ferricyanide is added to the bc_1 complex, superoxide generation and slow reduction of cytochrome *b* is observed, confirming the stigmatellin-induced oxidative nature of the ISC.

ADVISER'S APPROVAL: Dr. Chang-an Yu